The Thesis Committee for Jack Riley McLaughlin
Certifies that this is the approved version of the following Thesis:

Evaluating Abnormalities in Daily Transpiration Patterns Across Tree Species in a Semi-Arid Climate

APPROVED BY
SUPERVISING COMMITTEE:

Ashley Matheny, Supervisor
Daniella Rempe
Joel Johnson

Evaluating Abnormalities in Daily Transpiration Patterns Across Tree Species in a Semi-Arid Climate

by

Jack Riley McLaughlin

Thesis

Presented to the Faculty of the Graduate School of

The University of Texas at Austin

in Partial Fulfillment

of the Requirements

for the Degree of

Master of Science in Geological Sciences

The University of Texas at Austin

May 2022

Acknowledgements

First, I would like to thank my advisor, Ashley Matheny, for guiding me through my research and degree plan. I have learned invaluable skills and lessons along the way that will surely serve me for the rest of my life. I would also like to thank my friends and lab mates Suvan Cabraal, Ana Maria Restrepo Acevedo, Maria Ulatowski, Lily Beaman and Myriam Loving. Your company and help in the field, lab, and classroom saved me countless hours of struggle, and I have forged friendships with each of you that I will forever hold dear. Lastly, I would like to thank my family, especially my mom and dad. Thank you for always pushing me and supporting me in my education, hobbies, and life in general.

Abstract

Evaluating Abnormalities in Daily Transpiration Patterns Across Tree Species in a Semi-Arid Climate

Jack Riley McLaughlin, M. S. GeoSci

The University of Texas at Austin, 2022

Supervisor: Ashley Matheny

Climate change causes shifts in precipitation, temperature, shifting climate zones and more, thus affecting the ecology and hydrologic feedbacks of many environments, specifically those existing in already warm, arid climates. Vegetation affects the local hydrologic cycle, as it promotes multiple feedback mechanisms, such as the extraction of soil water via roots, the re-wetting of the atmospheric boundary layer and lowering temperatures through transpiration. This study focuses on transpiration patters in a hot semi-arid environment, which is defined as having a total annual precipitation between one-fifth and one-half of potential evapotranspiration and an annual mean temperature above 18°C. Meteorological conditions, sap flow, leaf water potential, carbon assimilation, and stomatal conductance were all recorded during 2021 in order to observe the drivers of transpiration among ashe juniper, lacey oak and pinyon pines, along with abnormalities in

their diurnal sap flow patterns, where the majority of sap flow occurs at dawn and dusk instead of midday. Sap flow was shown to increase in magnitude (up to 350% in pinyon pines' case) when environmental conditions such as vapor pressure deficit (VPD), temperature and soil water potential (SWP) are favorable. Ashe juniper was found to have a weak relationship between leaf water potential (LWP) and VPD, along with a stronger relationship between LWP and SWP. Oaks were found to have a very strong relationship between LWP and VPD, while pines were found to have a weak relationship between LWP and VPD. Of the three species, only the oaks were found to have a relationship between carbon assimilation rates and VPD, carbon assimilation rates and SWP, and stomatal conductance and SWP. This makes oaks the most vulnerable of the three species to future climate change and shifting climate zones. Better understanding of plant responses to stressful climatic conditions and in arid environments will provide insight in plant durability and adaptations to a warming climate, all of which are important as our global and local climates continue to change.

Table of Contents

List of Tables

List of Figures

Chapter 1: Introduction

1.1 Climate and Forest Dynamics

Vegetation plays a vital role in regulating multiple climatic feedback loops (Oki & Kanae, 2006). For example, vegetation affects the climate by mediating fluxes of energy and water from the land surface to the atmosphere (Anderegg et al., 2019). These feedbacks occur because plants normally lose water in order to obtain CO_2 and photosynthesize. This water loss is not of direct benefit the plants but is an unavoidable byproduct of opening their stomata to allow CO_2 in from the atmosphere. This process is known as transpiration. Transpiration rates and volumes vary around the globe and with different climates and vegetation assemblages, but universally it lowers the air temperature, raises humidity, and influences cloud cover via adding water to the boundary layer (Asawa & Fujiwara, 2020). As one would expect, drought and other stressful climatic conditions (e.g., extreme heat, saline soils) cause changes in transpiration (Anderegg et al., 2019). Unfortunately, global warming is expected to exacerbate drought conditions, and potentially cause shifting climate zones, with many becoming more arid — especially those regions which are already dry, such as hot semi-arid regions like the one in this study. At present, semi-arid regions make up 15.2% of Earth's terrestrial surface and are home to 1.1 billion people (Scholes, 2020). Semi-arid environments are those where the annual precipitation is between one-fifth and one-half of potential evapotranspiration. Hot semi-arid regions (Köppen class BSh) are further defined by having a mean annual temperature above 18°C. The identifying characteristics of a hot semi-arid climate region are as follows: high solar

radiation and temperature, low humidity and precipitation, ‘rainy’ and ‘dry’ seasons, and a high inter-annual variability in precipitation (Scholes, 2020). It has been shown that increasing temperatures and lower soil-water availability decrease gas exchange from plants (Kholová et al., 2010). Consequently, this limits their productivity (i.e., carbon uptake) and ultimately their ability to survive. Therefore, it is crucial to strengthen our understanding of vegetation behavior in hot semi-arid regions as the global climate continues to change.

1.2 Drivers of Transpiration

Transpiration is controlled by a multitude of factors, such as changes in atmospheric vapor pressure deficit (VPD), solar radiation, ambient and intra-ceullular CO_2 concentrations, air temperature, wind speed, humidity, soil water, soil temperature, hormonal signals and more (Mirfenderesgi et al., 2016; Oogathoo et al., 2020). Ultimately, one of the most important drivers of transpiration is changes in the atmospheric VPD (Belko et al., 2013; Kholová et al., 2010; Kirschbaum, 2004; Oogathoo et al., 2020). VPD is the difference between saturation vapor pressure and the observed vapor pressure (Grossiord et al., 2020). VPD serves as the driving force of transpiration, pulling water from the moist interior of the leaf into the drier atmosphere. This release of water vapor into the atmosphere is regulated by stomatal conductance to water vapor (Nizinski & Saugier, 1989). During favorable environmental conditions, plants open their stomata to take in the maximum amount of CO_2 for photosynthesis. However, when conditions become overly hot or dry, plants can restrict stomatal openness in order to

conserve water(Matheny et al., 2014). Water availability in the root zone, often referred to as soil moisture, has also been identified as a key control of transpiration (Gartner et al., 2009; Mitchell et al., 2012). Taken together, soil water content provides the water 'supply' for transpiration, while atmospheric VPD acts as the 'demand.' Studies regarding transpiration have been conducted for decades, regarding many different tree species across numerous environments around the globe. However, the complex nature of the phenomenon, the biotic and abiotic drivers of transpiration, and plant and species-specific dynamics of this critical flux differ based on locality, species, and environmental factors, cause it to remain an important field of scientific inquiry that is still yet to be fully understood.

1.3 Hot Semi-Arid Plant Behavior

In this study, we investigate the drivers of transpiration and the occurrence of abnormalities observed in diurnal sap flux dynamics for three common, canopy-dominant tree species: ashe juniper (*Juniperus ashei*), lacey oak (*Quercus laceyi*), and pinyon pine (*Pinus remota*). The Köppen Climate classification for the study region on the Edwards Plateau in West Central Texas is a hot semi-arid climate. A previous study at this field site revealed anomalies in tree water use, particularly during periods of high VPD and very low soil moisture (Rechner, 2020). Here, we seek to shed additional light on the causes and ramifications of these unusual behaviors. A typical tree under optimal conditions will generally transpire following the daily pattern of insolation (low at dawn, highest at solar noon, low at dusk and night), with minimum sap flow values occurring

overnight. Therefore, if one were to make a line plot of transpiration throughout the day, it would look similar to an upside-down parabola with the apex in the middle of the afternoon. However, in the xeric climate of Edwards County, Texas, an anomalous pattern of transpiration is observed, where the maximum values occur at dawn and dusk, and minimum values during the heat of the day (**Figure 1**).

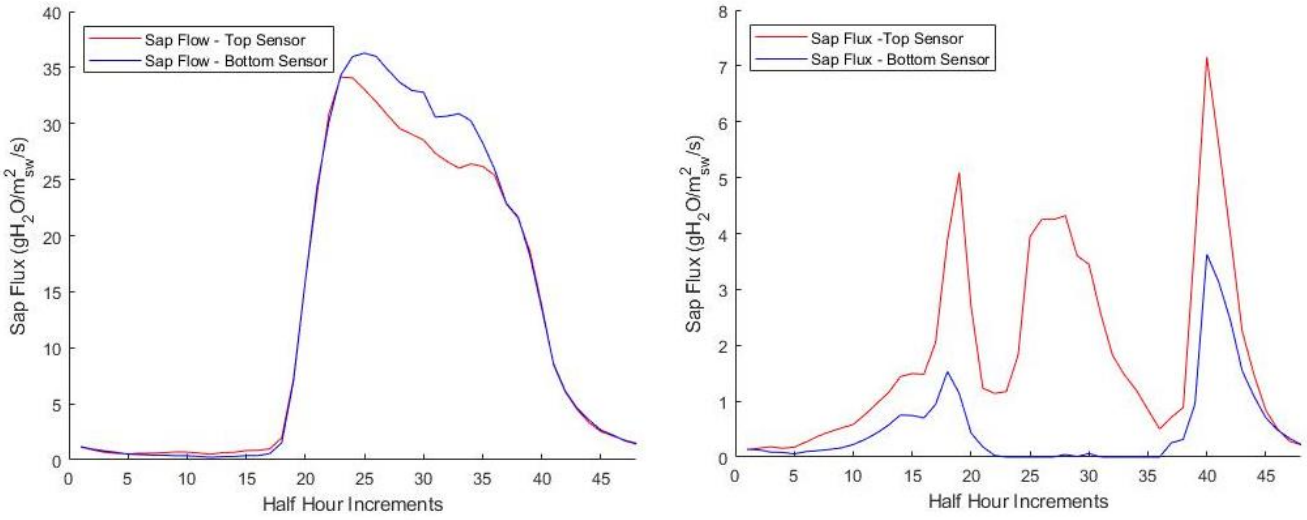

Figure 1: (Left) *An example of a typical diurnal pattern resembling an inverted parabola with the majority of the sap flow occurring during the afternoon.* ***(Right)*** *An example of the sap flow abnormality where the majority of sap flow occurs near dawn and dusk.*

A less extreme form of this pattern has been well documented as midday stomatal closure, when transpiration slows as water potentials within the xylem become too negative and stomata shut to avoid desiccation (Matheny et al., 2014). However, the pattern observed by Rechner shows a near complete cessation in sap flux during midday (2020). A second possible explanation for this phenomenon could potentially be a temperature artifact in sap flux data, with maximum flow occurring at night when wood

water content becomes so low that temperature dissipation in the xylem becomes uneven (Kukowski et al., 2013). Along with exploring the drivers of transpiration for these species, another key goal of this study is to investigate whether the observed transpiration anomaly in this hot, semi-arid forest is, in fact, the previously postulated sap flow artifact, or if the data is caused by plant adaptations to the xeric (very dry) climate. To disentangle these phenomena, we compared the sap flow measurements with leaf water potential, stomatal conductance, and net carbon assimilation observations over the course of the 2021 growing season.

Chapter 2: Methods

2.1 Field Site Description

This study was conducted on a privately owned ranch in Edwards County, roughly 20 miles southwest of Rocksprings, Texas (29.885519°, -100.495890°). The study area encompasses an elevation range of 650 to 700 m, and the average annual temperature is ~20.01°C based on daily data observations from 2019-2021. The mean annual rainfall at this location is 148 mm during the growing season, which is defined as approximately day of year (DOY) 120-300. These days were selected to include only days when both deciduous and evergreen species have full foliage. The property lies on the Edwards Plateau, which is a large, uplifted portion of southwest Texas composed of carbonate beds (limestones and dolomites), with some siliciclastic beds and igneous intrusions scattered across the landscape. The thin, rocky limestone soils of Edwards County give refuge to

flora that are characteristic of a semiarid region, like grasses, shrubs and certain small trees such as juniper, several oak species, mesquites and others(Long et al., 1963). The study area — like much of the Edwards Plateau — is underlain by Lower Cretaceous age carbonate and siliciclastic units that were deposited on a marine continental shelf due to rifting and subsidence in the Gulf of Mexico (Barker & Ardis, 1996). Mainly, the Segovia Member of the Edwards Limestone (found in the Fredricksburg Group) is exposed at the surface, with the Upper and Lower Glen Rose Members of the Trinity Group found below (Barker et al., 1994; Long et al., 1963; *Texas Water Science Center (USGS TWSC)*, 2014). These limestone units form karst features at and near the surface, where conduits, fractures, sinkholes, and more form due to the carbonate rock being soluble with water (Gams, 1993; Palmer, Arthur, 1991). This in turn creates a highly porous and permeable subsurface, with unknown amounts of water content and flow paths, complicating the local water budget.

Figure 2: *A view from the highest point on the property, looking downhill to where the sap flux array is installed.*

2.2 SAP FLUX

2.2.1 Sensor Theory

Sap flux measurements act as the most reliable proxy for transpiration at the individual plant scale. In simple terms, this proxy works because any water that moves upward through the xylem of a tree must be lost, eventually, to the atmosphere via transpiration. We measure sap flux using hand-manufactured Granier-style thermal dissipation sensors (Granier, 1985). These sensors consist of two thermocouple-bearing needles that are placed 10 cm apart vertically in the tree's xylem. The top needle is wound in a constantan wire which produces heat when powered by 0.2W. Sap flux measurements are based on the recorded temperature difference between the two thermocouples. Throughout the day, fluctuations in thermal dissipation from the top

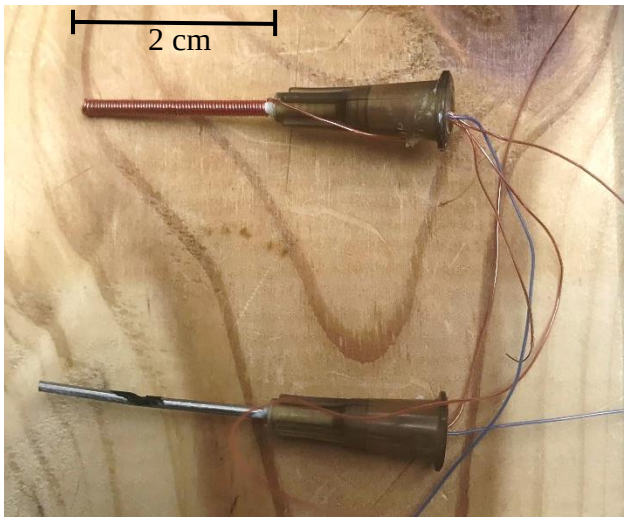

Figure 3: *A handmade Granier-style sap flux sensor with the heating needle on top*

needle are compared to the normal temperate of the tree's xylem (Davis et al., 2012). The top needle measures how much heat is dissipating as sap flux carries the heat away

vertically, away from the thermocouples. The bottom needle measures the reference temperature of the sapwood without any heat added. If the temperature between the two thermocouples is roughly the same, sap flux will be relatively high, as the vertical movement of water is carrying heat away from the top needle, causing the two needles to experience similar temperatures. If the top needle is warmer than the bottom needle, sap flux is relatively low, because there is no vertical movement of water to carry the heat away from the upper needle. Ultimately, this quantitative temperature difference (measure in millivolts) is proportional to sap flux velocity.

2.2.2 Sensor Construction

The sap flux sensors used in this study are hand manufactured. To start, each sensor consists of two 19-guage hypodermic needles (Becton Dickinson, Franklin Lakes, NJ, USA) that have been trimmed and polished to 1 or 2 cm, typically with a Dremel tool. 1 cm long sensors were used to observe sap flux in trees and branches having narrow sap wood. Using the Dremel, a 'window' is cut into the side of the needles at the midway point (1 cm or .5 cm mark) by letting the Dremel lightly touch the needle until a small hole appears. This window is used to view and secure the thermocouple in position. Since only one of the needles has the heating element, a .0125 mm hole is drilled in the plastic base of the needle that will have the heating wired wrapped around it. The two needles are then connected through the plastic bases of the needles using a 30 cm constantan wire of .127 mm diameter (TFCC-005-100, Omega Engineering, Stamford, CT, USA). Both needles also have a 15 cm copper wire (TFCP-005-100, Omega

Engineering, Stamford, CT, USA) of .125 mm diameter through the plastic base. At this point, the heating wire is inserted into the heating needle, which is a 50 cm piece of constantan wire of the same design. This wire should hang free with ~95% of its length protruding from the needle. Lastly, the thermocouple is constructed for both needles by stripping roughly a cm of insulation from the ends of the 30 cm constantan wire and the 15 cm copper wires and twisting them together. The thermocouples can then be pulled down into the viewing windows of each needle. Next, the thermocouples are glued into place (where they can be seen in the window) using a flexible rubber adhesive (Loctite 308 Black Max, Henkel, Dusseldorf, Germany). The glue is allowed to set for a week to ensure that it has completely cured. Once the glue dries, the 50 cm heating is wrapped tightly around the heating needle, starting from the tip and working towards the base. It is important to be sure that this wire is wound tightly and no gaps are visible between the coils of the wire. Once the wire is wound to the base, the excess wire is threaded through the hole in the plastic base of the needle was drilled earlier. The plastic bases of both needles are then filled with white craft glue to hold the wires in place and to ensure that the heating wire stays tightly wound. The sensors are then hung upside down and left to dry typically for one or two days. A multimeter is used to test the resistance between each of the connections as a way to perform a quality control check and ensure that each sensor is functioning properly and within the same measurement range. The acceptable ranges of values can be found in the table below (**Table 1**).

***Table 1**: Targeted resistance ranges of wired connections after sap flux sensor assembly*

Wires	Connection	Resistance (Ω)
Constantan – Constantan	Heating wire to self	22-24
Copper – Copper	Thermocouple to thermocouple	14-16
Copper - Constantan	Heating wire to either thermocouple	Infinite/NaN

2.3 FIELD SITE SETUP

We installed four individual trees with sap flux sensors in each of ashe juniper (*J. ashei),* lacey oaks *(Q. laceyi),* and pinyon pines *(P. remota).* Each tree was instrumented with one sensor on the main trunk at breast height (1.37 m) and another, at the base of the live crown, typically near twice breast height. Sensors were installed in pairs (2 sensors per tree) to verify the timing of sap flow from trunk to crown. All 24 sensors were connected to a datalogger (CR1000x Campbell Scientific, Logan, UT, USA) via ethernet cable placed inside of a weatherproof enclosure (**Figure 4**). The enclosure was located under an elevated hunting blind with a solar panel on the roof, continuously supplying the logger and sensors with power.

Figure 4*: Weatherproof housing for datalogger with sensor cables entering from below*

Tree allometric data at each sensor location has been compiled in **Table 2** and **Table 3** for all 12 trees. For convenience, we will refer to the sensor located at breast height the "bottom sensor," in reference to its lower position on the trunk. The "top sensor" is the sensor located within the tree's crown.

***Table 2**: Data for all sensors placed at breast height (bottom sensor)*

Tree	Diameter at Breast Height — DBH (cm)	Sap Wood Area at DBH (cm^2)	Sensor Height Above ground (cm)	Tree Height (m)	Tree Crown Area (m^2)
Juniper 1	27.3	271.41	137.2	8.1	46.1
Juniper 3	31.4	331.27	137.2	11	46.2
Juniper 6	36.4	404.27	137.2	15.9	37.9
Juniper 7	24.3	227.61	137.2	11.6	30.8
Oak 1	14.4	75.560	137.2	11.9	34.4
Oak 4	19.9	151.90	137.2	21.9	48.9
Oak 5	31.7	315.67	137.2	13.9	73.3
Oak 6	24	208.81	137.2	15.9	79.9
Pine 2	14.8	112.21	137.2	7.0	19.6
Pine 4	30.8	314.29	137.2	13.4	59.5
Pine 6	19.1	166.52	137.2	10.9	25.1
Pine 7	25.5	247.36	137.2	11.8	52.4

Table 3: *Data Measurements taken at all top sensor locations*

Tree	**Diameter at Top Sensor (cm)**	**Sap Wood Area at Top sensor (cm^2)**	**Sensor Height Above ground (cm)**	**Tree Height (m)**	**Tree Crown Area (m^2)**
Juniper 1	12.95	61.96	278.2	8.1	46.1
Juniper 3	21.84	191.75	282.2	11	46.2
Juniper 6	13.71	73.08	267.2	15.9	37.9
Juniper 7	15.49	99.04	277.2	11.6	30.8
Oak 1	11.18	30.81	259.12	11.9	34.4
Oak 4	19.56	147.16	259.1	21.9	48.9
Oak 5	31.7	252.92	333.2	13.9	73.3
Oak 6	22.61	189.46	259.1	15.9	79.9
Pine 2	14.8	112.21	238.2	7.0	19.6
Pine 4	30.8	314.29	352.2	13.4	59.5
Pine 6	19.1	166.52	259.12	10.9	25.1
Pine 7	25.5	247.36	323.2	11.8	52.4

2.3.1 Sensor Installation

Sap flux sensors are installed on the north side of the tree, away from any large knot, scar, or branching points that may interrupt the flow path. Whenever possible, we chose sensor locations where both sensors would be unobstructed, and were close to being aligned with each other vertically (i.e., on the same side of the tree).

Figure 5: (Left) *Sap Flux sensor installed in a tree and connected to the ethernet cables.* ***(Right)*** *An example of a tree that has 2 fully installed and wrapped sap flow sensors*

Once a spot has been chosen for the sensor to be installed, the outer bark of the tree must be scraped away to the cambium using a draw knife. The needles of an individual sensor must be placed 10 cm apart vertically, and sufficient bark must be removed for such that the cambium is visible in both needle locations enabling the sensor to be installed directly

into the hydroactive xylem. Next, two holes are drilled in the tree where the needles are inserted using a 3/32-inch diameter drill bit to a depth of 2 cm (or 1cm for smaller branches). Top sensors in Juniper 1, Oak 1, and Pine 2 were all 1cm long. After the holes have been drilled, a piece of 14-guage aluminum hypodermic tubing (Grainger Industrial, Lake Forest, IL, USA) that is the same length of the sensor needles (either 1 or 2 cm) is inserted into each hole. The purpose of these 'heat shields' is to ensure consistent heating around the entire needle, as well as protecting the tree and the needles from harming one another. The last step before inserting the needles into the heat shields is to cover them in conductive thermal paste (ThermalCote 250G, Aavid Thermolly, Concord, NH, USA) to ensure uniform heat dissipation. Once the needles are all inserted in the tree such that the plastic base of the needles are flush with the outer edge, the sensors are soldered to a CAT-5 ethernet cable (CAT-5E, Priority Wires and Cables, INC, Little Rock, AR, USA), which is connected to the datalogger and power supply. Power is supplied to the sensors from custom-built circuit boards inside the weatherproof enclosure, which provides each sensor with 0.2W of heating power. The temperature difference, measured in voltage, between the thermocouples is recorded every 60 seconds and averaged to a half-hourly timestep. The final step for sensor installation is to wrap the sensor and tree with a piece of reflective insulation (Reflectix Radiant Barrier, Reflextix Inc, Markelville, IN, USA). This provides the sensors with protection from solar radiation and environmental threats, such as birds.

2.4 Tree Height and Crown Area

Tree height and crown area were measured for each study tree (**Table 2** and **Table 3**). Tree height (h in m) was measured using a digital protractor and trigonometric functions. To do this, someone ('the spotter') walks away from the tree being measured until the apex of the canopy is in view of the digital protractor. Then, 'the spotter' notes the angle (θ in degrees) from the horizontal where they are standing to the canopy using the digital protractor. The height of the spotter's eye level is measured (y in cm) as well as the total distance 'the spotter' is standing away from the tree (d). The total tree height was calculated using **Equation 1** below.

Equation 1

$$h = d\ tan(\theta) + y$$

Tree crown area was also approximated as the projected area of an ellipse. The major and minor axes of the tree crown are measured to their furthest extents from the ground using a survey tape.

2.5 Leaf Water Potential

Leaf Water Potential (LWP) measurements are used to determine leaf hydration status. LWP measurements were taken using pressure chambers (PMS Model 600 and 600D, Albany, OR, USA) at different times throughout the day: predawn (6:00 am), midday (12-1 pm), and dusk (6-7 pm) for six weekend-long Trips throughout the year. On some occasions, LWP measurements were also taken at 3:00 am and 10:00 pm to

investigate nocturnal plant water status. These measurements were recorded from three trees (one per species): AJ1, O6, and P7.

Figure 6: *PMS Model 600 pressure chamber attached to nitrogen tank*

First, a small distal branch segment or leaf is trimmed using handheld garden shears. Next, the cut stem must be cut cleanly at the end with a razor, such that the cut surface is flat and smooth, with an unbranched segment or petiole of sufficient length to pass through the chamber gasket. The lid to the pressure chamber is then removed, where in the middle a small gasket the aperture will open/close as the lid is rotated, making it smaller or larger. The smooth stem is then inserted into the aperture from the bottom of the lid, so the foliage will be enclosed in the pressure chamber with only the end of the stem (~1 cm or so) sticking through the top of the lid for the operator to view. After tightening the aperture to form an airtight seal with the stem, the foliage is loaded into the pressure chamber, making sure that none of the leaves/needles become pinched when the chamber closes. Once the

lid is secured on the pressure chamber, tare the pressure at 0 MPa inside the chamber. Nitrogen gas is slowly added to the chamber, while the operator meticulously watches for bubbles on the cut cross section of the stem. The pressure at which bubbles first appear on the stem cross-section is equivalent to the water pressure within the leaf. Therefore, it is important to increase the pressure slowly to get as accurate of a reading as possible. Measurements were conducted in Triplicate for each time point at each sample tree in order to ensure high quality data. These measurements were recorded in 2021 for all the days spent in the field. Those days are reported below in **Table 4**. All LWP measurements from this study can be seen in **Table S1** in the appendix.

Table 4: *Different Trip dates over the course of 2021 where LWP and Licor measurements were recorded.*

	Julian Start Day	**Julian End Day**	**Calendar Dates**
Trip 1	29	32	Jan 29 – Feb 1
Trip 2	175	179	July 24 – July 28
Trip 3	218	221	Aug 6 – Aug 9
Trip 4	250	254	Sep 7 – Sep 11
Trip 5	297	300	Oct 24 – Oct 27
Trip 6	316	319	Nov 12 – Nov 15

2.6 PHOTOSYNTHESIS AND STOMATAL CONDUCTANCE

Figure 7: *Portable Licor 6800 capable of making gas exchange measurements*

The LI-6800 portable photosynthesis system (LI-COR Biosciences, Lincoln, NB, USA) is a machine that measures gas exchange from an individual leaf. LI-6800 observations include CO_2 and H_2O fluxes, stomatal conductance, net photosynthesis and more.

The LI-6800 is a handheld apparatus that clamps around a leaf, creating a closed system. After calibration, the machine supplies an air stream ('reference') with known concentrations of CO_2 and H_2O to the leaf. Trace gas fluxes are then calculated as the difference in concentration of CO_2 and H_2O in the reference and sample lines. The exchange of gas is then used by software in the LI-6800 to calculate the leaf's net photosynthetic assimilation rate of carbon (A_{net}) and stomatal conductance (GSW). The carbon assimilation rate, or photosynthesis rate, is how much carbon the plant is assimilating and photosynthesizing, while stomatal conductance refers to how open or closed the stomata are. These measurements were recorded concurrently with diurnal LWP (6:00 am, 1:00

pm, 6:00 pm) and during the same days, which can be seen above in **Table 4**. For all LI-6800 measurements, light levels, fan speed, reference humidity, and CO_2 concentrations were held constant to ensure consistent measurements.

2.7 METEOROLOGICAL MONITORING STATION

In a small clearing adjacent to the sap flow network, a micrometeorological station was installed to measure ambient air temperature, relative humidity (EE181-L10-PT, Logan, UT, USA) and air pressure (CS 100, Logan, UT, USA). Soil water content (SWC) was measured at 10 cm depth, where bedrock prohibits deeper installation (CS655-17-PT-DS, Logan, UT, USA). However, the SWC sensor was accidentally removed from the ground from DOY 290-318, presumably by either feral pigs rooting for food, or a brush-clearing team hired by the landowner. Broad-spectrum shortwave radiation was measured (CS320-T5, Logan, UT, USA) along with photosynthetically active radiation (LI190R-L15-PT, Logan, UT, USA). A tipping bucket system was used to measure precipitation (TE525WS-L25-PT, Logan, UT, USA). Leaf wetness, or water accumulation on the leaf surface, was recorded as an indicator of intercepted rainfall or dew (LWS-L15-PT, Logan, UT, USA). Lastly, wind speed and direction were measured (windsonic1-L14-PT, Logan, UT, USA). All data were recorded every 5 minutes on a datalogger inside a weatherproof enclosure (CR6, Campbell Scientific, Logan, UT, USA).

2.8 DATA PROCESSING

When dealing with nature and vegetation, correlations are expected to be weak, as no single variable can be isolated as the determining factor of a plant's success. Often, forcing variables are highly auto correlated (e.g., temperature, VPD, and soil moisture). Therefore, in this study, any P-value less than .06 is considered significant, where any R^2 value above .1 is considered a correlation (Dennis Baldocchi, 2014).

2.8.1 Meteorological Data Processing

Meteorological data was recorded every 5 minutes, and then averaged to half hour intervals. VPD was calculated by taking the difference of the saturation vapor pressure ($e_{saturated}$ in kPa), and ambient vapor pressure *(e* in kPa) based on observed air temperature (°C) and relative humidity. The deriving equations for these variables can be seen below (**Equation 2**, **Equation 3**, **Equation 4**) (Howell & Dusek, 1995).

Equation 2

$$e_{saturated} = .611e^{\frac{17.502*T}{T+240.97}}$$

Equation 3

$$e = \left(\frac{RH}{100}\right) * e_{saturated}$$

Equation 4

$$VPD = (e_{saturated} - e)$$

Assuming a soil type of sandy loam, soil water content was converted to soil water potential using **Equation 5** (Campbell, 1974). SWP is used in comparison to LWP instead of SWC

because not all water in the soil is available for plants to use. SWP provides a more informative point of comparison, as it is directly related to how easily extractable soil water is for plants. More negative SWP values indicate more stressful field conditions, while less negative values indicate more water availability.

Equation 5 $$|\psi(\theta)| = |\psi_{ae}| \cdot \left(\frac{\phi}{\theta}\right)^{b}, \theta^{*} < 1$$

2.8.2 Sap Flux Data Processing

Raw sap flow data is originally recorded in millivolts (mV) and later converted into sap flux density ($g_{water}/m^2{}_{sapwood}/s$) following the equations originally developed by Granier (1985, 1987) below in equations 5, 6 and 7. In order to take into account minor variations in hand-made sensors, sensor installation, sensor drift, and potentially nocturnal transpiration, each sensor is calibrated and baselined to itself every night following the Oishi baselining technique (Oishi et al., 2008, 2016). The maximum temperature difference (ΔT_{max} in mV) recorded by a sensor represents a no flow condition in the xylem, as no heat is being carried away from the heating needle. To ensure that these baseline points (ΔT_{max}) occur during flow conditions, a VPD threshold value of 0.5 kPa is used (Oishi et al., 2016). The baseline points are selected for times when VPD has a two-hour average less than 0.5 kPa and when the standard deviation of the four highest ΔT values are less than 0.5% of the average of the four values. These criteria, or nightly conditions, may not be met every single night, which gives this method the ability to account for potential nocturnal flow (Oishi et al., 2008). After the determination of the ΔT_{max} points, a linearly interpolated baseline for ΔT_{max} is calculated. ΔT_{max} is then paired

with the half hourly temperature difference data from every single sensor to calculate K (dimensionless, seen in **Equation 6**) (Granier, 1987).

Equation 6

$$K = \frac{\Delta Tmax}{\Delta Tsensor} - 1$$

The mean sap flux density (u, $g_{water}/m^2_{sapwood}/s$) can be calculated from K. Mean sap flux density is the instantaneous mass of water flowing per square meter of sapwood. A one-hour moving average was applied to u for every day in 2021 (**Equation 7**) (Granier, 1987).

Equation 7

$$u = 119 * K^{1.123}$$

For this study, transpiration (kg_{water}/day) is regarded as the amount of water being lost to the atmosphere over a daily period. Daily transpiration values (**Equation 8**) come from calculating the integral of u multiplied by sapwood area (S_A in m^2), where b is time at day's end and a is time at day's beginning (Granier, 1987).

Equation 8

$$F = \int_a^b u * S_A * dt$$

2.8.3 Photosynthesis and Stomatal Conductance Data Processing

The LI-6800 records the datafiles as a .CSV, which can be imported into Excel or MATLAB. LI-6800 measurements were assigned a species number (Juniper as 1, Oak as 2, and Pine as 3) and a column was added to record Julian day of year. Any negative values

for carbon uptake (indicating respiration) or stomatal conductance were removed to eliminate measurement points when the leaf chamber was not properly sealed around the leaf. Lastly, regression plots for assimilation and stomatal conductance (**Figure S3-Figure S6**, **Figure 67-Figure 70** & **Figure S7**, and **Figure S8-Figure S11**) do not show all the recordings. This is due to multiple recordings being taken in the span of just a few seconds, so when the data is averaged to align temporally with sap flow data, the fast measurement values become a single point.

Chapter 3: Results

3.1 Meteorological Results and Yearly Variability

Meteorological data was recorded continuously from 2018 to 2021 (**Table 5**).

Table 5: *Mean meteorological data for the growing season (day of year 120-300) for years 2018 through 2021. Values in parenthesis are standard deviations.*

Yearly Meteorological Variables				
	2018 (DOY 120-300)	**2019 (DOY 120-300)**	**2020 (DOY 120-300)**	**2021 (DOY 120-300)**
Temperature (°C)	24.9 (±6.2)	25.4 (±5.9)	23.64 (±6.19)	24.63 (±5.23)
Total Precipitation (mm)	156	160	137	131
VPD (kPa)	1.30 (±1.28)	1.36 (±1.13)	1.47 (±1.26)	1.14 (±1.05)

Soil Water Content (m^3_{water}/m^3_{soil})	0.248 (±0.14)	0.175 (±0.13)	0.192 (±.10)	0.204 (±.08)
Relative Humidity (%)	68.3 (±23.1)	64.7 (±20.8)	62.7 (±22.25)	69.7 (±21.21)

Mean temperature increased by 4.19% from 2020 to 2021, but 2021 was not abnormally warm, as 2018 and 2019 both had warmer growing season temperatures on average. The warmest day of 2021 was DOY 208, recording a temperature of 37.46°C. 2021 had the lowest mean VPD on record for the four years of data at this field site at 1.14 kPa, a 22% decrease from the highest mean VOD on record (the 2020 growing season). Temperature and VPD can be seen for all of 2021 in **Figure 8** below.

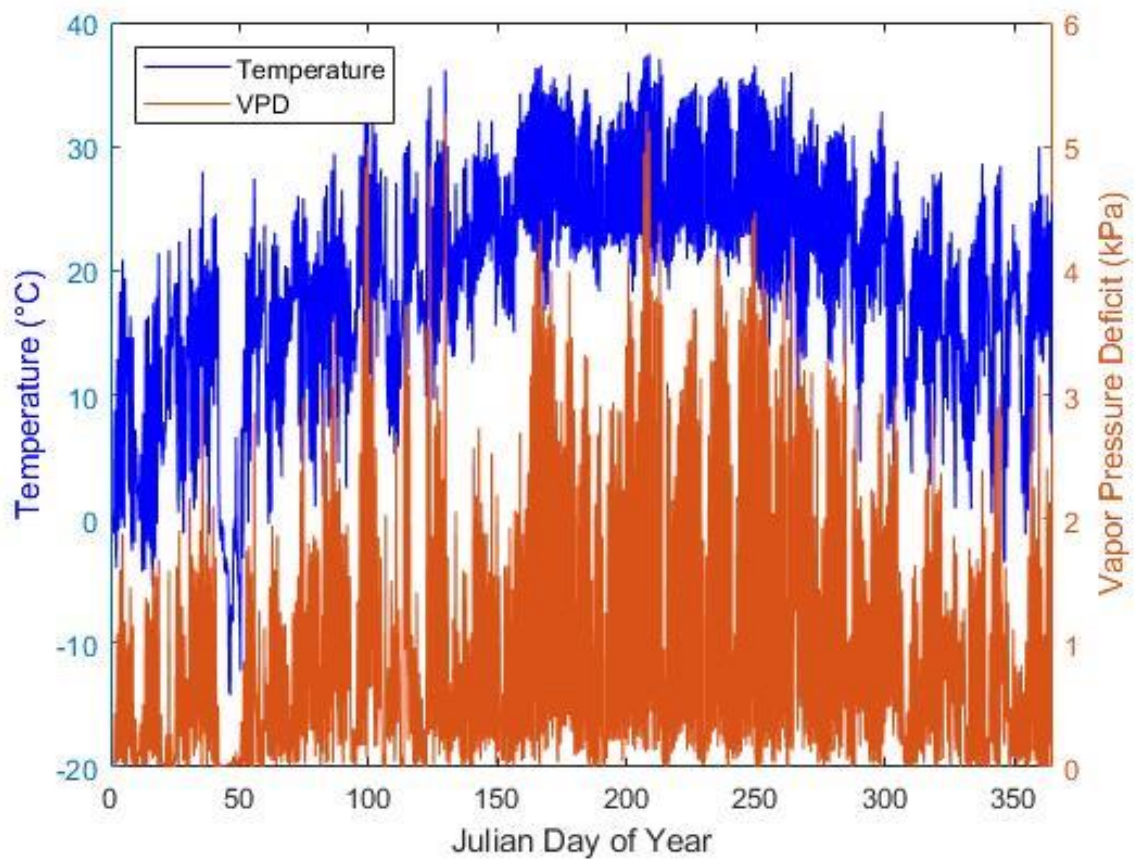

Figure 8: *Temperature and Vapor Pressure Deficit recorded for all of 2021*

As one would expect based on annual VPD averages (**Table 5**), this means 2021 had the highest humidity out of all 4 years at 69.7%, an 11% increase from 2020. However, 2021 was the driest of our four-year measurement period, receiving only 131 mm of precipitation during the growing season, a 4.38% decrease from 2020 and an 18.13% decrease from 2019. For the first month of the 2021 growing season, however, there were four precipitation events over 4 mm, which greatly increased SWC during this period (**Figure 9**). Consequently, mean soil water content (SWC) increased from 0.192 to 0.204,

a change of 6.25% from 2020 to 2021. Note that SWC values are missing at the end of the year due to the sensor being found out of the ground.

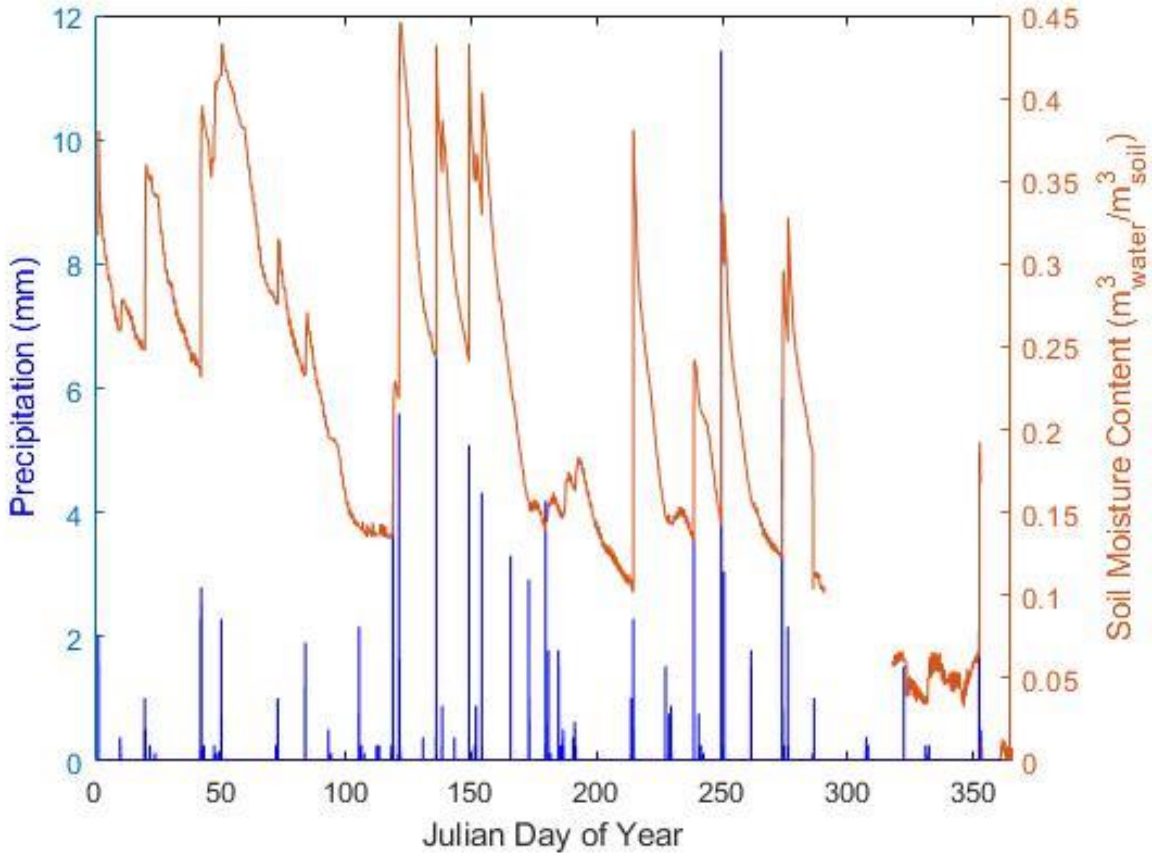

***Figure 9**: Precipitation and Soil Water Content for all of 2021*

Daily average temperature, VPD and photosynthetic active radiation (PAR) for 2021 can be seen below in **Figure 10**.

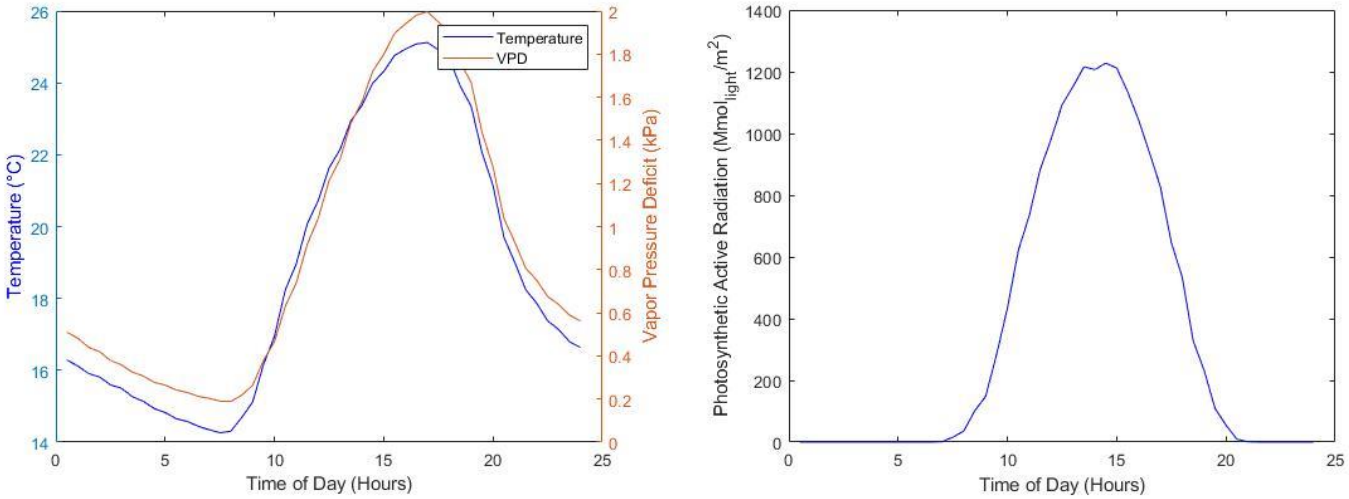

Figure 10: (Left) *Daily averaged temperature and Vapor Pressure Deficit (VPD).* ***(Right)*** *Daily averaged Photosynthetic Active Radiation (PAR) for the duration of 2021*

3.1.1 Meteorological Results — Stressful Period

In order to analyze the influence of meteorological conditions on tree hydrodynamic behaviors, we selected two periods from the growing season — a stressful period and a favorable period. The stressful period was chosen to encompass the highest temperature and VPD maxima for the year, with no precipitation events (**Figure 11**). These variables are found to increase leaf-water stress and decrease soil water potential. The stressful period extends from DOY 200 (June 12, 2021) to DOY 212 (June 24, 2021). The mean daily temperature during this period was 27.67°C. Consequently, the SWC dropped to the lowest point during the growing season at just 0.12 m^3m^{-3}, and the mean daily VPD was 1.74 kPa (**Figure 11** and **Figure 12**).

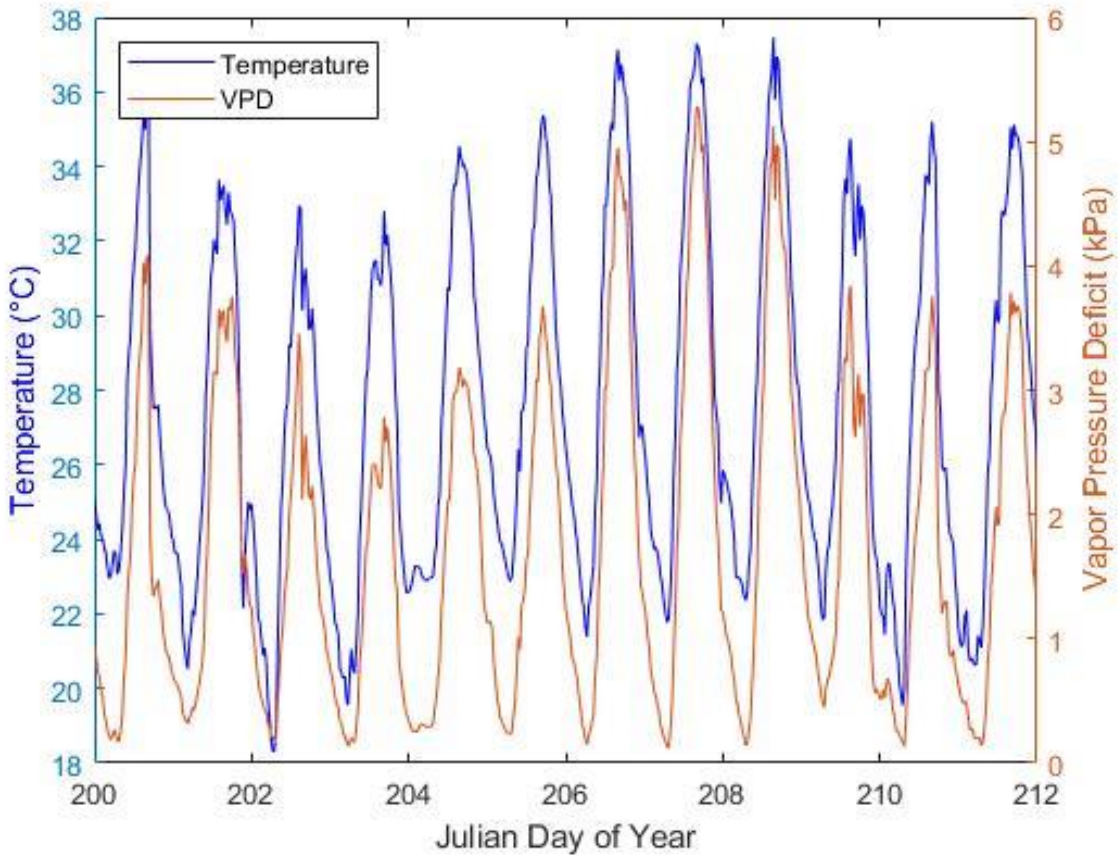

Figure 11: *Temperature and VPD over the course of the stressful period (DOY 200-212)*

DOY 208 had the highest recorded temperature of the year at 37.46° C, and every day during this period had a temperature above 32° C. As one would expect, VPD becomes very high as well — above 5 kPa.

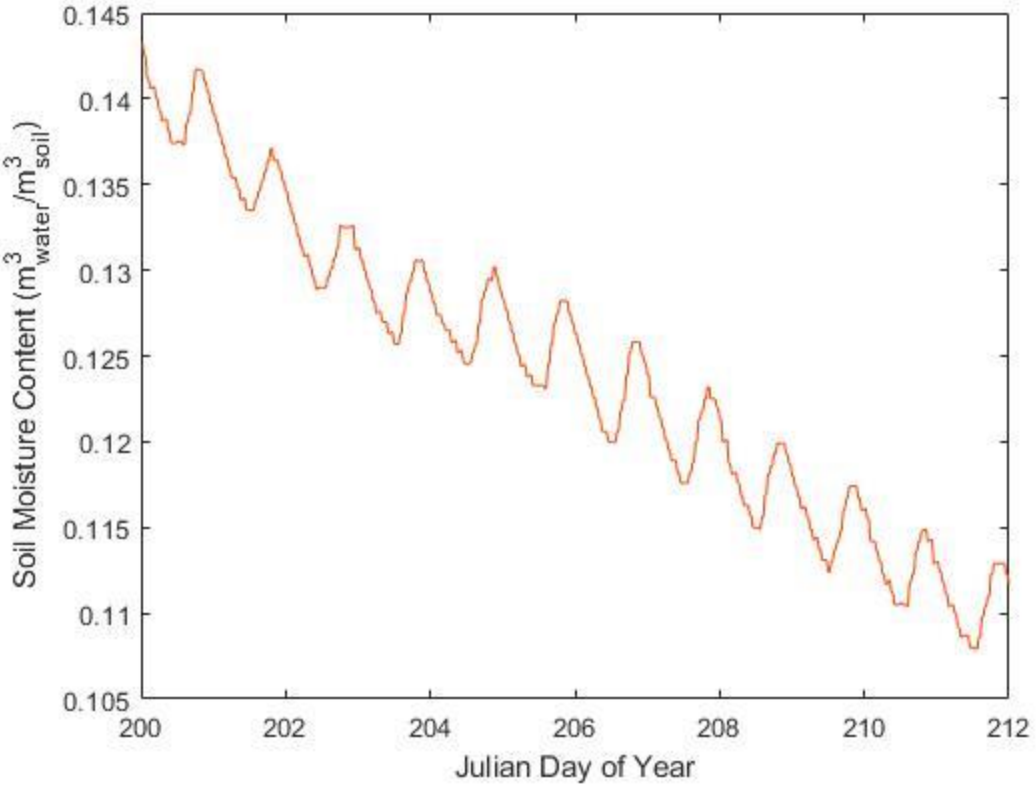

Figure 12: *Soil water content (SWC), or soil moisture content, for the stressful period (DOY 200-212).*

3.1.2 Meteorological Results — Favorable Period

The favorable period extends from DOY 250 (August 1, 2021) to DOY 72 (August 11, 2021). These dates were chosen to include some of the highest SWC with relatively mild temperatures for the growing season 2021. The mean daily temperature for this period was 24.85°C and the mean daily VPD was 1.35 kPa (**Figure 13**).

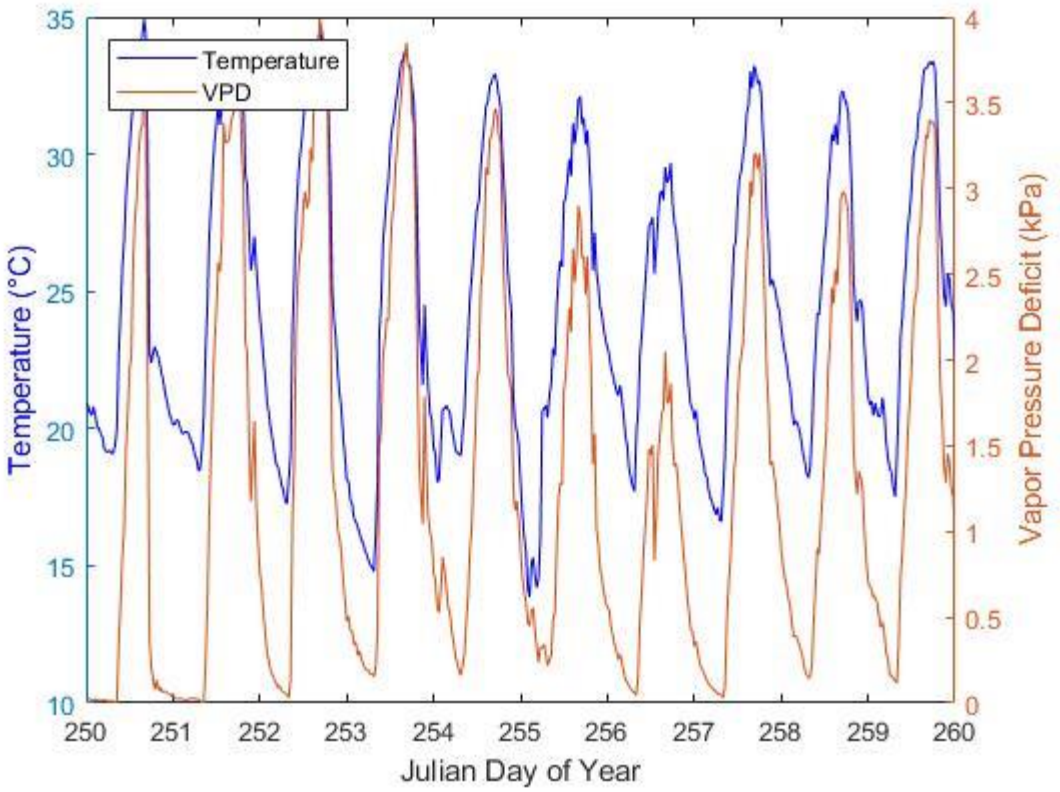

Figure 13: *Temperature and VPD over the course of the favorable period (DOY 250-260)*

This is still a warm 10-day stretch, with daily max temperatures above 30° C. However, this period started with just over 3 mm of rain, so SWC is above 0.32 m^3m^{-3} near the beginning (**Figure 14**).

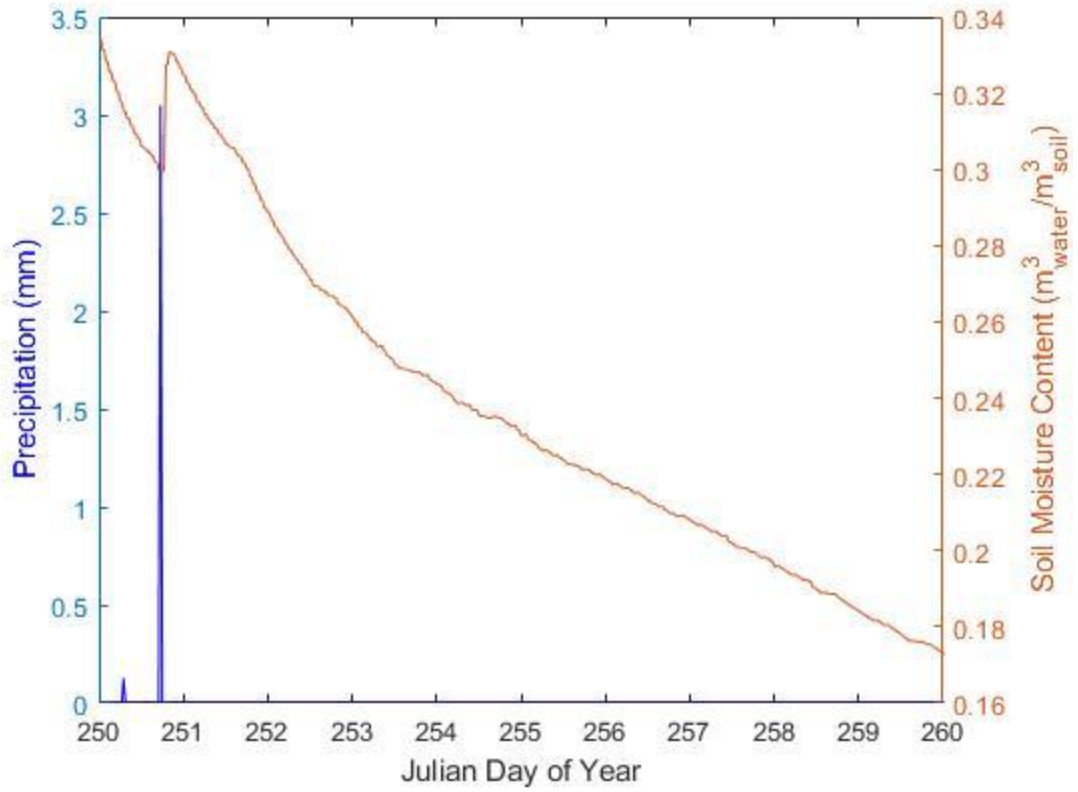

Figure 14: *Precipitation and Soil Water Content over the course of the favorable period (DOY 250-260)*

3.1.3 Meteorological Results — Trips 1-6

LWP measurements were recorded over 6 weekend-long Trips to the field site in 2021. The environmental conditions most closely related to plant-water relations — average VPD, temperature, and SWC — are reported for each Trip in **Table 6**. Due to sensor malfunction, SWC for Trip 5 (and much of Trip 6) was not recorded.

Table 6: *Average VPD, Temperature and Soil Water Content for each Trip in 2021. Note that the SWC sensor was out of the ground from DOY 290-318, so SWC values for Trip 5 are missing.*

	Mean VPD (%)	**Mean Temp (°C)**	**Mean SWC (g_{water}/g_{soil})**
Trip 1	.61	11.93	.29
Trip 2	1.46	27.78	.15
Trip 3	1.22	27.02	.248
Trip 4	1.38	24.90	.287
Trip 5	.91	24.09	N/A
Trip 6	.95	14.79	.06

3.2 SAP FLUX RESULTS

3.2.1 Yearly Sap Flux Results — Ashe Juniper

We observed sap flux in two locations in each of four mature juniper trees (AJ1, AJ3, AJ6 & AJ7). A continuous sap flux record from each juniper's top and bottom sensor can be seen below in **Figure 15** for 2021. Gaps in the data occasionally occur due to sensor malfunctions; data reported in Figure 13 is not gap-filled.

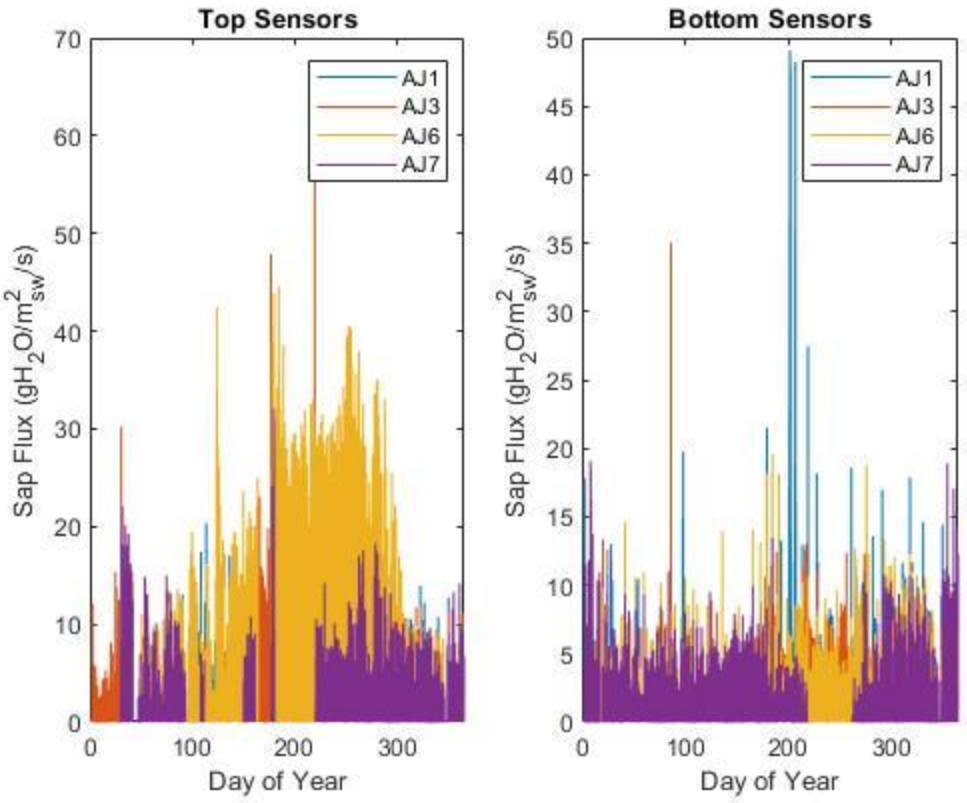

Figure 15: *All Juniper sap flux data for top and bottom sensors in 2021*

At first glance, the top sensors seem to record higher magnitudes of sap flux than the bottom sensors, excluding some instances, in particular AJ1. This is verified for some Juniper trees by the daily average sap flux plots in **Figure 16**. These daily average figures demonstrate the sap flux abnormality we seek to explain.

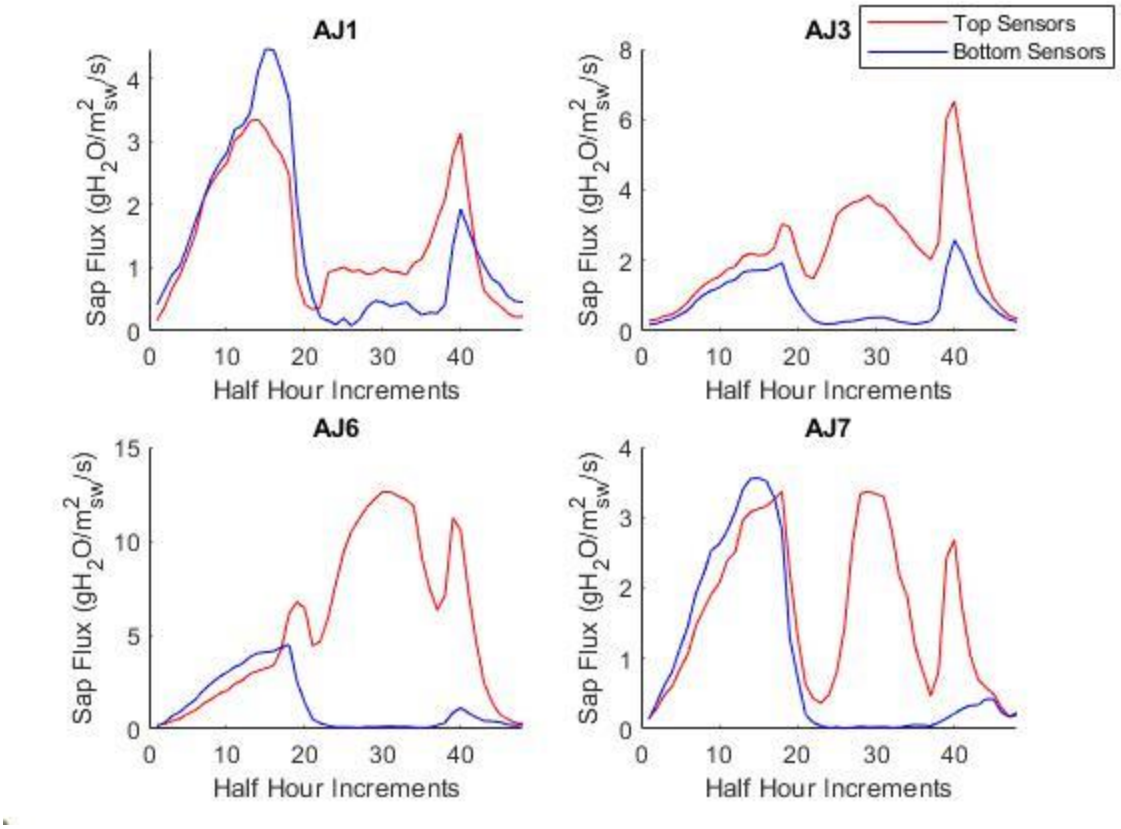

Figure 16: *Daily averages of all Juniper sensors. These show average daily patterns for sap flux across the 2021 growing season. The x axis shows a full day in half hour increments, with zero being midnight.*

For an average day (Figure 10) juniper water use is characterized by a large spike in sap flow at dawn followed by a decrease in the late morning, a slight increase during midday for some trees (except AJ6 and AJ7 have large midday sap flux), a decrease in the late afternoon, and a spike again at dusk. The bottom sensors generally have higher sap flow rates in the morning than the evening, excluding AJ3's sap flow spikes being similar in magnitude between the top and bottom sensor. Top sensors show similar patterns with spikes at dawn and dusk, but they also typically show spikes in the middle of the day

when transpiration would generally be highest. The only juniper tree that produced a 'typical' diurnal pattern of sap flux (e.g. an upside-down parabola) is AJ7. However, even this signal is shifted towards the early morning with maximum values near 7 am rather than solar noon. AJ1 and AJ7 have similar sap flow magnitudes between top and bottom sensors, while AJ3 and AJ6 have a top sensor which recorded much larger values than their bottom sensors. Top and bottom sensors in AJ1 and AJ3 produced similar diurnal patterns, regardless of differences in magnitudes.

3.2.2 Stressed Period vs Favorable Period Sap Flux Results — Ashe Juniper

Daily averages are a useful tool to observe a tree's generalized behavior. However, the weather changes drastically over the course of the year, as well as from day to day. Therefore, we compared typical behaviors during an environmentally favorable period and an environmentally stressful period, using the same days as described in the Meteorological Results (sections 3.1.1 and 3.1.2). Daily average sap flow for junipers during the stressful period (DOY 200-212) can be seen below in **Figure 17**, and the sap flow abnormality is shown for three out of the four junipers (AJ7 is the exception).

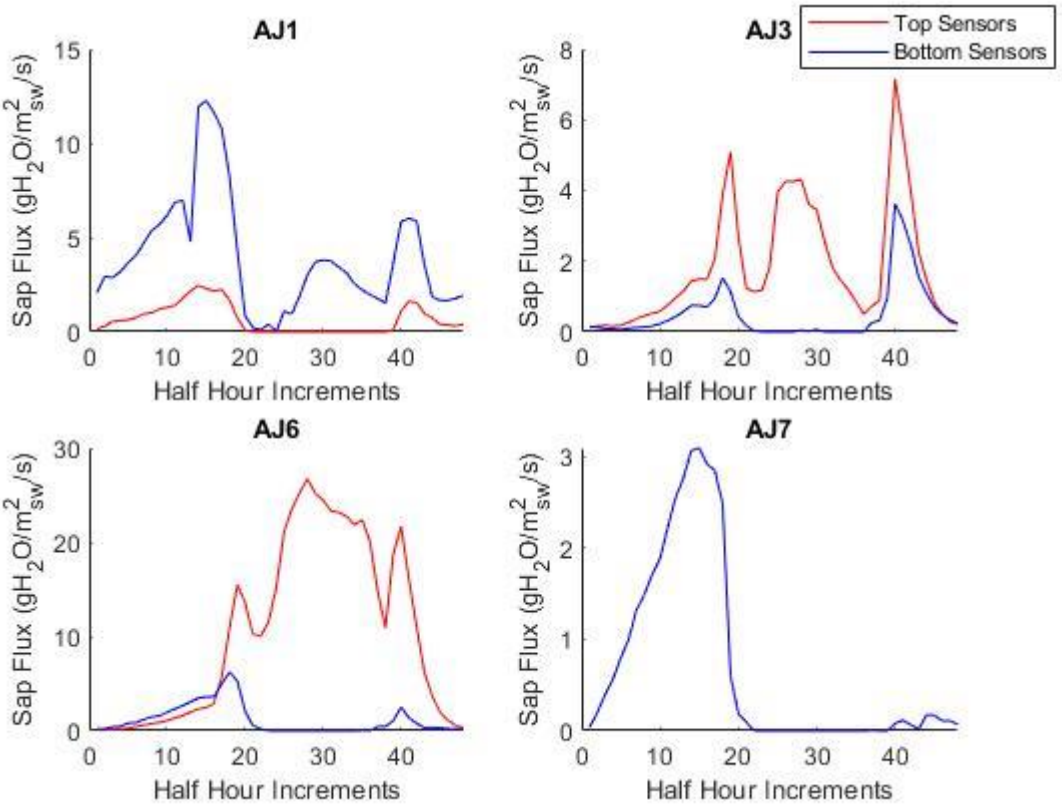

Figure 17: *Daily averaged sap flux for all Junipers during the stressful period (DOY 200-212). These show average daily patterns for sap flux across the 2021 growing season. The x axis represents a full day in half hour increments, with zero being midnight.*

Note that the top sensor in AJ7 was malfunctioning during the 'stressful' observation period and therefore has no data provided. The same is true for the bottom sensor of AJ7 during the favorable period (**Figure 18**).

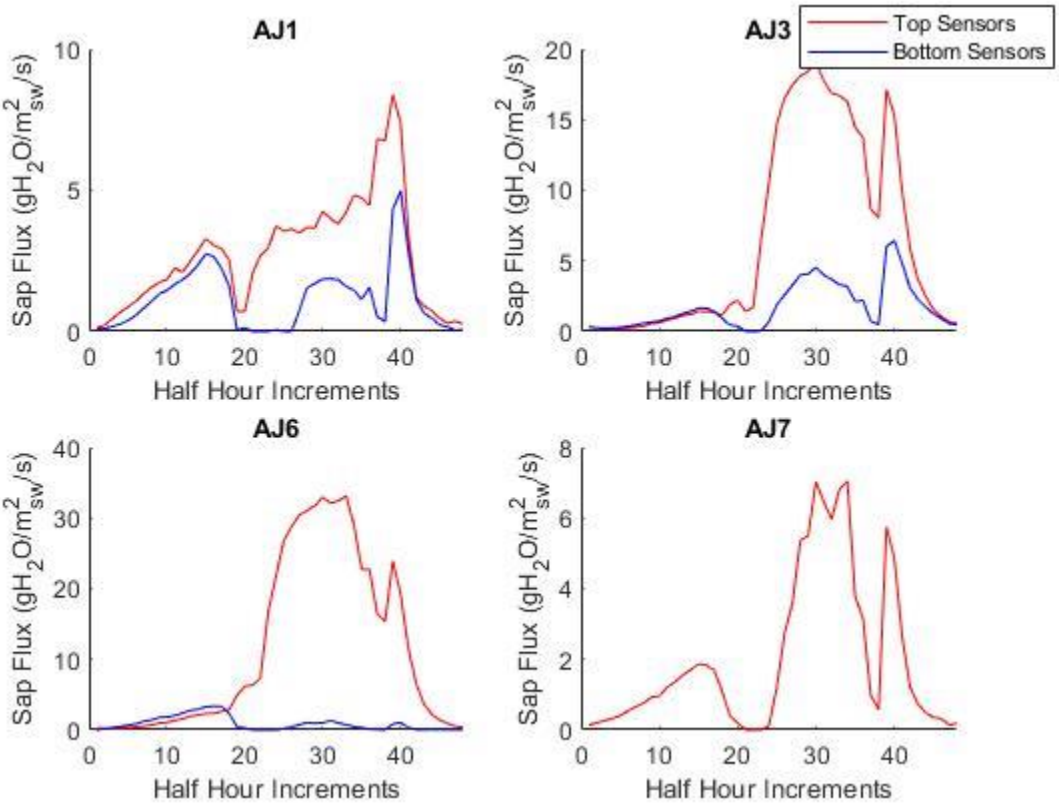

Figure 18: *Daily averaged sap flux for all Junipers during the favorable period (DOY 250-260). These show average daily patterns for sap flux across the 2021 growing season. The x axis represents a full day in half hour increments, with zero being midnight..*

Compared to the stressed period in **Figure 17**, sap flux patterns during the favorable period are notably different, with the majority of sap flow later in the day. For example, only AJ1 and AJ7 show sap flux spikes in the morning, and even then, theses sap flow spikes are less than half of the daily maximum. Instead, AJ6 and AJ3 show a more typical diurnal sap flow pattern, with the majority of sap flow occurring in the midafternoon. However, all show an evening spike in sap flux near dusk. Top sensor magnitude outweighs bottom

sensors in all instances during the favorable period (**Figure 18**), but the opposite was true for AJ1 in the stressful period (**Figure 17**). Overall, larger sap flow magnitude and more typical shapes can be observed during the favorable period easily in **Figure 19**.

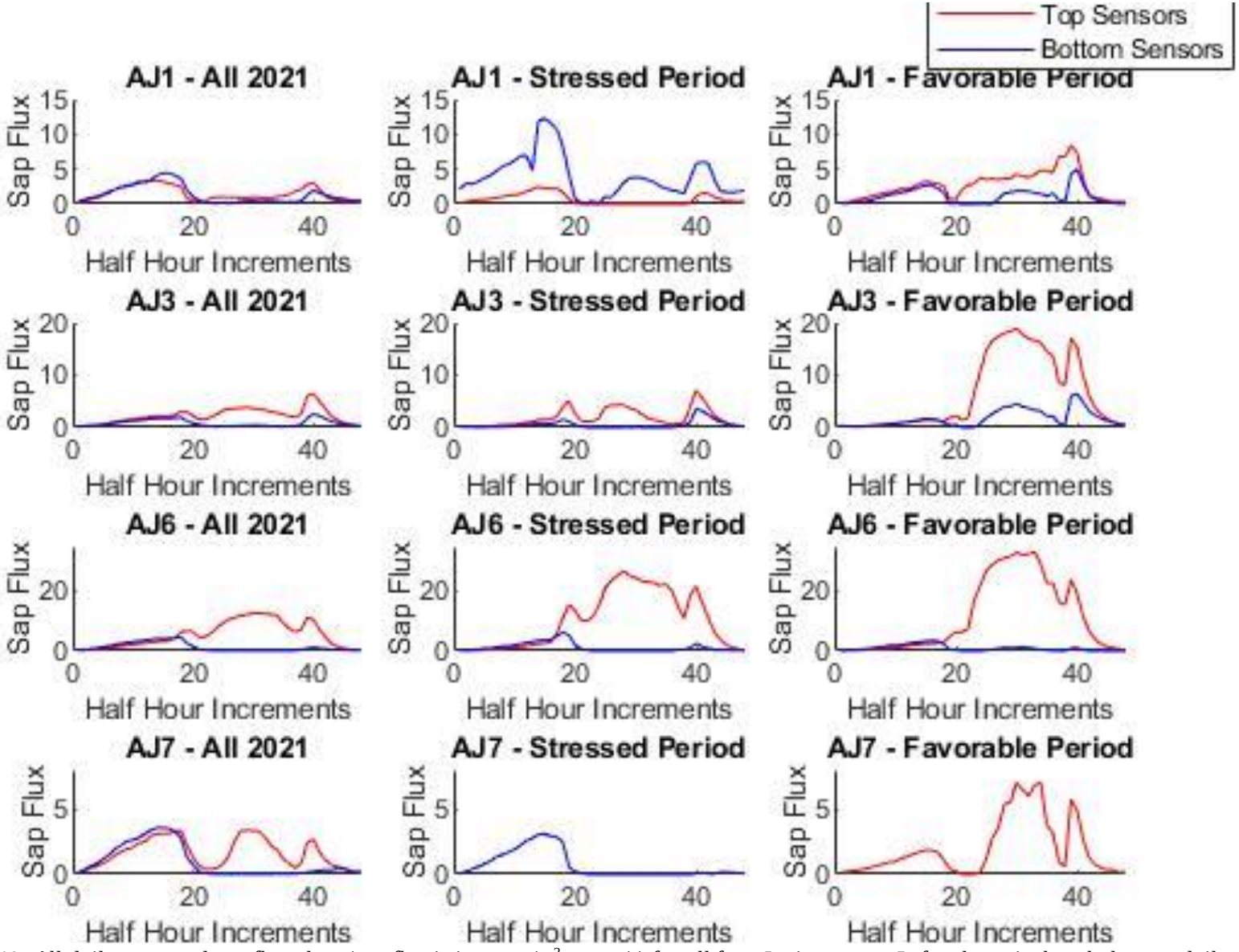

Figure 19: *All daily averaged sap flux plots (sap flux is in $g_{water}/m^2_{sapwood}/s$) for all four Juniper trees. Left column is the whole year daily averaged, middle column is the stressed period daily averaged, and right column is the favorable period daily averaged.*

3.2.3 Yearly Sap Flux Results — Lacey Oak

We instrumented 4 lacey oak trees (Oak 1, 4, 5, and 6) with both top and bottom sap flux sensors (**Figure 20**).

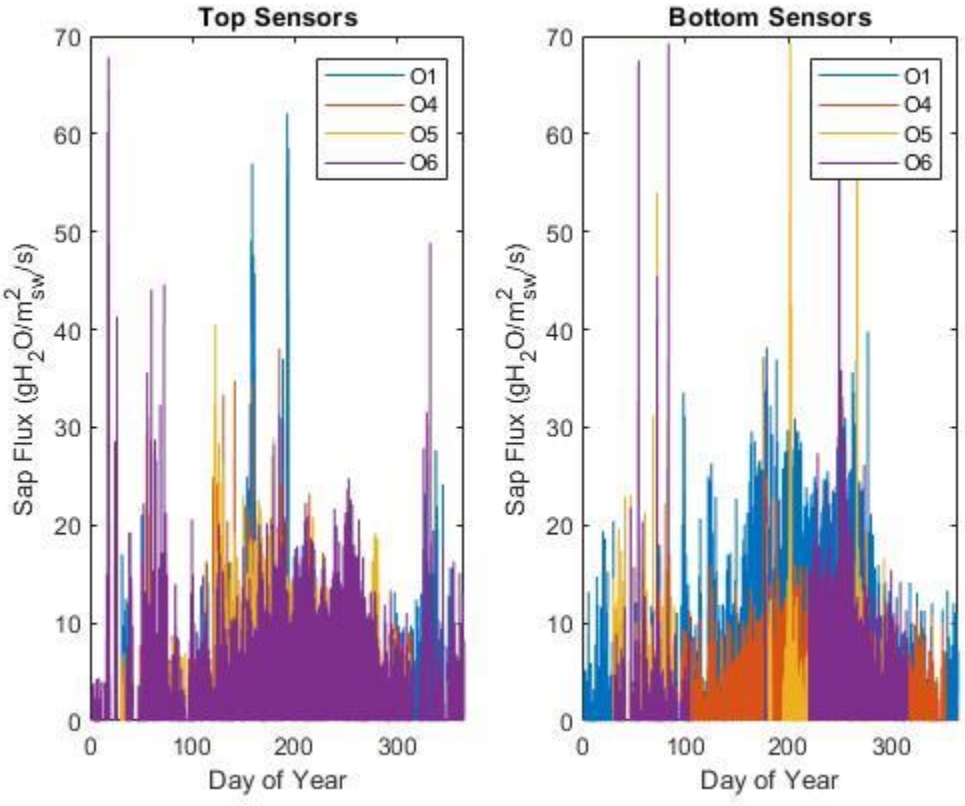

Figure 20: *All Lacey Oak sap flux data for top and bottom sensors in 2021*

Over the course of 2021, the magnitudes of sap flux observed in the bottom and tops of the oak trees were more similar to one another than the top and bottom sensors in the junipers (**Figure 15).** Oak trees showed a similar average daily pattern of sap flux featuring the 'abnormal' characteristics of spikes early and late in the day (**Figure 21**).

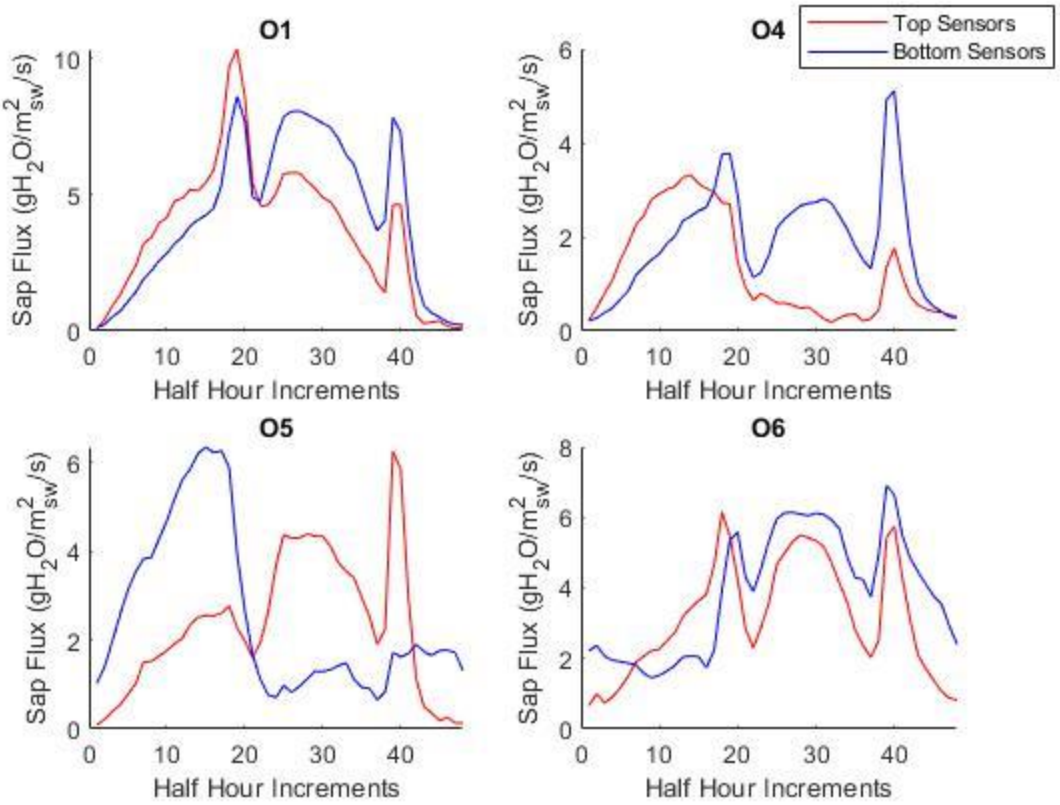

Figure 21: *Daily averaged sap flow patterns for both top and bottom sensors for all Oaks. These show average daily patterns for sap flux across the 2021 growing season. The x axis represents a full day in half hour increments, with zero being midnight.*

While the oaks all show significant sap flow during midday, the maximum flow rates still occur near dawn and/or dusk. Notice that oak 5's bottom sensor produces a pattern of sap flux that is very similar to AJ7's bottom sensor (**Figure 16**), where maximum sap flow values occur around dawn and remain more or less steady throughout the remainder of the day. However, the same sensor is less predictable for the rest of the average day than that in AJ7, signaling more variability in this sensor than the others over the course of 2021. Lastly, O1 and O6 both report the same pattern for their top and bottom sensors, similar to what was observed in AJ1 and AJ3 (**Figure 16**).

3.2.4 Stressed Period vs Favorable Period Sap Flux Results — Lacey Oak

The dates of the stressed and favorable periods were kept constant for a uniform analysis across all tree species. Figures here will be displayed in the same order as they were for ashe junipers: daily averages over the stressed period (**Figure 22**), daily averages over the favorable period (**Figure 23**), and finally both periods' plots and the whole year plots side-by-side to facilitate comparison (**Figure 24**).

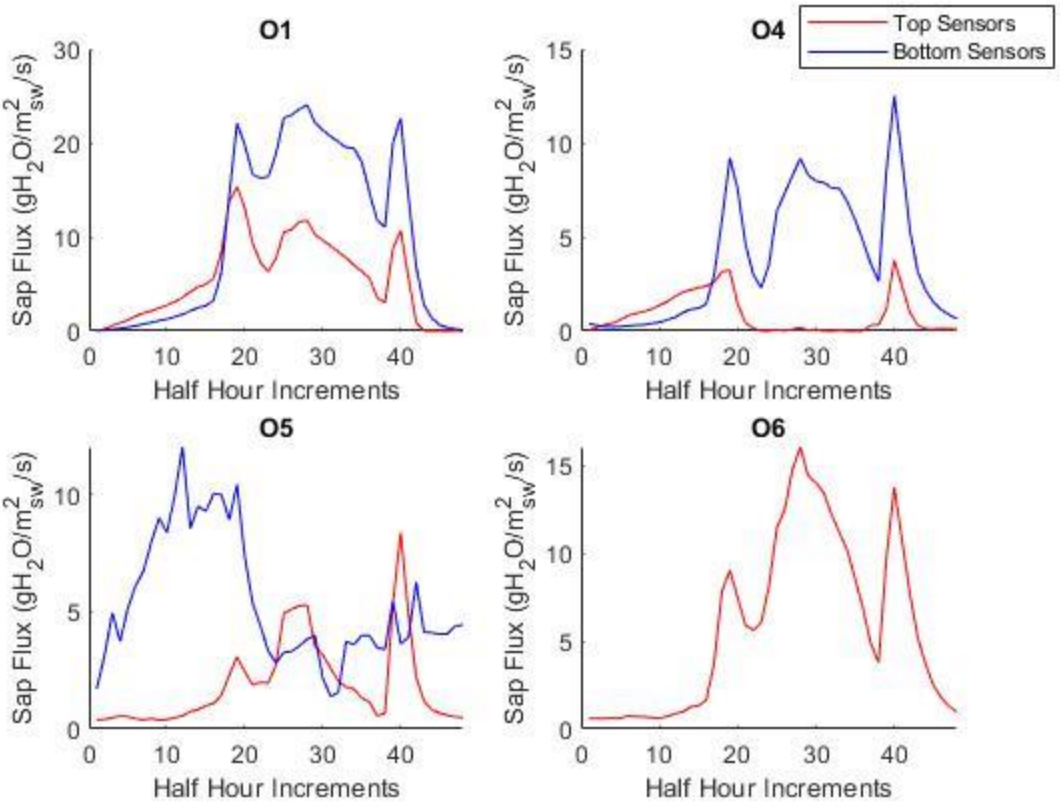

Figure 22: *Daily averaged sap flow patterns for all Oaks during the stressful period (DOY 200-212). These show average daily patterns for sap flux across the 2021 growing season. The x axis represents a full day in half hour increments, with zero being midnight.*

While O1 produced the same curve for both top and bottom sensors, the magnitude of diurnal sap flux increased substantially (225% in O6's case) between the stressful and favorable periods (**Figure 22** and **Figure 23**). Notice how the sap flow pattern during the

stressful period has dawn sap flow spikes occurring just shy of 10:00 am and dusk spikes at 8:00 pm (**Figure 22**), whereas the favorable period produces a smoother, more upside-down parabola like pattern with maximum sap flow around 3:00 pm (**Figure 23**).

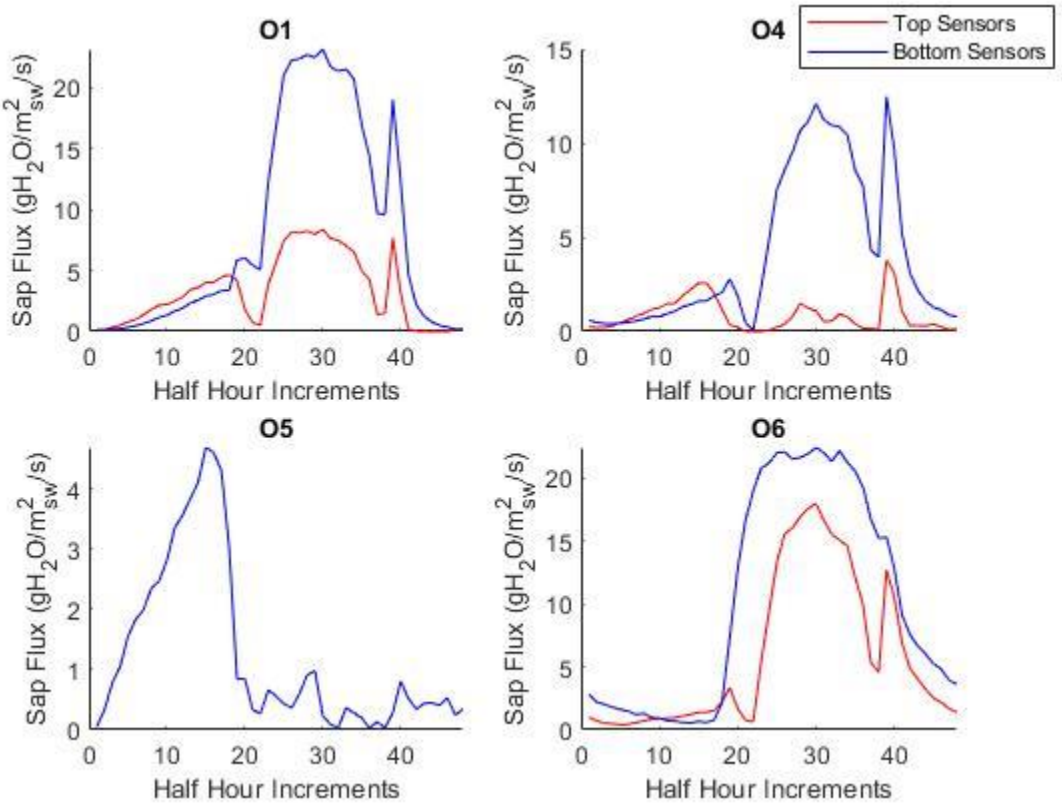

Figure 23: *Daily averaged sap flow plots for all oaks during the favorable period (DOY 250-260). These show average daily patterns for sap flux across the 2021 growing season. The x axis represents a full day in half hour increments, with zero being midnight.*

With the exception of O5 (which experienced a top sensor malfunction), it's clear to see that sap flow has shifted to occur mostly during midday in the favorable period. There are practically no morning sap flow spikes, but there are still evening sap flow spikes, just as there were in junipers (**Figure 18**). Below is **Figure 24**, where all three daily average plots are side-by-side for comparison of magnitude and shape. As we saw with junipers (**Figure 19**), the largest flow magnitudes and more-typical diurnal patterns are found in **Figure 24**.

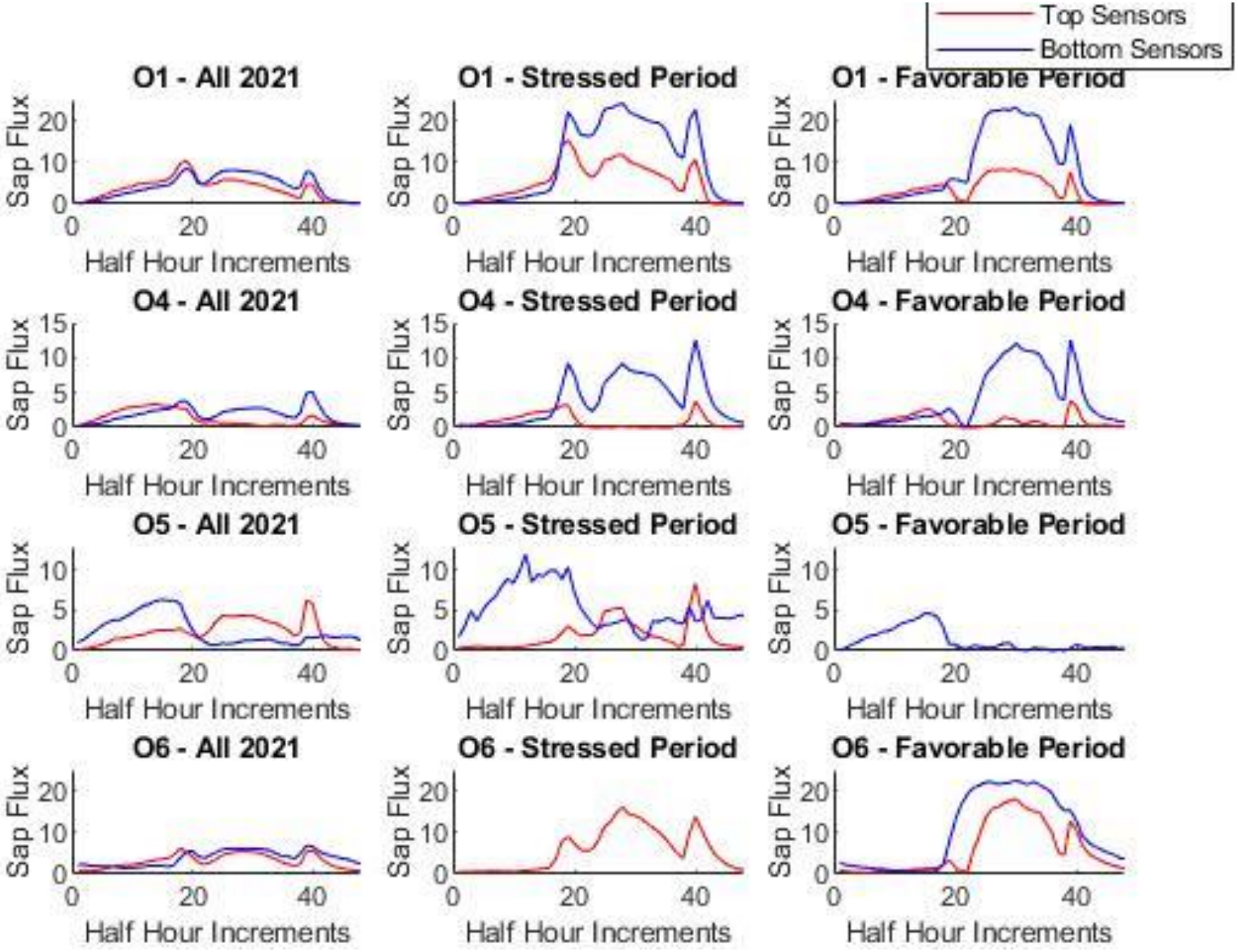

Figure 24: *All daily averaged sap flux plots (sap flux is in $g_{water}/m^2_{sapwood}/s$) for all four Oak trees. Left column is the whole year daily averaged, middle column is the stressed period daily averaged, and right column is the favorable period daily averaged.*

3.2.5 Yearly Sap Flux Results — Pinyon Pine

We instrumented four pinyon pines (P2, P4, P6 and P7) with top and bottom sap flux sensors in the same manner as the junipers and oaks. As before, yearly sap flux for all Pinyon Pine top and bottom sensors for can be seen in **Figure 25**.

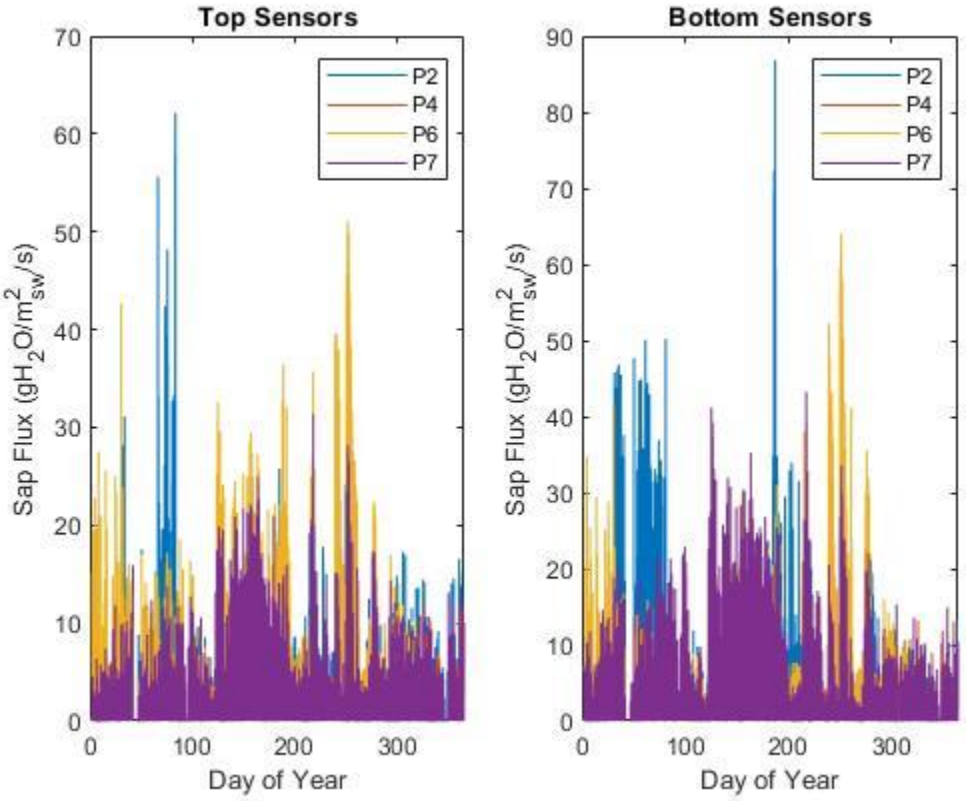

Figure 25: *All Pinyon Pine sap flux data for top and bottom sensors in 2021*

Sap flow magnitude for the entire year appear mostly equivalent between top and bottom sensors (except for a few spikes in P2), similarly to what was observed in the lacey oaks. In **Figure 26** below, the sap flux abnormality is still readily apparent for P4 and P7 and is present for P6. P2 is the only pine that has daily average sap flux over the whole year that follow typically observed patterns (i.e., inverted parabolas), with sap flux peaks in the midafternoon (2:00 pm) featuring only a slight decline during midday. The top sensor for

P2 produces a similar pattern to the bottom sensors of AJ7 (**Figure 16**) and O5 (**Figure 21**), where the maximum sap flow occurs near dawn and decreases for the rest of the day.

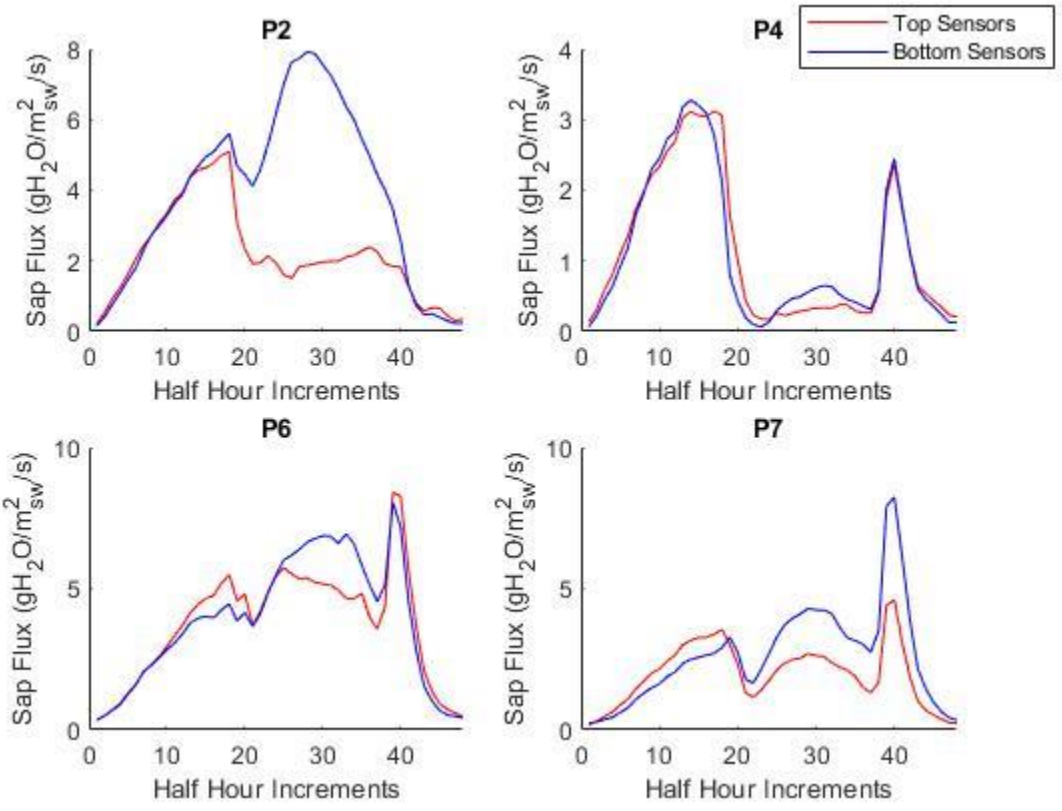

Figure 26: *Daily averages of all pinyon pine sensors. These show average daily patterns for sap flux across the 2021 growing season. The x axis represents a full day in half hour increments, with zero being midnight.*

3.2.6 Stressed Period vs Favorable Period Sap Flux Results — Pinyon Pine

The daily average plots for Pinyon Pines during the stressed period are below in **Figure 27**. Daily averages for the favorable period can be found after that in **Figure 28**, and daily

averages for all three time periods (stressful period, favorable period and the entire year) can be found at the end of this section in **Figure 29**.

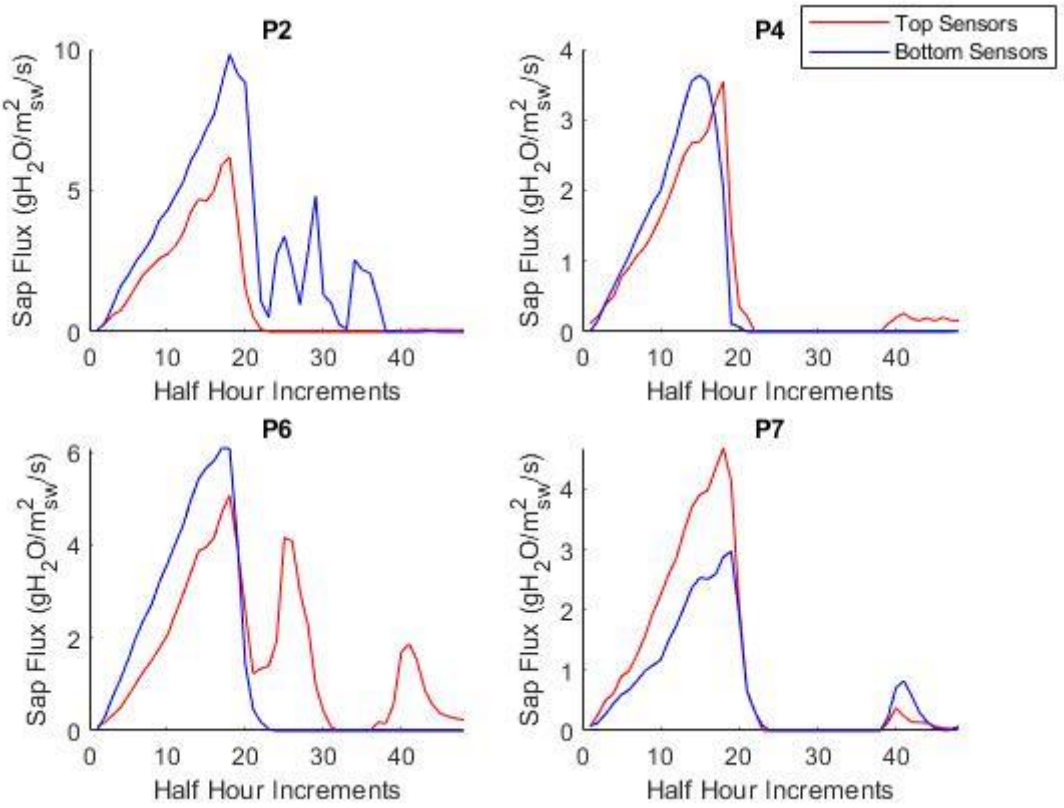

Figure 27: *Daily averaged sap flow patterns for all pines during the stressful period (DOY 200-212). These show average daily patterns for sap flux across the 2021 growing season. The x axis represents a full day in half hour increments, with zero being midnight.*

Sap flow in the pines shifted its maxima to early morning hours when environmental conditions are stressful (**Figure 27**). In fact, P4 and P7 almost have no sap flow activity during the day. P2's bottom sensor shows substantial variability after the morning hours, while P6's top sensor recorded the only midday increase in sap flux. Overall, nearly all sap flow occurs in the morning during the stressful period. Daily averages for the favorable period can be seen below in **Figure 28**.

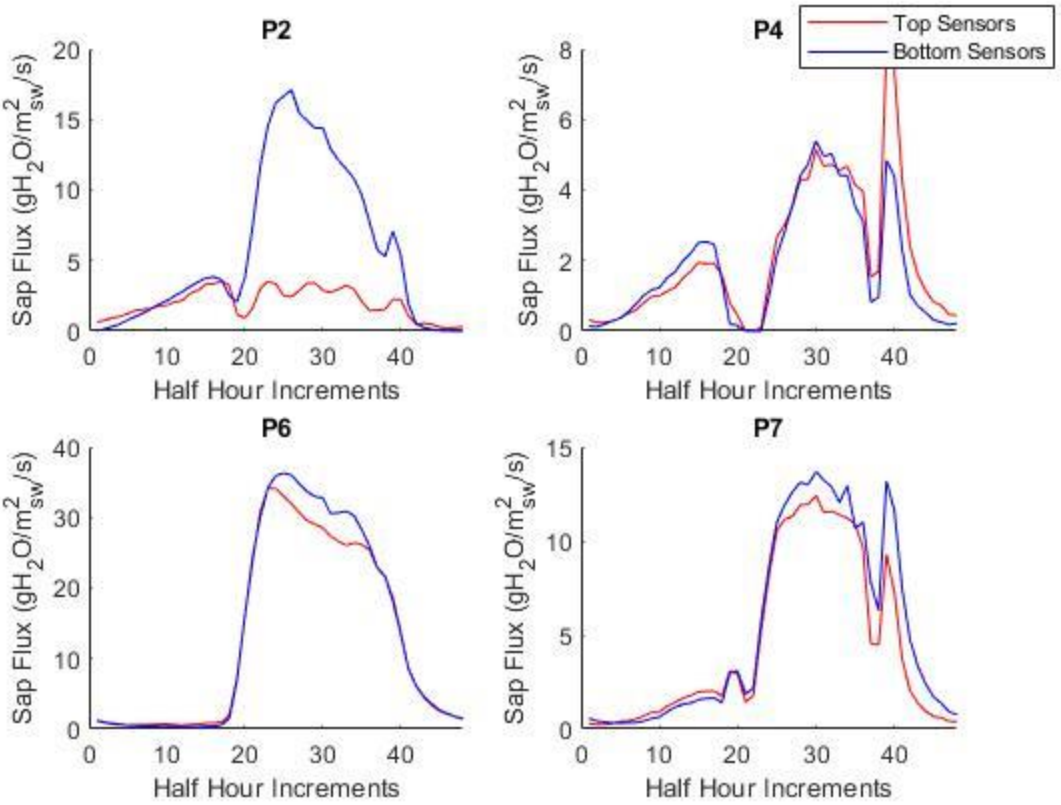

Figure 28: *Daily averaged sap flow patterns for all pines during the favorable period (DOY 250-260). These show average daily patterns for sap flux across the 2021 growing season. The x axis represents a full day in half hour increments, with zero being midnight.*

The pines generally produced typical sap flux patterns (i.e., inverted parabolas) when environmental conditions were favorable. Both sensors for P6 have the typical upside-down parabola shapes, with the bottom sensor of P2 recording something similar. P7 and P4 exhibit similar behavior, but P4 still has both a morning and evening spike, where P7 just has an evening sap flow spike. As seen with junipers (**Figure 19**) and oaks (**Figure 24**), daily averages from all three periods show that sap flow magnitudes are higher and diurnal patterns are more typical during the favorable period (**Figure 29**).

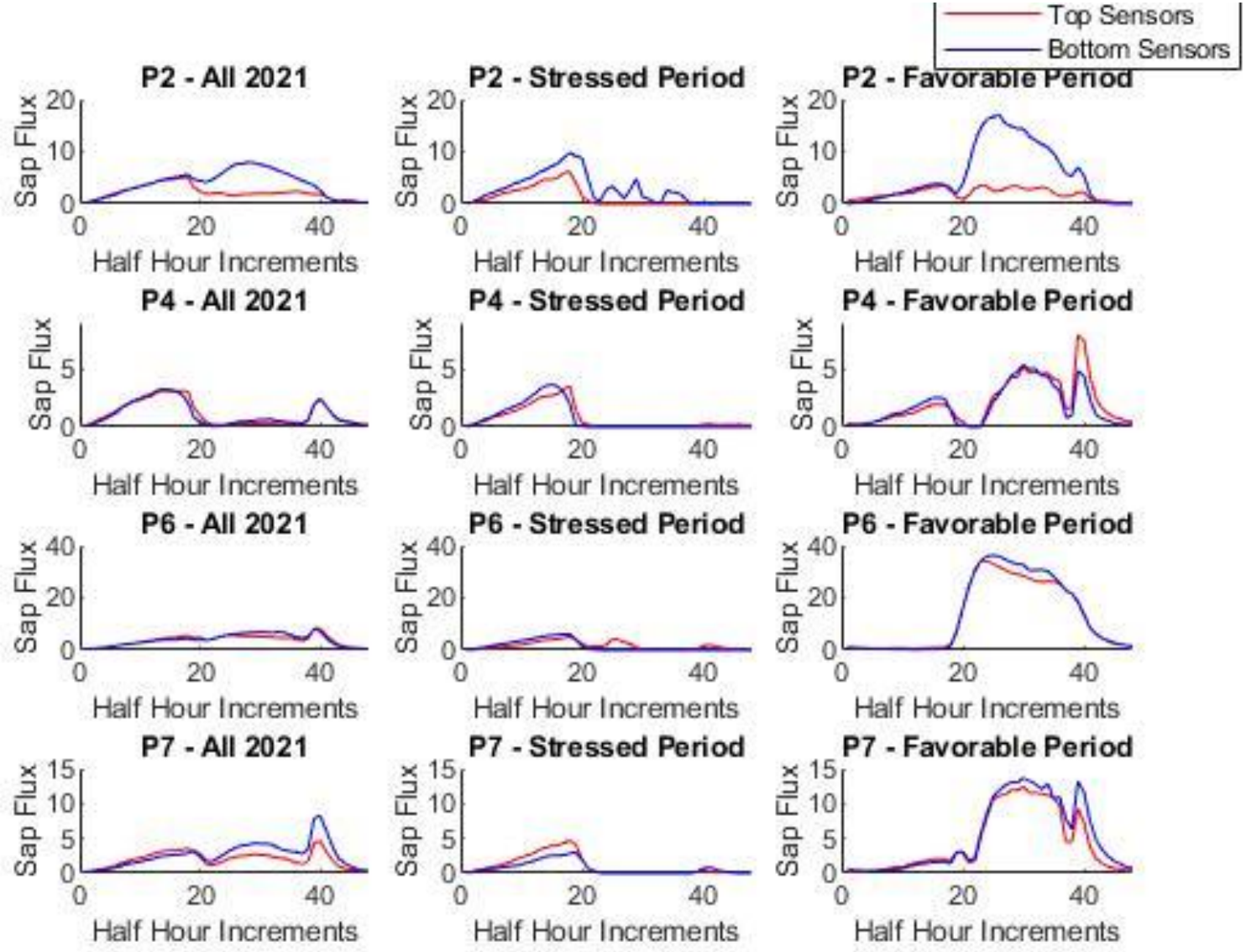

Figure 29: *All daily averaged sap flux plots (sap flux is in gwater/m2sapwood/s) for all four pine trees. Left column is the whole year daily averaged, middle column is the stressed period daily averaged, and right column is the favorable period daily averaged.*

3.3 LEAF WATER POTENTIAL RESULTS

Leaf water potential measurements were taken consistently from three trees (one per species): AJ1, O6, and P7. LWP was assessed in comparison to many data types (sap flow, SWP, VPD, etc.); for organization purposes, results will be broken up by individual trees, starting with ashe juniper and ending in pinyon pine. Furthermore, each tree's LWP results will be split into two sections: LWP in response to sap flux and LWP in response to meteorological conditions. The former covers LWP comparison as sap flow changes over the course of all six field site visits, referred to as Trips 1 through 6. However, for Trips 5 and 6, sap flow data was gap. The latter section compares LWP to different meteorological conditions. The first analysis to be made is to observe the relationship between predawn leaf water potential measurements and predawn soil water potential. In theory, these variables should match, as the plant will equilibrate to soil water potential values (Donovan et al., 1999). The results can be found below in **Figure 30**.

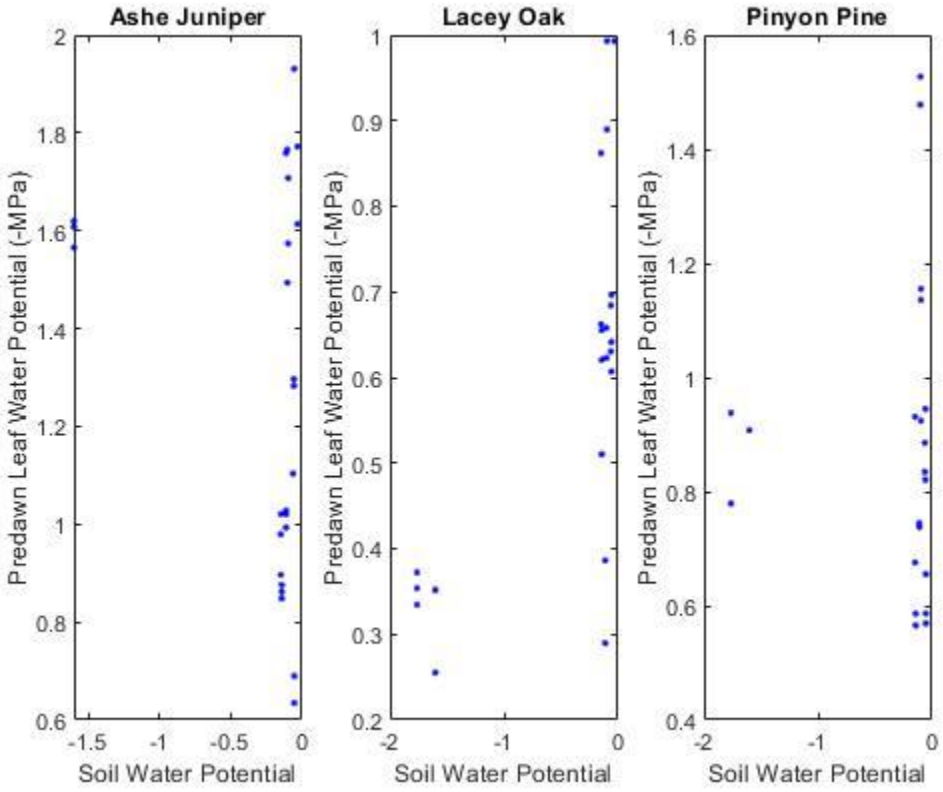

Figure 30: *Predawn LWP values for each species with corresponding SWP values (m^3_{water}/m^3_{soil}).*

As seen above, SWP values are generally near zero (less negative) right before dawn. However, LWP measurements for each species have a large range of values, with ashe juniper having the most negative (indicating increased water-stress) range of values, followed by pinyon pine, and then lacey oak. This indicates that SWP and LWP are not in equilibrium right before dawn for any of the three species. There are two possible explanations for this. First, the trees could be getting moisture from a different source, such as water stored in the bedrock or water found in karst features like conduits and perched water tables (Palmer, Arthur, 1991; Rempe & Dietrich, 2018). Second, this could

be caused by the trees transpiring at night, so they are never able to reach hydrostatic equilibrium with the soil (Donovan et al., 1999).

3.3.1 LWP Results — Ashe Juniper 1 (AJ1)

AJ1 is the ashe juniper in which all juniper LWP measurements were taken. Every LWP measurement taken in 2021 for AJ1 can be seen below in **Figure 31**. This includes measurements from predawn, afternoon, and dusk measurements, as well as nighttime measurements in some cases.

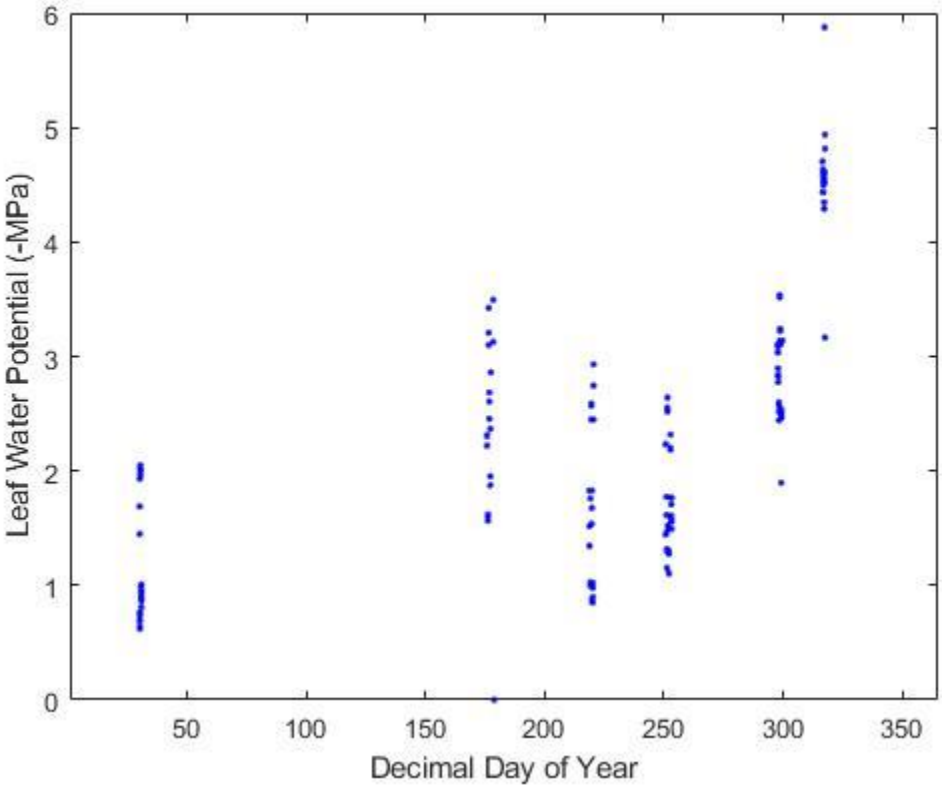

Figure 31: *All LWP measurements taken from AJ1 in 2021.*

The six field site Trips for 2021 can be seen above. Juniper leaf water potentials were highly variable across days and across the season ranging from -0.62 MPa to -5.87 MPa, with more negative variables meaning higher water-stress (**Figure 31**). In the next section, LWP and sap flow are compared for each Trip.

3.3.1a LWP in Response to Sap Flux — Ashe Juniper 1 (AJ1)

Trip 1 occurred from DOY 29 to DOY 32. LWP and sap flow over this period can be seen below in **Figure 32**.

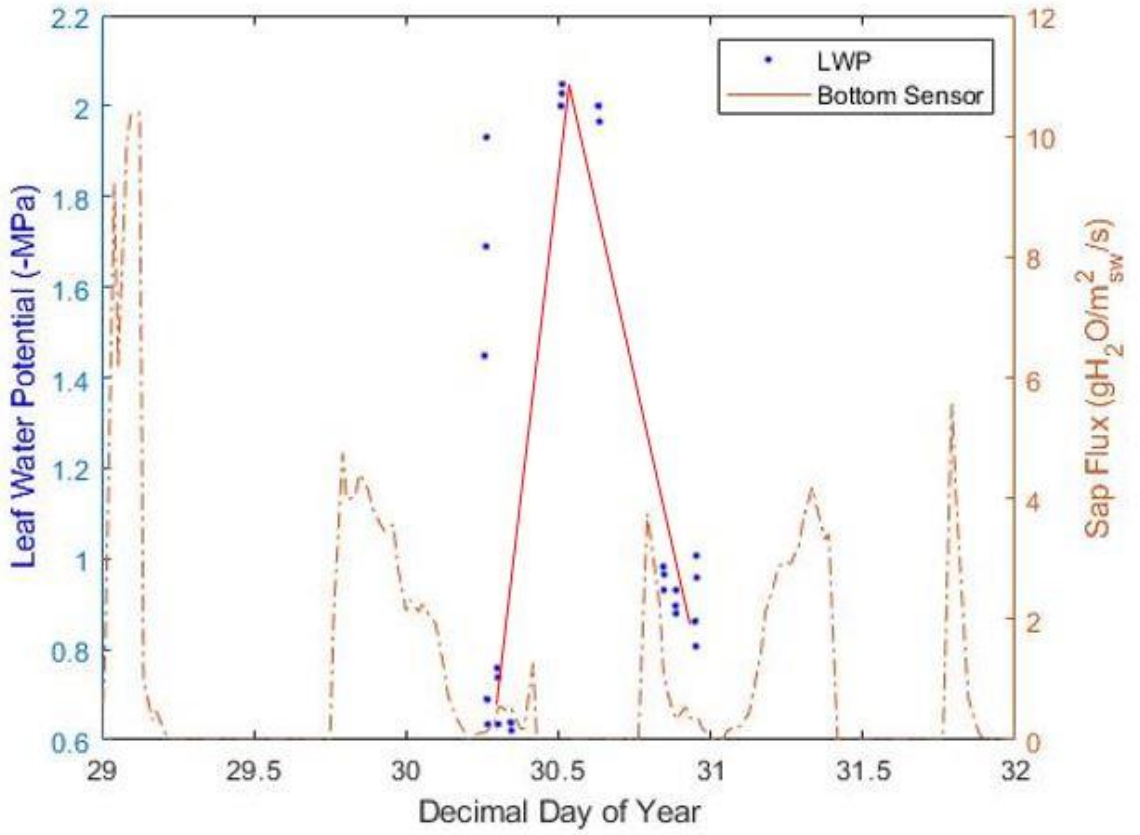

Figure 32: *LWP and sap flow for AJ1 during Trip 1 (DOY 29-DOY 32). Whole numbers on the x-axis are midnight. Numbers with half decimals (i.e, 31.5) represent noon of that day. LWP trend is in red.*

There is no sap flow data from the top sensor during this period, as it had malfunctioned and was not replaced until the end of the Trip. LWP measurements began in the morning of DOY 30 and were repeated into the night of DOY 30 before the nitrogen tanks were depleted. In **Figure 32**, sap flux shows the opposite of the typical diurnal pattern that we would expect (resembling an inverse parabola). Instead, here sap flux occurs only in the late evening, night, and early morning for DOY 29-31. LWP measurements early in DOY 30 (right as sap flow is ending) are the lowest, signaling that AJ1 is not water-stressed. Then just after noon in the heat of the day, LWP is highest (above -2 MPa), meaning AJ1 is the most water-stressed at this time. LWP is again less negative a few hours before midnight, just as sap flow is starting again. It is important to note that Trip 1 occurred prior to the start of the growing season, which may be responsible for the unusual pattern of sap flow at this time.

Trip 2 was from DOY 175 to DOY 179; LWP and sap flow during this Trip are found in **Figure 33**.

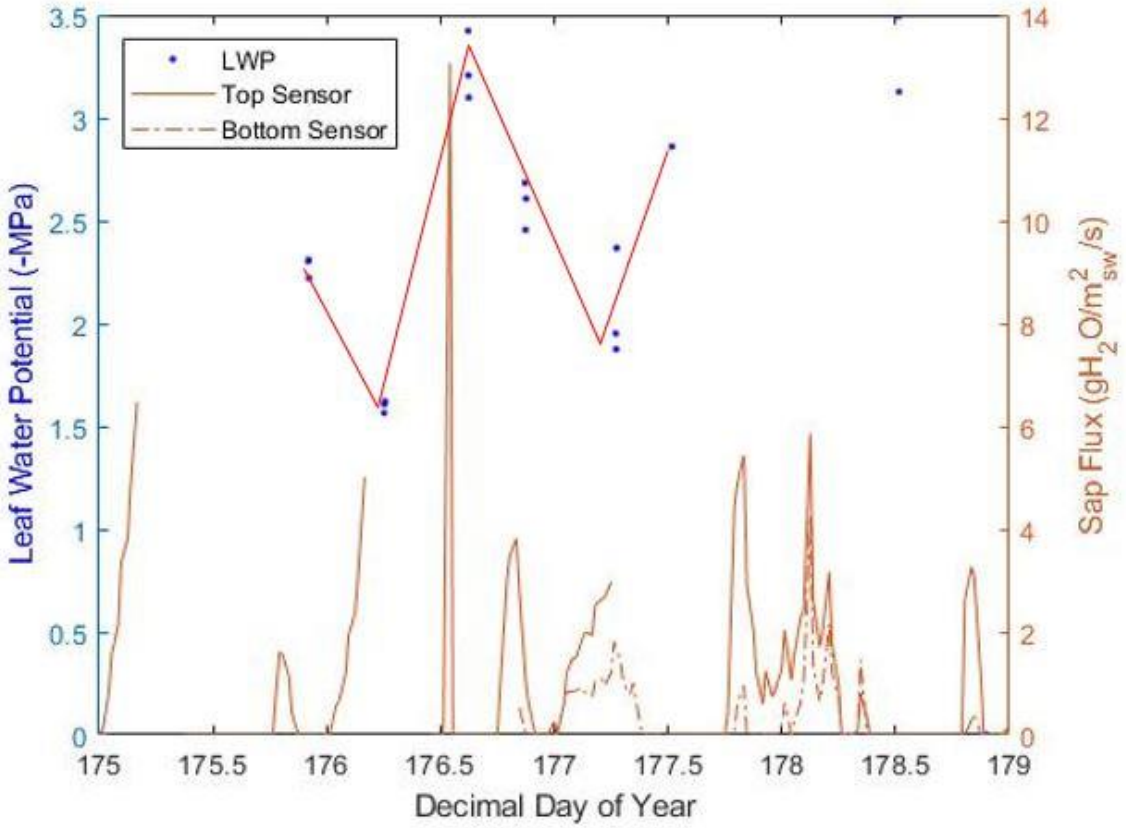

Figure 33: *LWP and sap flow for AJ1 during Trip 2 (DOY 175-DOY 179). Whole numbers on the x-axis are midnight. Numbers with half decimals (i.e, 176.5) represent noon of that day. LWP trend is in red.*

AJ1's bottom sensor was malfunctioned for Trip 2 until it was replaced late DOY 176. As with Trip 1 (**Figure 32**), LWP is most negative during the afternoon between 1:00 and 2:00 pm, signaling that this is when AJ1 is most water-stressed. LWP is the least negative at night and early morning still. While sap flux data is very unpredictable, there is little to no sap flow data being recorded during the middle of the day when LWP is most negative.

Sap flow and LWP for Trip 3 are found in **Figure 34** below.

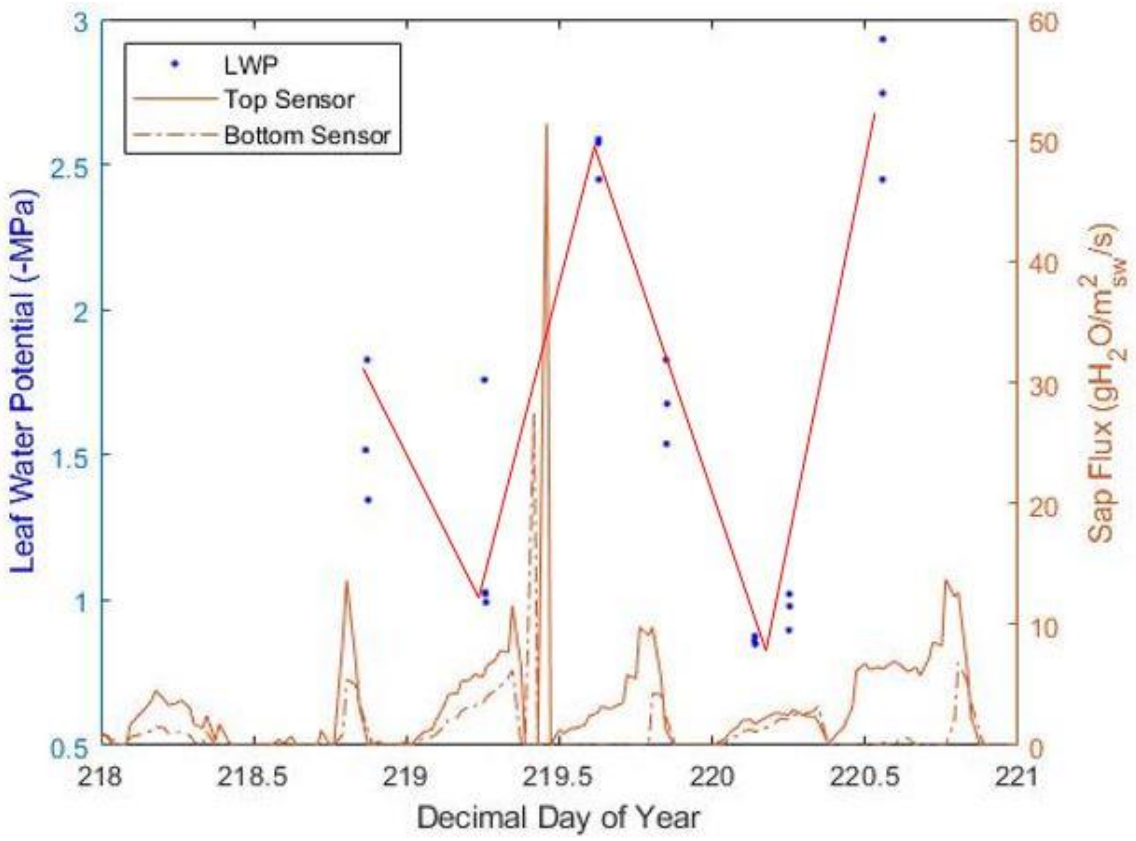

Figure 34: *LWP and sap flow for AJ1 during Trip 3 (DOY 218-DOY 221). Whole numbers on the x-axis are midnight. Numbers with half decimals (ie, 219.5) represent noon of that day. LWP trend is in red.*

Sap flow for Trip 3 differs from the first two Trips, as days 219 and 220 show sap flux start to increase after midnight, decrease in the late morning, picking back up again for the evening before ending for the night. LWP is least negative in the early mornings, just as sap flow is starting to increase. As indicated by the more negative LWP values, AJ1 is most water-stressed in the afternoon, before LWP decreases throughout the night and early morning.

LWP and sap flow values for Trip 4 are found in **Figure 35**.

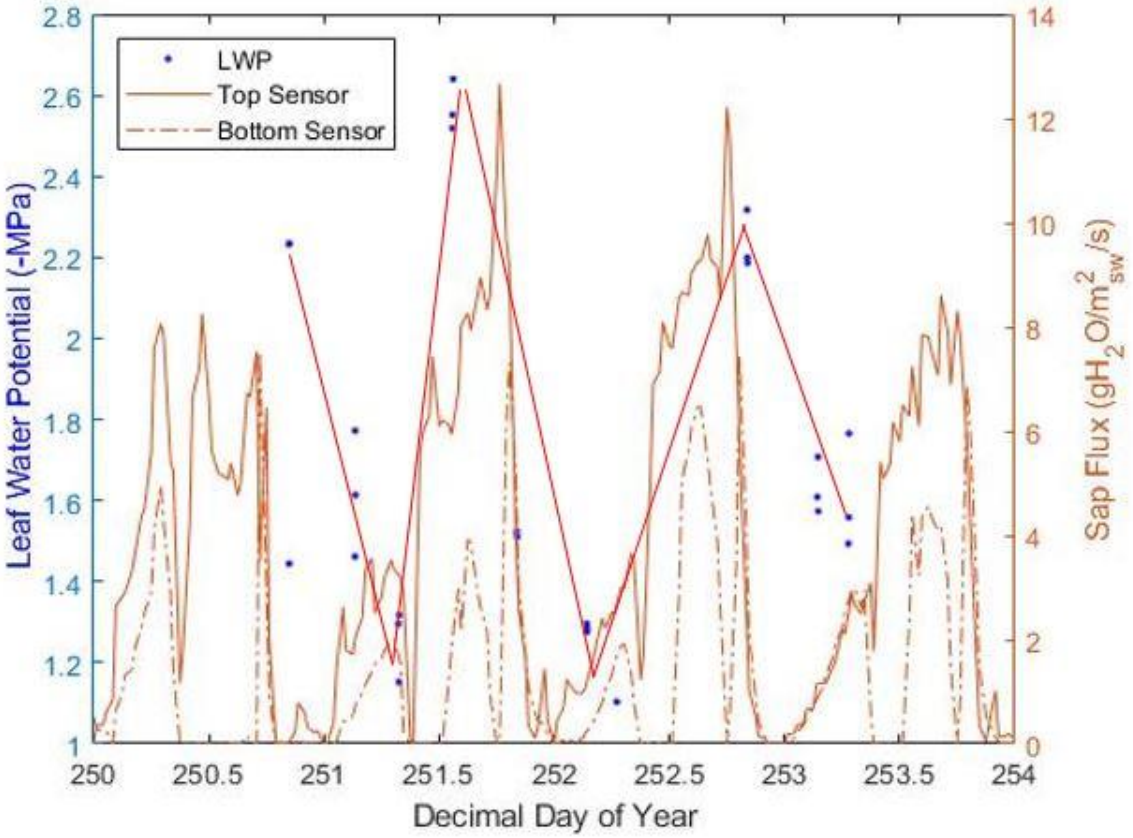

Figure 35: *LWP and sap flow for AJ1 during Trip 4 (DOY 250-DOY 254). Whole numbers on the x-axis are midnight. Numbers with half decimals (ie, 251.5) represent noon of that day. LWP trend is in red.*

Out of all the Trips for AJ1, Trip 4 shows the best example of what is expected for sap flow and LWP (Thomsen et al., 2013), as Trip 4 is coincides with the beginning of the study's favorable period (DOY 250-260). Notice how the diurnal sap flow cycle is much more predictable, with sap flow increasing in the morning, peaking in the afternoon, and decreasing again in the evening, creating a shape similar to an inverse parabola. LWP increases throughout the day and is the most negative (high water-stress) around 1:00 to 2:00 in the afternoon, after a full day of transpiration. LWP falls during the night and into early morning, as the plant is not stressed from the night period.

LWP for Trip 5 is below in **Figure 36**. Note that there is no sap flow shown, as sap flow data was malfunctioned over this period.

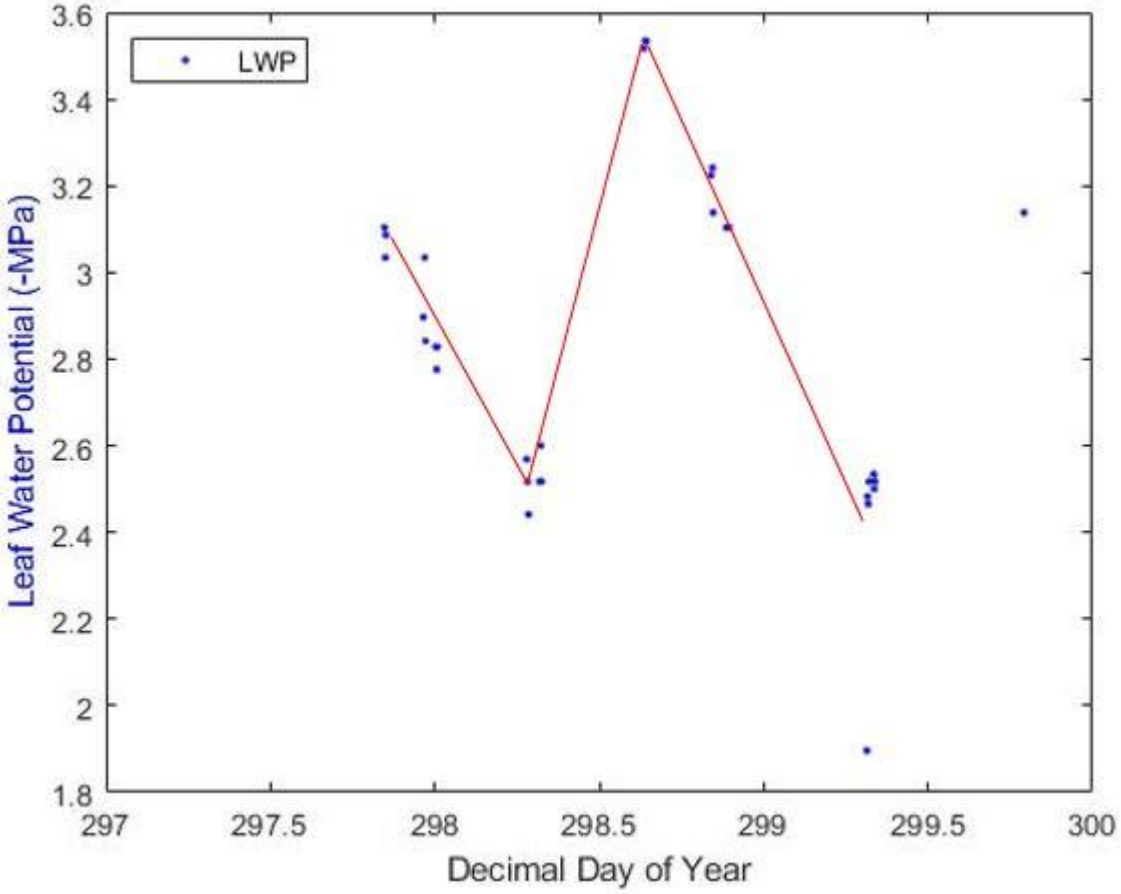

Figure 36: *LWP for AJ1 during Trip 5 (DOY 297-DOY 300). Whole numbers on the x-axis are midnight. Numbers with half decimals (ie, 298.5) represent noon of that day. LWP trend is in red.*

We can see that LWP decreases in the evening and over night before rising again in the morning. The maximum LWP is around 3:00 pm in DOY 298, showing this is when AJ1 was most water-stressed, before LWP approaches less negative values as the evening of DOY 298 progresses. LWP for Trip 6 is below in **Figure 37**.

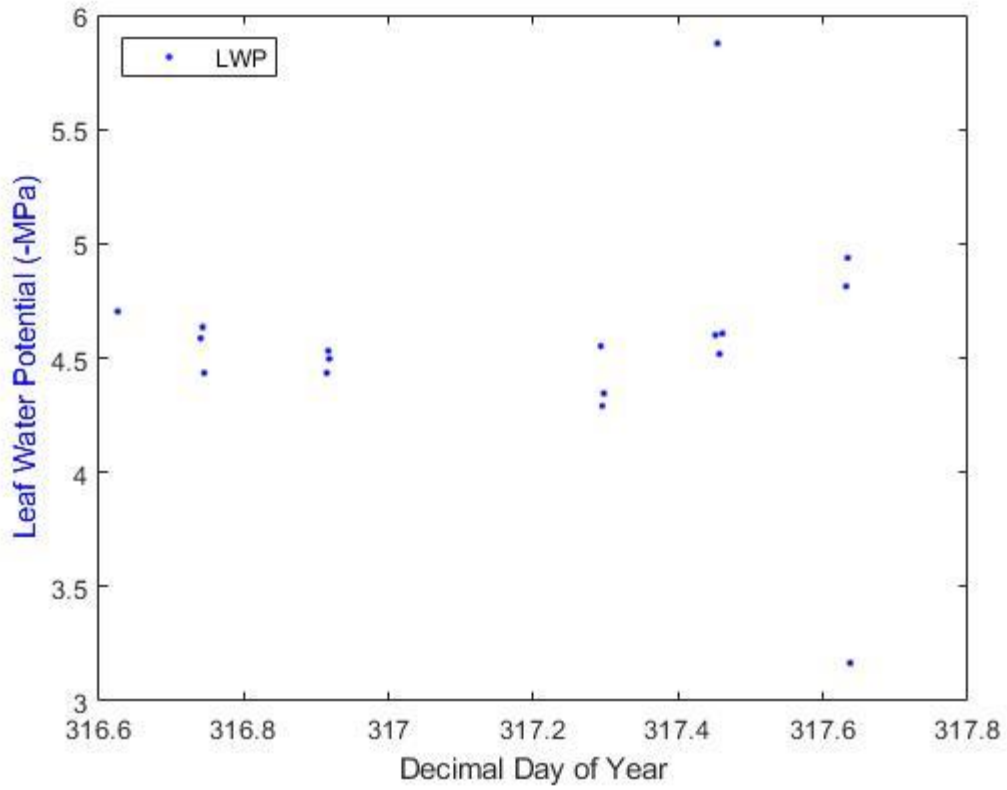

Figure 37: *LWP for AJ1 during Trip 6 (DOY 316-DOY 319). Whole numbers on the x-axis are midnight. Numbers with half decimals (ie, 317.5) represent noon of that day.*

As in Trip 5 (**Figure 36**), sap flow curves here have been gap-filled, meaning that these are only approximations of diurnal sap flow patterns. While LWP points here do not demonstrate an obvious trend as some other Trips, the most negative LWP values still

occurs just after midday (signaling water-stress), and the least negative LWP values occur at night and early morning.

3.3.1b LWP in Response to Meteorological Conditions — Ashe Juniper 1 (AJ1)

The relationship between LWP and VPD for AJ1 indicates a strong positive relationship, where LWP becomes increasingly negative as VPD increases (**Figure 38**).

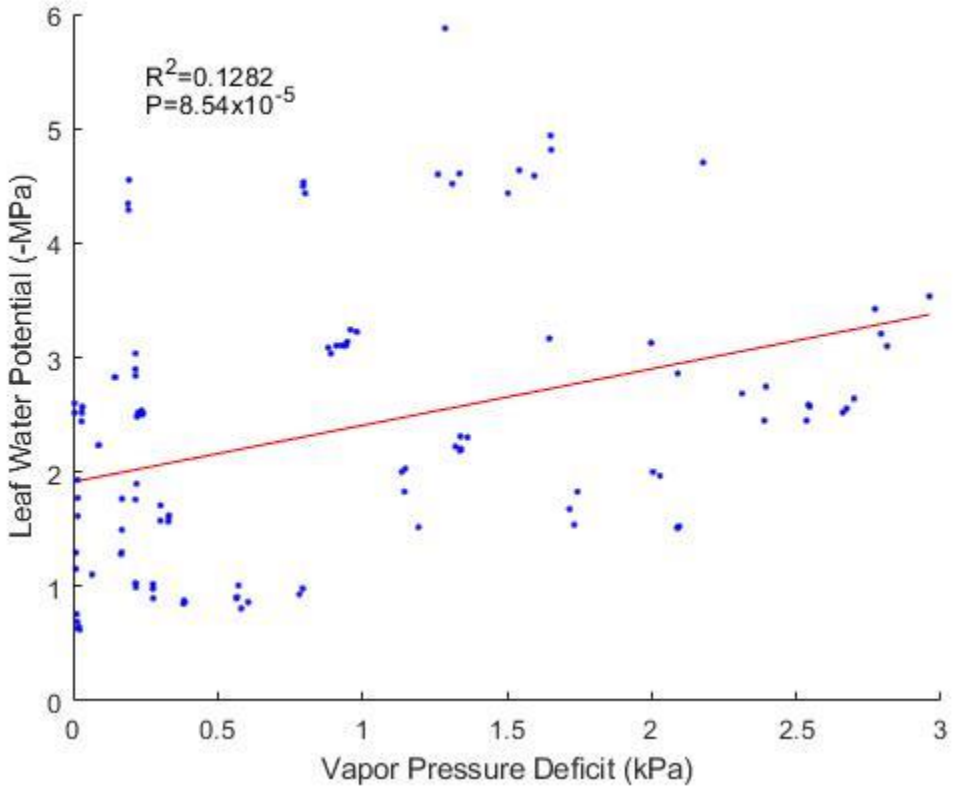

Figure 38: *LWP and VPD for all LWP measurements taken from AJ1 over the course of 2021. Best line of fit is in red, with R^2 and P value from linear regression listed.*

With such a small P value and an R^2 above .1, we have a significant but weak relationship between LWP and VPD for AJ1. Next, LWP and SWP values at the same corresponding time are plotted below (**Figure 39**).

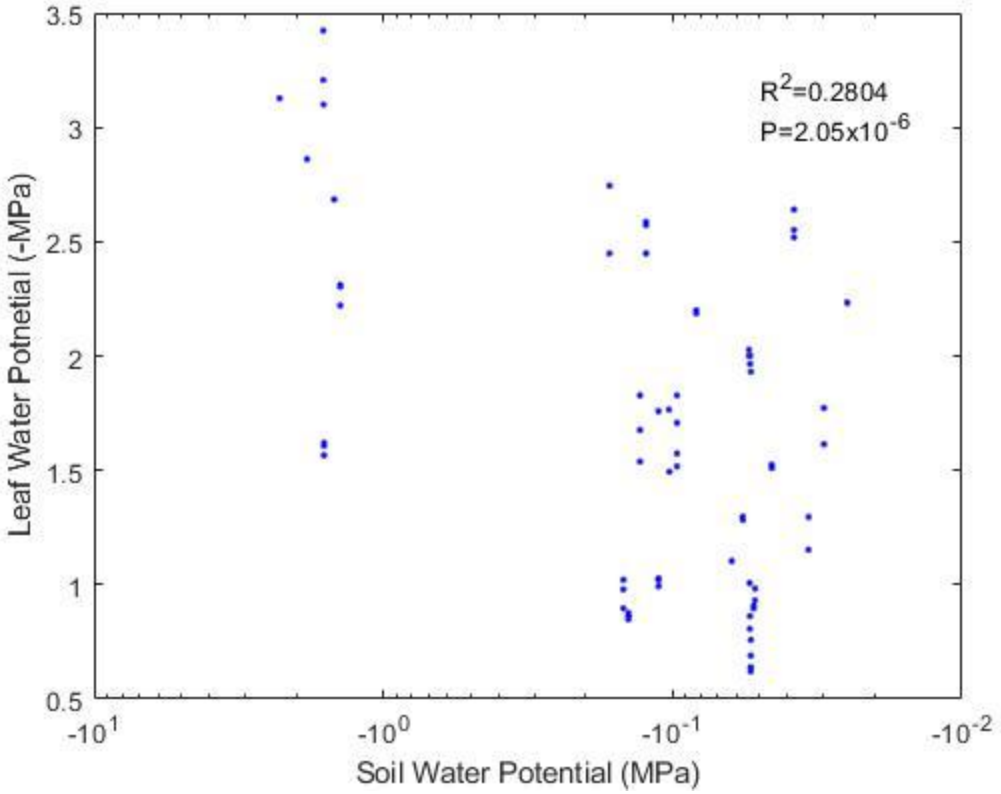

Figure 39: *LWP and SWP for AJ1 for all LWP measurements of 2021. R^2 and P values from linear regression are listed.*

As implied by the R^2 and P-value, the regression between LWP and SWP is significant and has a medium-strength correlation. This means that when SWP is less negative (farther right) LWP is likewise less negative (lower number), meaning AJ1 will be less water-stressed.

3.3.2 LWP Results — Lacey Oak 6 (O6)

Out of the four lacey oaks, O6 is the one which LWP measurements were taken from. All LWP recordings for 2021 can be found below in **Figure 40**.

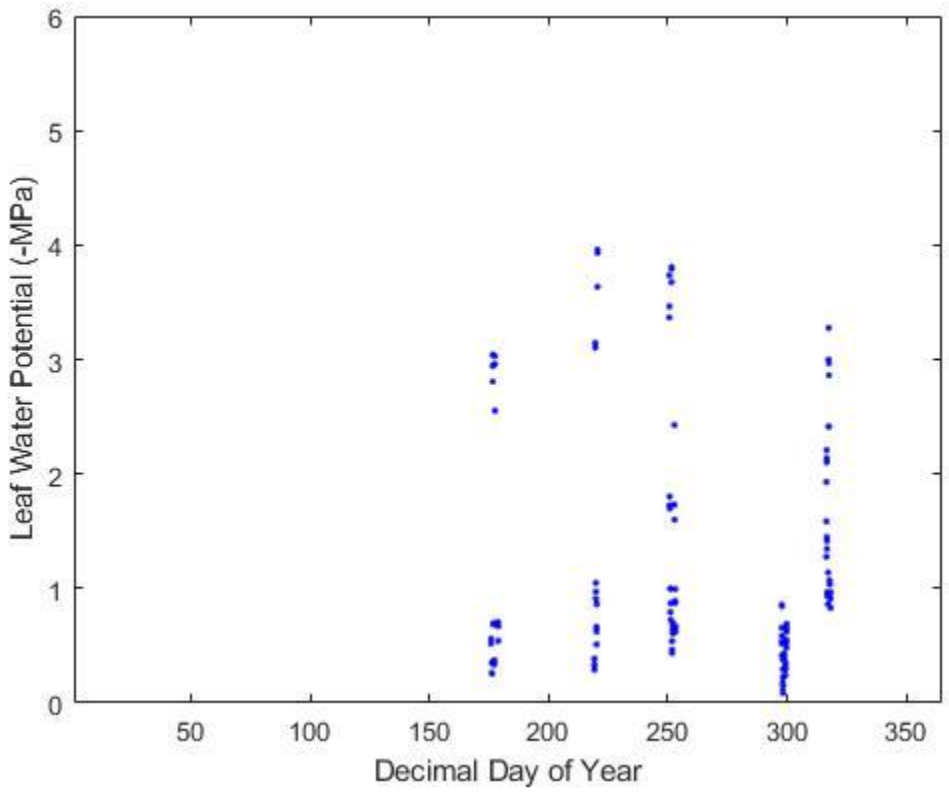

Figure 40: *All LWP measurements taken from O6 during 2021.*

Similar to juniper, oak shows a large range of LWP from -0.08 MPa to -3.96 MPa (**Figure 40**). Notice that there are only 5 Trips in which LWP measurements were recorded. This is because LWP was not recorded for the first Trip of the year (DOY 29-DOY 32), as the Trip fell outside of the growing season at a time when the cold deciduous oaks did not have foliage. Therefore, LWP data will only be reported for Trips 2-6 below. However,

sap flow data during the last Trip was completely absent due to both sensors malfunctioning, so only LWP will be presented for Trip 6.

3.3.2a LWP in Response to Sap Flux — Lacey Oak 6 (O6)

LWP and sap flow for O6 during Trip 2 can be seen below (**Figure 41**).

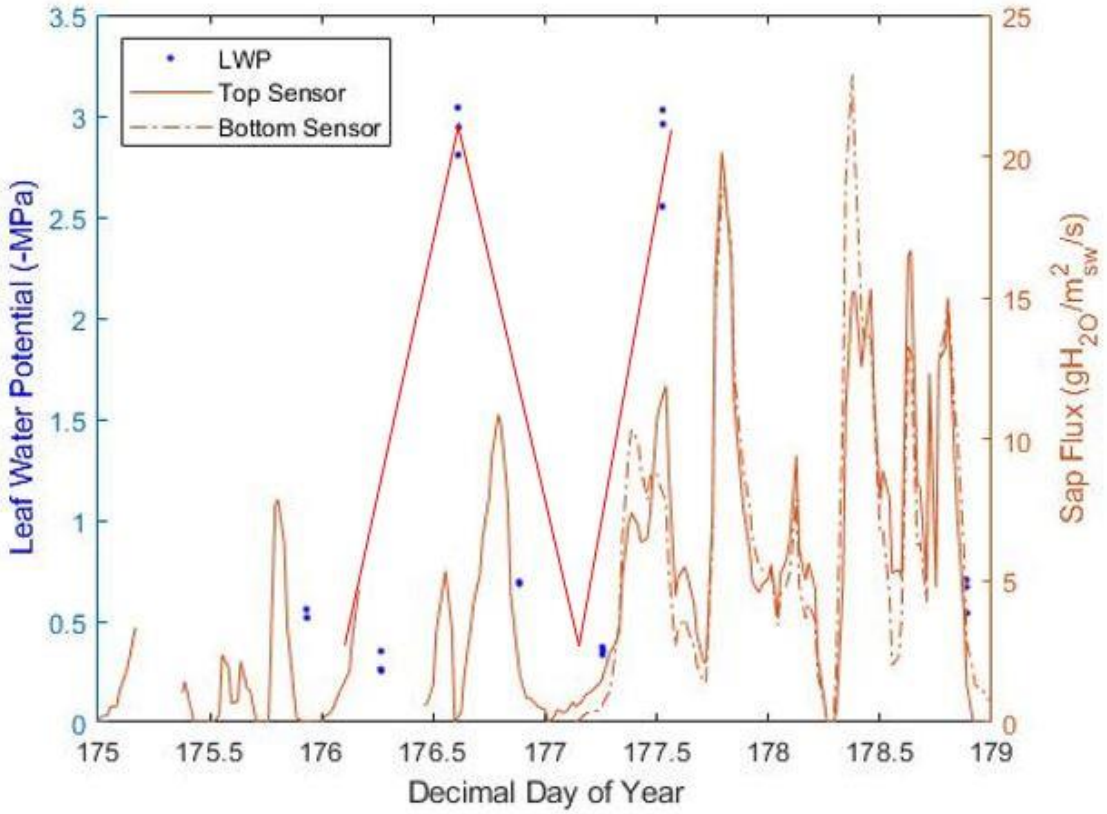

Figure 41: *LWP and sap flow for O6 during Trip 2 (DOY 175-DOY 179). Whole numbers on the x-axis are midnight. Numbers with half decimals (i.e, 176.5) represent noon of that day. LWP trend is in red.*

O6's bottom sensor malfunctioned and was not replaced until DOY 177. Sap flow during this period is highly variable, but it does show that O6 has sap flow during the afternoon.

Much like AJ1, O6 has more negative LWP values in the afternoon, and less negative values at night.

LWP and sap flow for Trip 3 can be found below in **Figure 42**.

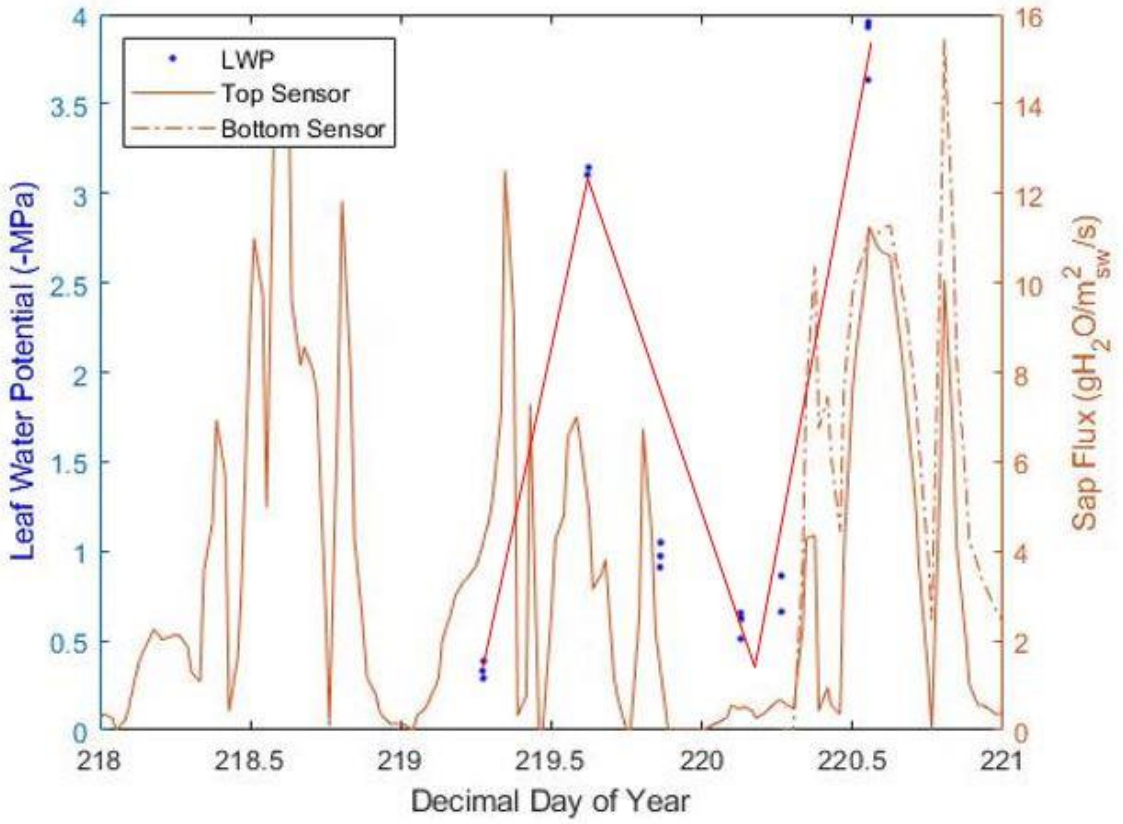

Figure 42: *LWP and sap flow for O6 during Trip 3 (DOY 218-DOY 221). Whole numbers on the x-axis are midnight. Numbers with half decimals (ie, 219.5) represent noon of that day. LWP trend is in red.*

As before, the top sensor malfunctioned and was not replaced until DOY 220. The diurnal sap flow pattern seen above is more typical, where sap flow is greatest in the afternoon, but the data has more peaks and valleys (i.e., not a smooth inverted parabola) than normal. Early in DOY 219 LWP is low, meaning O6 is well hydrated following night. After a day of transpiring, LWP is most negative (signaling water-stress) in the afternoon, before becoming less negative as the evening continues and O6 becomes less stressed.

Sap flow and LWP for Trip 4 are in **Figure 43** below.

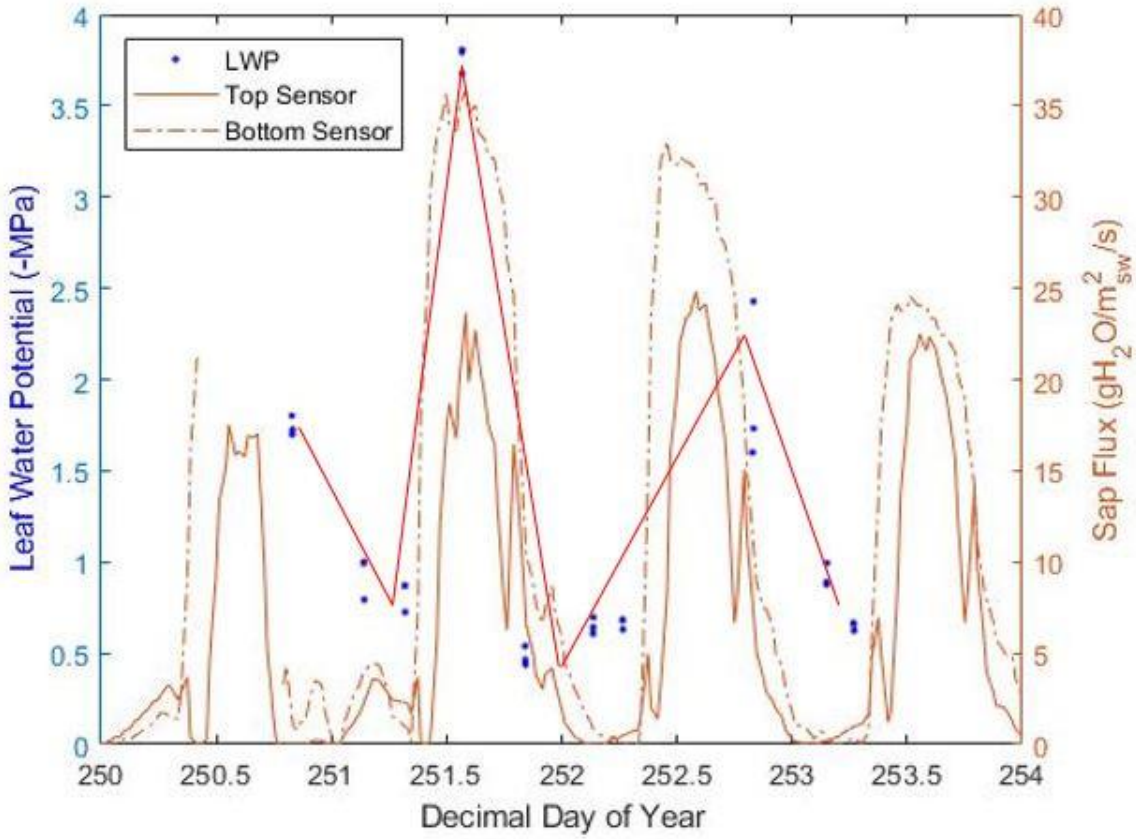

Figure 43: *LWP and sap flow for O6 during Trip 4 (DOY 250-DOY 254). Whole numbers on the x-axis are midnight. Numbers with half decimals (ie, 251.5) represent noon of that day. LWP trend is in red.*

This is arguably the best example of what sap flow and LWP are expected to look like (Thomsen et al., 2013). This is most likely because Trip 4 coincides with the beginning of the favorable study period (DOY 250-260). Sap flow data from both sensors resembles that of typical diurnal sap flow, with each day displaying smooth inverse parabolas. LWP values are less negative at night and become increasingly negative as sap flow increases, as seen in DOY 251 where the minimum (most negative) LWP coincides with maximum sap flow, when O6 is most stressed. LWP then trends less negative over the rest of DOY

251 as sap flow decreases. All of this indicates us that O6 is most water-stressed in the afternoon, after almost a full day of transpiring.

Trips 5's LWP and sap flow recordings can be seen below in **Figure 44**.

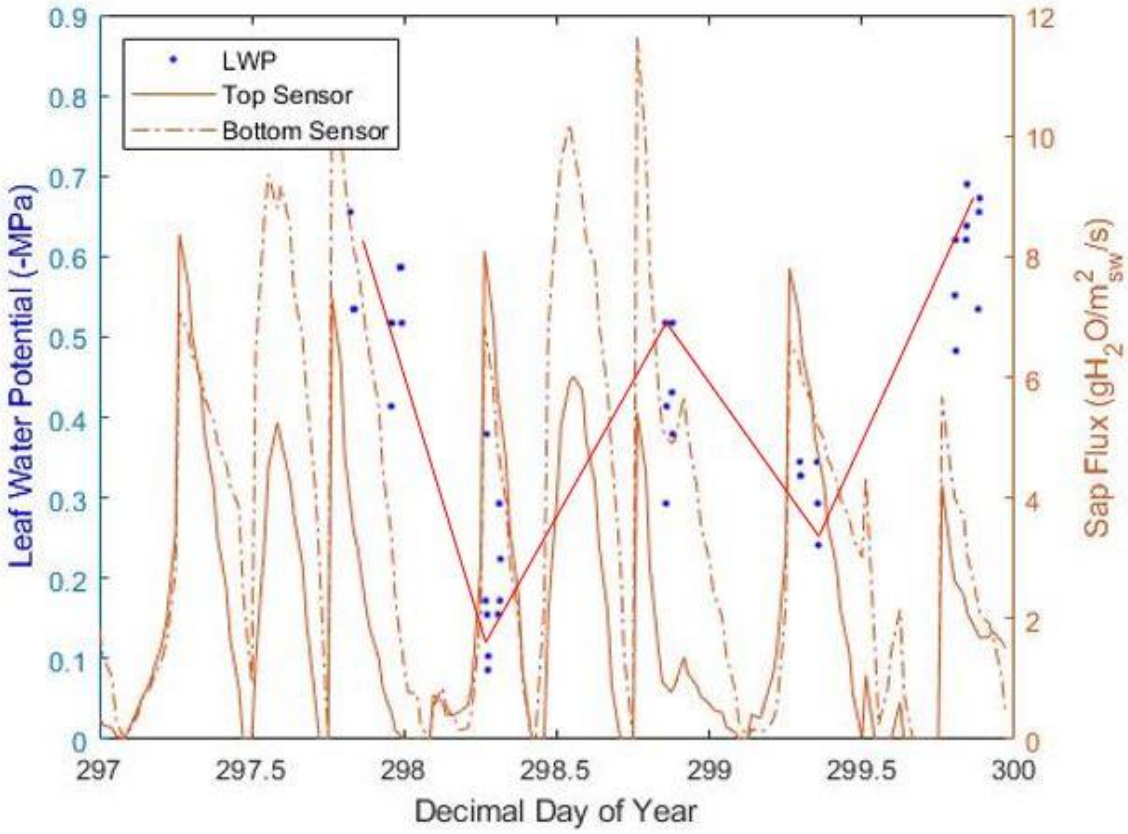

Figure 44: *LWP and sap flow for O6 during Trip 5 (DOY 297-DOY 300). Whole numbers on the x-axis are midnight. Numbers with half decimals (ie, 298.5) represent noon of that day. LWP trend is in red.*

O6's sap flow for Trip 5 is highly variable, but sap flow maximums coincide with midafternoon for each day. There seems to be 3 spikes in sap flow for each day; if the data would have been a smooth curve across the flow maximums (not having the valleys between the 3 peaks), then this would be considered a more typical sap flow pattern. LWP is most negative in the late afternoon of DOY 297 when sap flow is starting to decrease for the day, meaning O6 is water-stressed from a full day of transpiration. LWP is least

negative in the morning of DOY 298, meaning O6 has recovered, and trends more negative as sap flow increases into the afternoon.

As stated earlier, sap flow data O6 was not available for Trip 6, so only LWP is displayed (**Figure 45**).

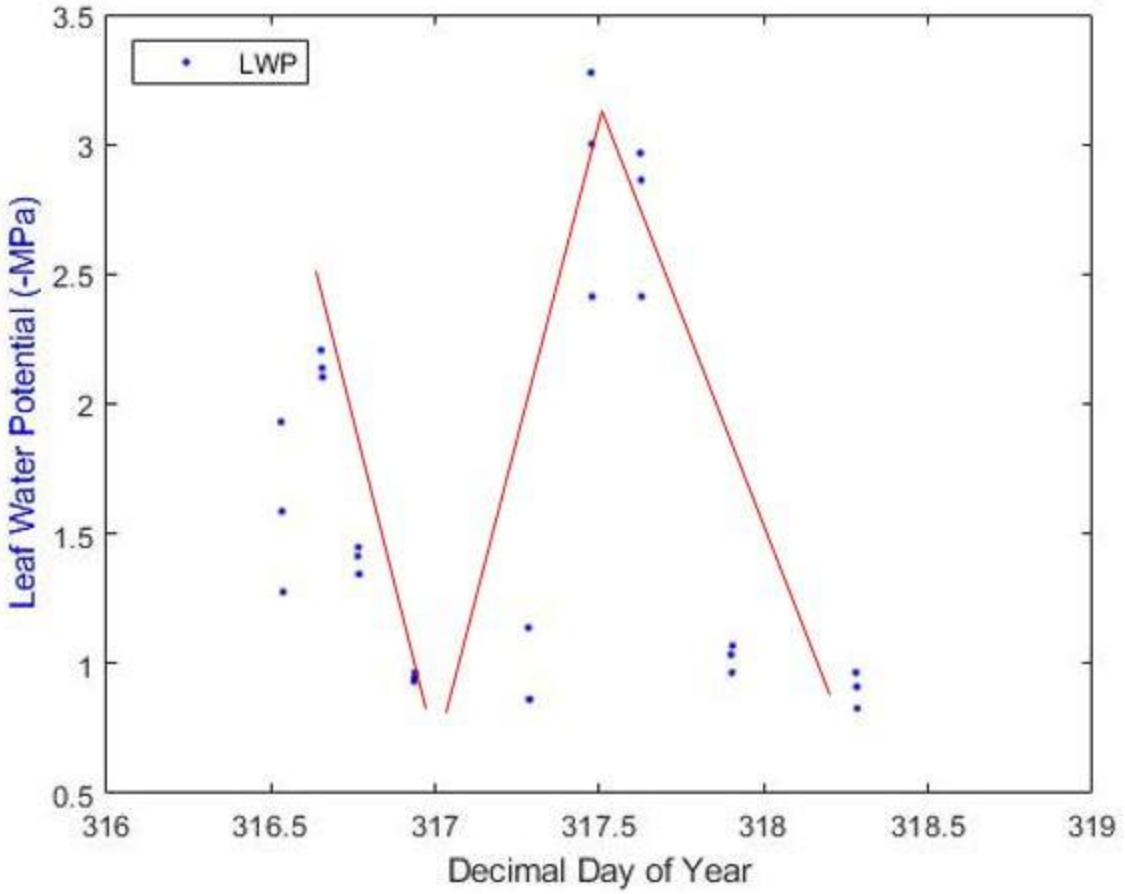

Figure 45: *LWP values for O6 during Trip 6. No sap flow data was recorded, as both sensors were malfunctioned during this period. LWP trend is in red.*

LWP is most negative in the midafternoon (signaling water-stress) and least negative at night.

3.3.2b LWP in Response to Meteorological Conditions — Lacey Oak 6 (O6)

O6 shows a strong positive correlation between LWP and VPD (**Figure 46**).

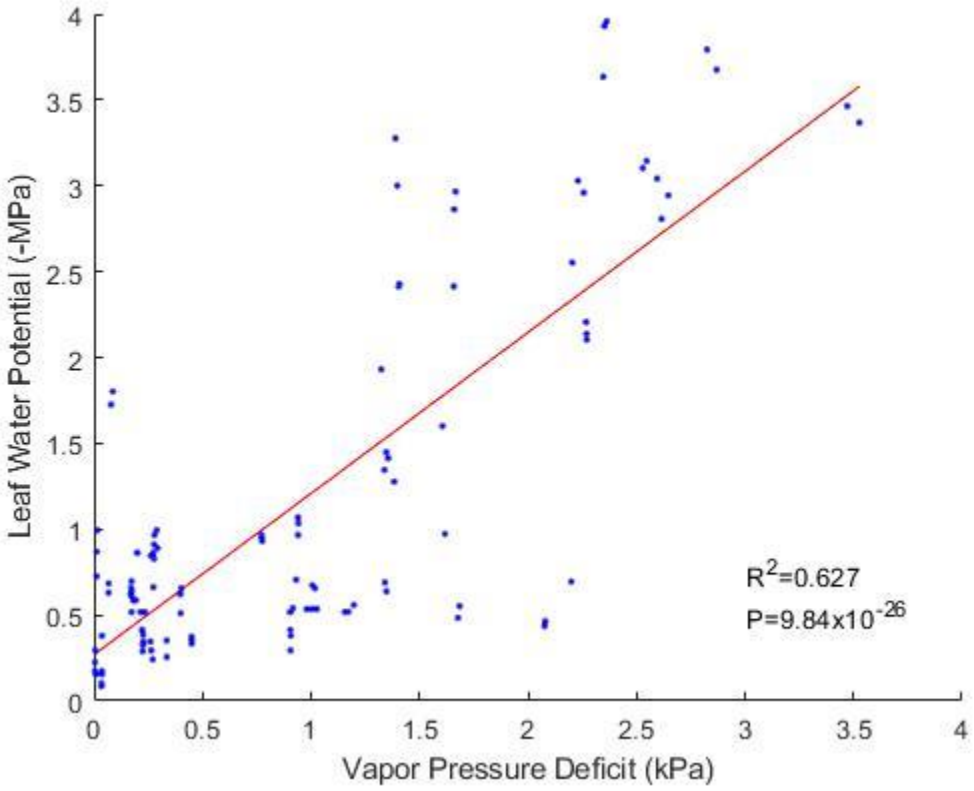

Figure 46: *LWP and VPD for all LWP measurements taken from O6 over the course of 2021. Best line of fit is in red, with R^2 and P value from linear regression listed.*

As indicated by the R^2 and P value, VPD and LWP have a much stronger and more significant correlation for O6 than observed in AJ1 (**Figure 38**). O6 did not show a strong or significant correlation between SWP and LWP (**Figure S1** in appendices) as was observed with AJ1 (**Figure 39**). In other words, LWP responses from O6 do not depend on soil water potential but are highly controlled by VPD.

3.3.3 LWP Results — Pinyon Pine (P7)

Pinyon pine 7 (P7) was chosen for LWP measurements to represent the pines for the first 4 Trips but was switched to P2 for the last two Trips. LWP values for pine were much less variable than those observed in oaks or junipers (**Figure 47**). LWP was recorded on all six Trips for 2021.

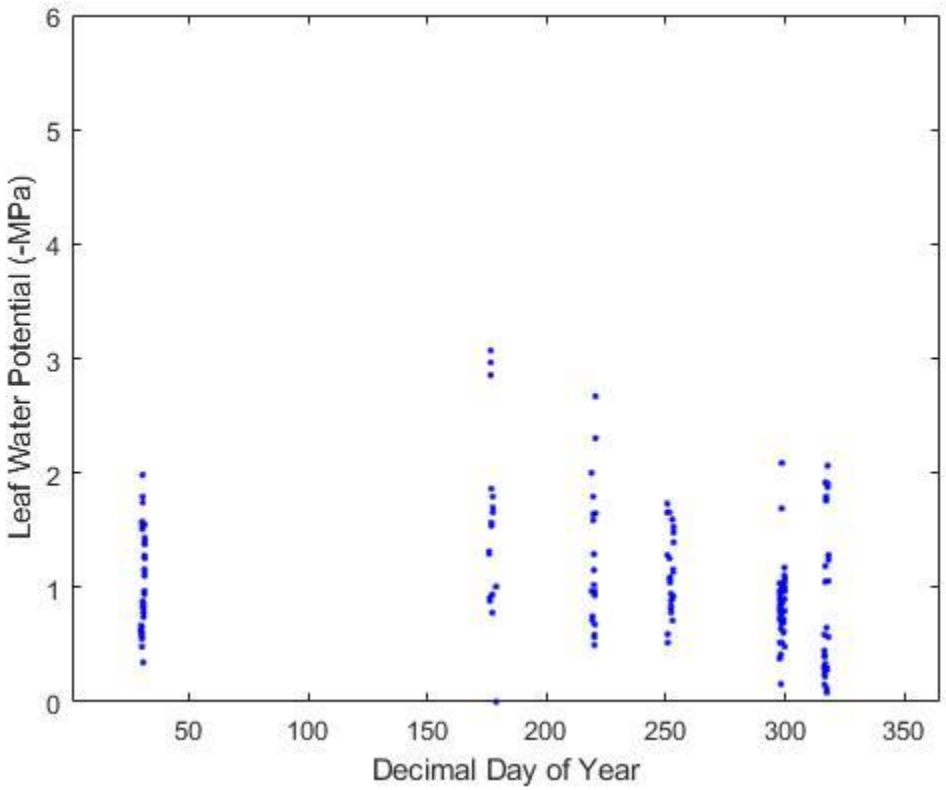

Figure 47: *All LWP measurements taken from P7 during 2021.*

3.3.3a LWP in Response to Sap Flux — Pinyon Pine (P7)

LWP measurements for P7 during Trip 1 are seen below (**Figure 48**).

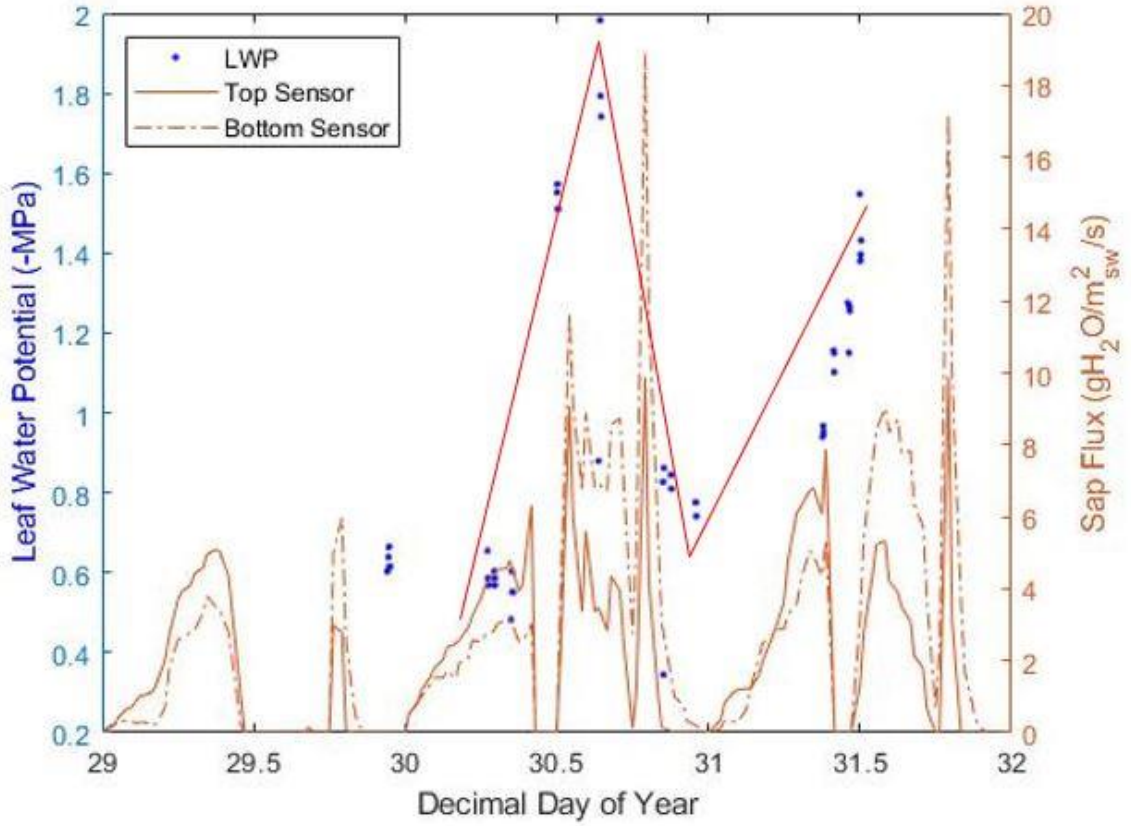

Figure 48: *LWP and sap flow for P7 during Trip 1 (DOY 29-DOY 32). Whole numbers on the x-axis are midnight. Numbers with half decimals (i.e, 3.5) represent noon of that day. LWP trend is in red.*

While both of P7's sensors were working, sap flow is rather variable. Every morning starts with an increase in sap flux, starting shortly after midnight, before stopping during the middle of the day. In the early afternoon (excluding DOY 29), sap flow increases again (sometimes spiking at dusk as in DOY 30 and 31), before ceasing at night. LWP is least negative (not water-stressed) just before midnight and in the mornings around 8:00 am, and most negative (indicating water-stress) around 3:00 pm, after a full day of transpiring indicated by sap flow measurements.

LWP and sap flow for Trip 2 can be found below in **Figure 49**.

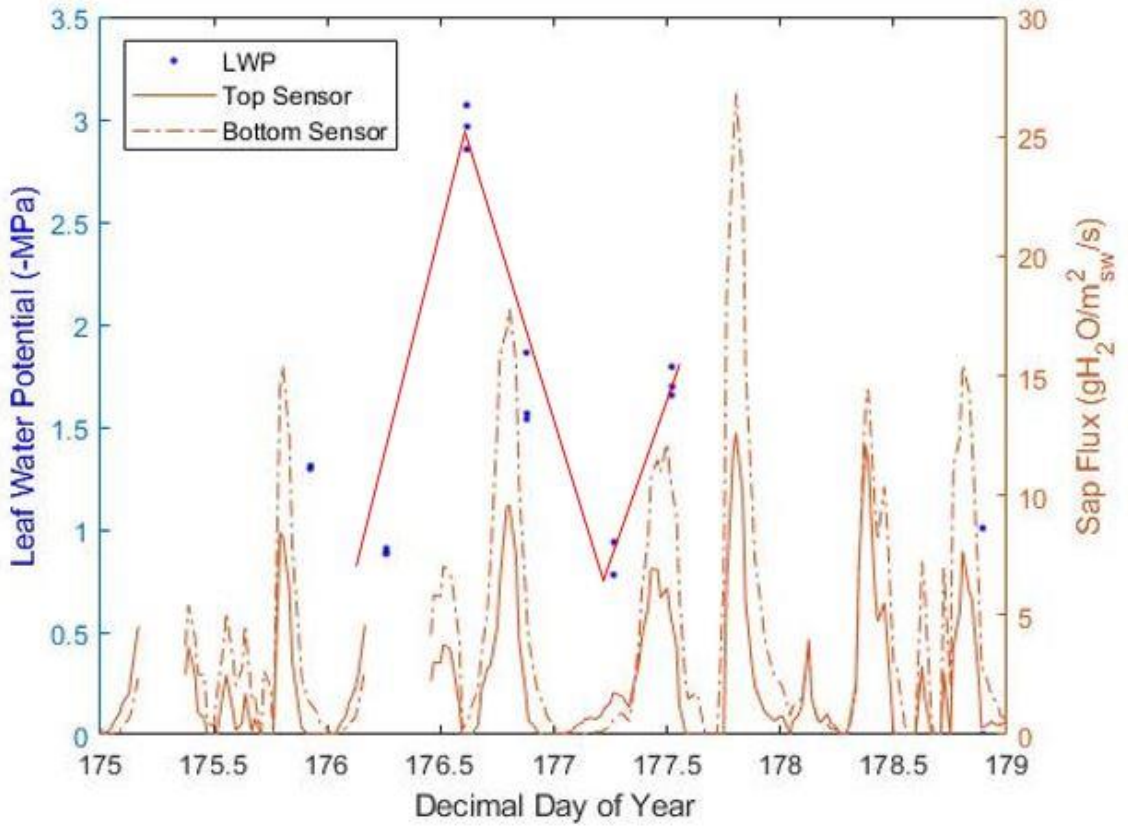

Figure 49: *LWP and sap flow for P7 during Trip 2 (DOY 175-DOY 179). Whole numbers on the x-axis are midnight. Numbers with half decimals (i.e, 176.5) represent noon of that day. LWP trend is in red.*

Once again, P7's sap flow is inconsistent from a typical diurnal sap flow pattern's standpoint. Both P7's sensors show maximum sap flow for each day at dusk, with other sap flow spikes around noon. Once again, LWP is most negative in the heat of the afternoon (1:00 - 2:00 pm) and least negative right before dawn at 7:00 am, again signaling that P7 is most water-stressed after transpiring for most of the day.

P7's LWP and sap flow data for Trip 3 can be found in **Figure 50**.

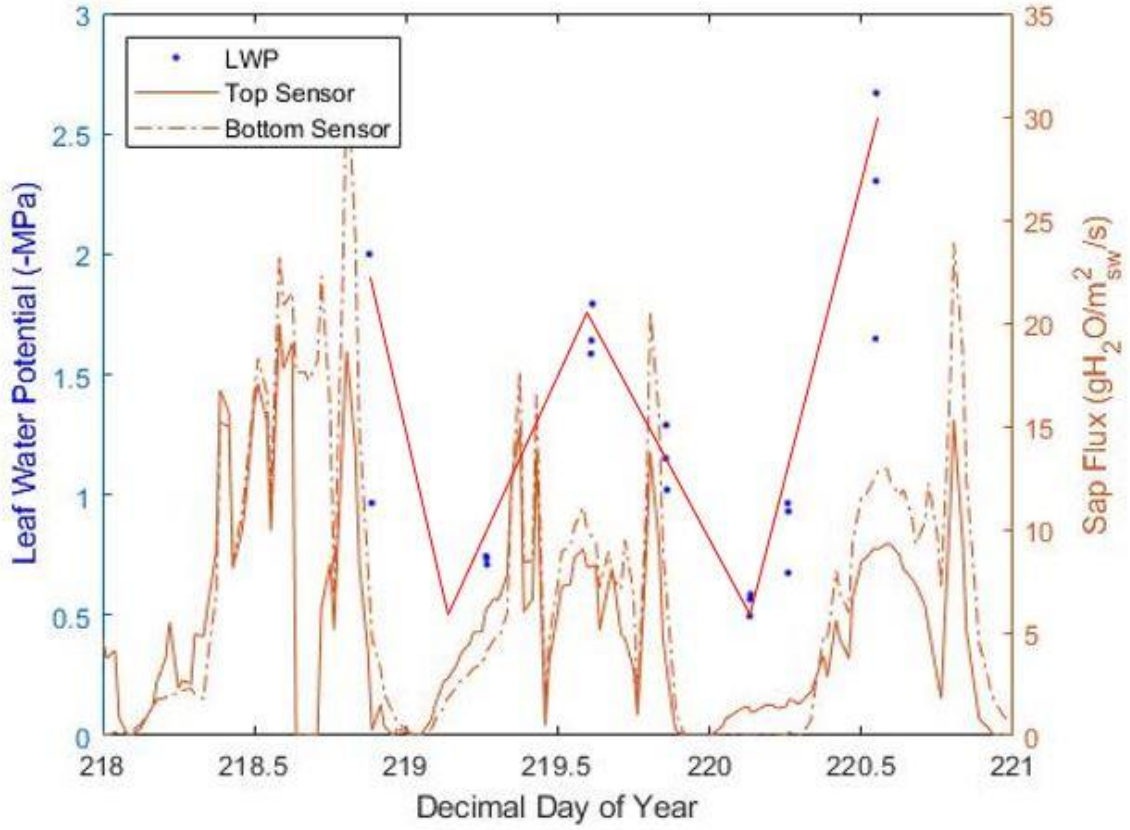

Figure 50: *LWP and sap flow for P7 during Trip 3 (DOY 218-DOY 221). Whole numbers on the x-axis are midnight. Numbers with half decimals (ie, 219.5) represent noon of that day. LWP trend is in red.*

Diurnal sap flow patterns for this Trip have a similar shape to O6's for Trip 3 (**Figure 42**), where sap flux occurs mainly during the day, but the curve is less regular than expected for a typical inverse parabola. DOY 218 has many sap flow peaks but generally assumes an inverse parabolic shape, and DOY 219 has maximum sap flow at dawn and dusk. Sap flow during DOY 220 is as close to a typical diurnal sap flow pattern as will be observed for this Trip, with just one additional sap flow spike occurring at dusk. LWP for Trip 3 is consistent; it's most negative around 2:00 pm (signaling water-stress after transpiring all day), and least negative just before dawn, signaling P7 has recovered from the previous day's water-stress.

Sap flow and LWP for Trip 4 can be seen below in (**Figure 51**).

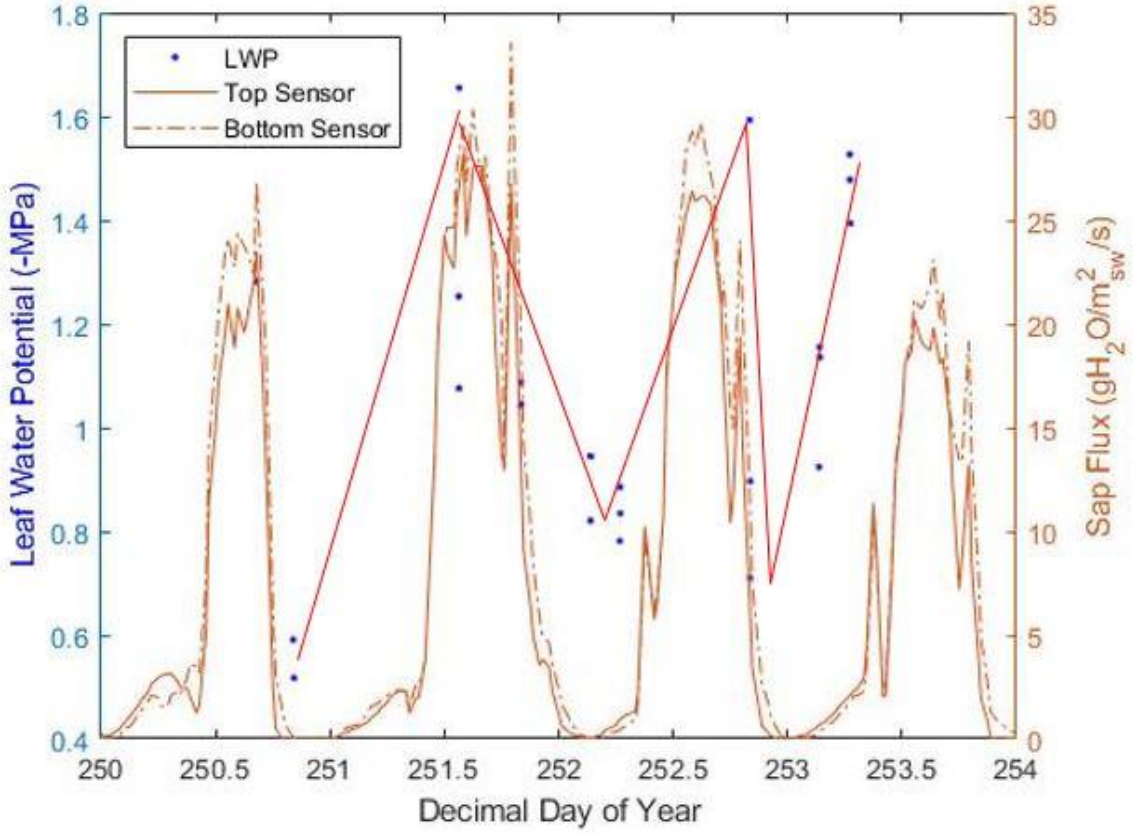

Figure 51: *LWP and sap flow for P7 during Trip 4 (DOY 250-DOY 254). Whole numbers on the x-axis are midnight. Numbers with half decimals (ie, 251.5) represent noon of that day. LWP trend is in red.*

As seen in the other two species' diurnal sap flow patterns for Trip 4 (**Figure 35** and **Figure 43**), sap flow for P7 is the most typical and expected here out of all six Trips, as Trip 4 coincides with the favorable period chosen earlier (DOY 250-260). Sap flow strongly resembles an inverse parabola, although spikes in sap flow can still be seen in the morning and evening after DOY 250. LWP is the most negative from 1:00 – 3:00 in the afternoon, suggesting that P7 is the most water-stressed after transpiring all day. LWP then shifts towards less negative values as P7 recovers throughout the night and early morning.

Both Trip 5 and Trip 6 do not have sap flow data for P7, as the sensors were malfunctioned. LWP and sap flow for Trip 5 can be seen below in **Figure 52**.

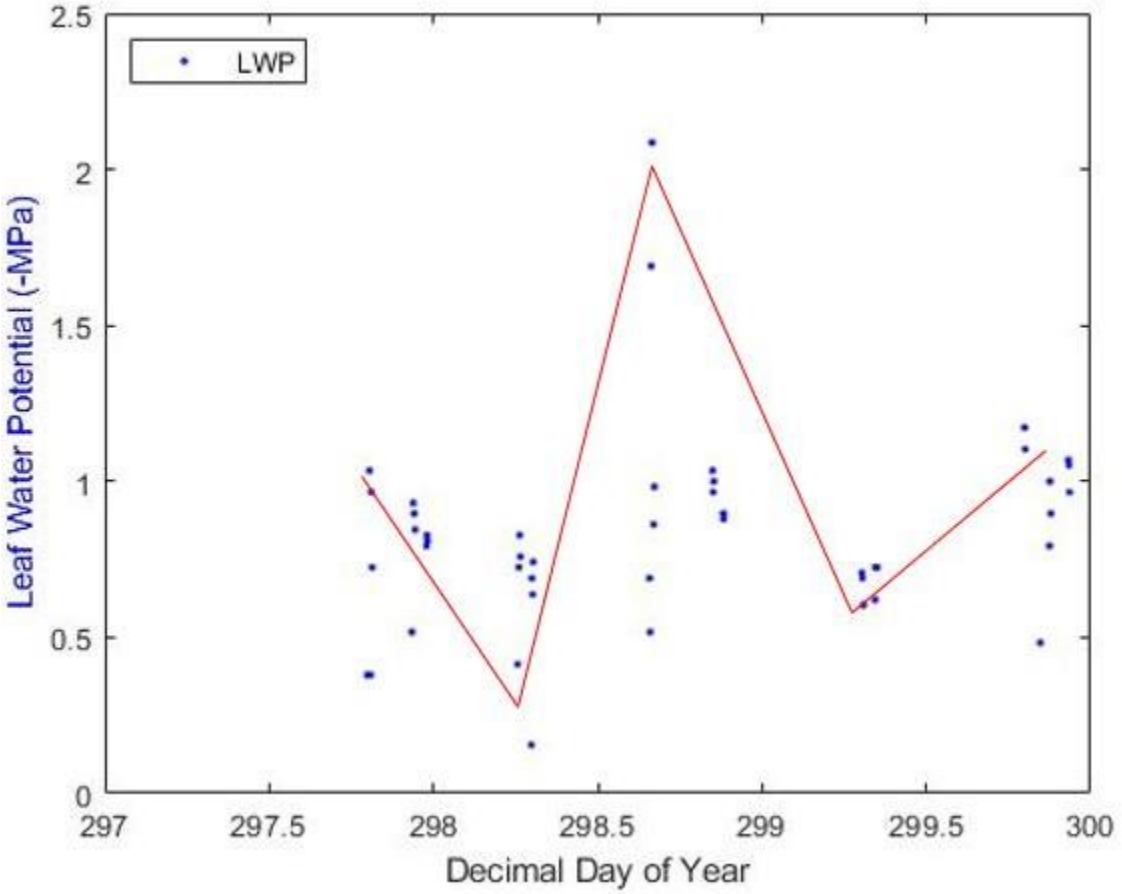

Figure 52: *LWP for P7 during Trip 5 (DOY 297-DOY 300). Whole numbers on the x-axis are midnight. Numbers with half decimals (ie, 298.5) represent noon of that day. LWP trend is in red.*

LWP is at its most negative around 3:00 pm of DOY 298, indicating this was P7's most water-stressed moment of Trip 5. Most of the LWP measurements are remarkably similar to each other, regardless of time of day, but generally, LWP appears less negative (less stressed) at night and early morning and get more negative during the afternoon.

LWP for Trip 6 can be seen below in **Figure 53**.

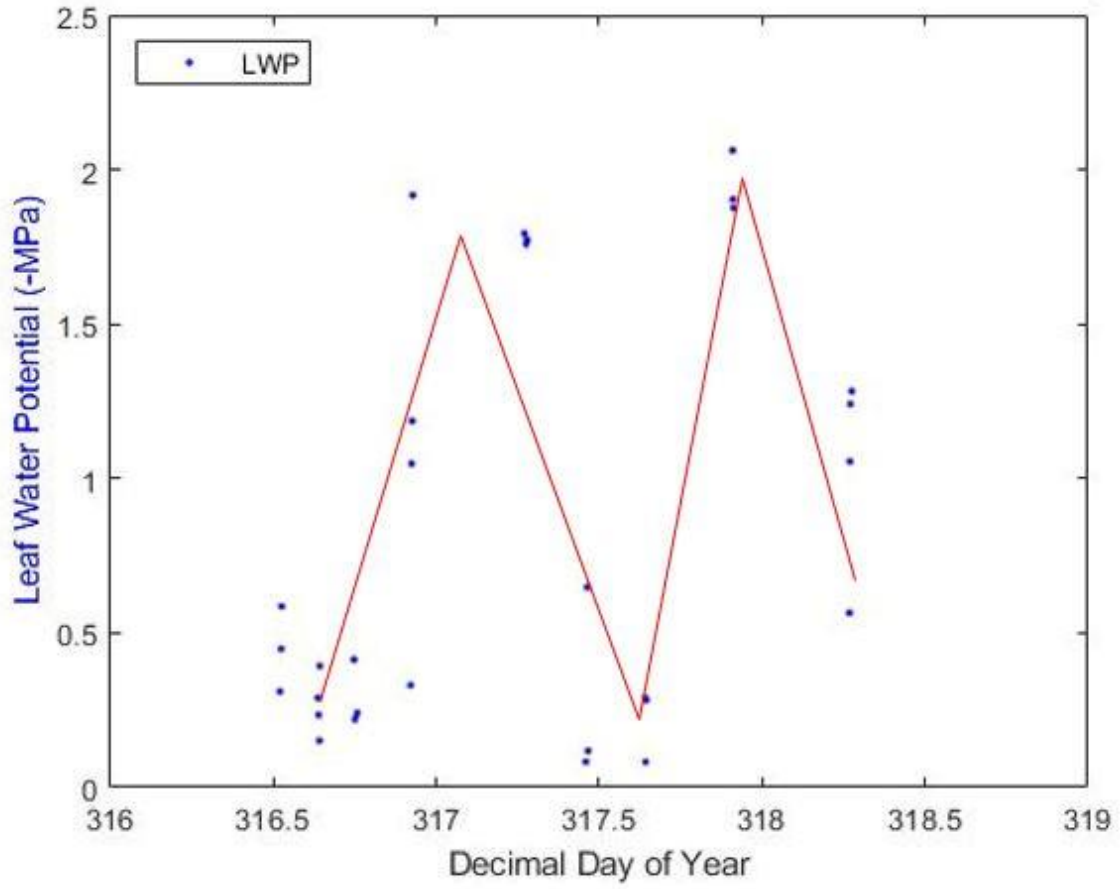

Figure 53: *LWP for P7 during Trip 6 (DOY 316-DOY 319). Whole numbers on the x-axis are midnight. Numbers with half decimals (i.e., 317.5) represent noon of that day. LWP trend is in red.*

LWP measurements here have much more variability than for Trip 5 (**Figure 52**). Interestingly, this is the only instance across all Trips and species where LWP is the most negative at night and least negative during the middle of the day.

3.3.3b LWP in Response to Meteorological Conditions — Pinyon pine (P2/P7)

The pines presented a positive relationship between LWP and VPD (**Figure 54**).

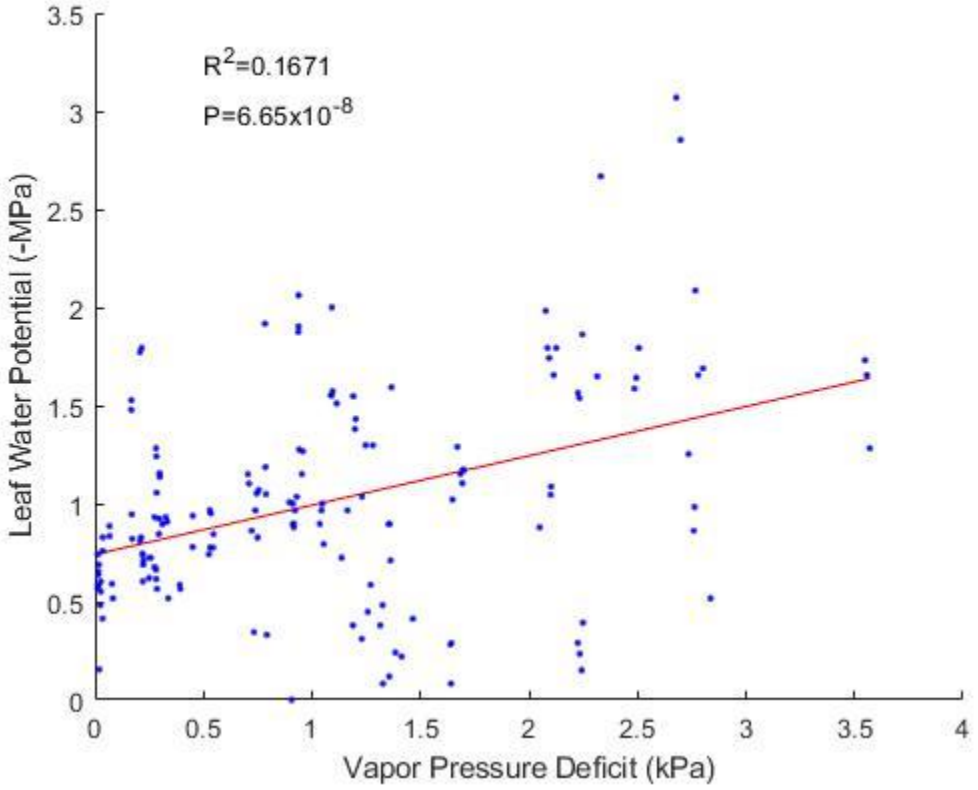

Figure 54: *LWP and VPD for all LWP measurements taken from P7 over the course of 2021. Best line of fit is in red, with R^2 and P value from linear regression listed.*

With such a small P value and an R-squared greater than 0.1, there is a significant albeit weak relationship between LWP and VPD for P7. This means that higher VPD will cause P7 to be more water-stressed. No significance or correlation was found between LWP and SWP for P7 (**Figure S2** in appendices).

3.4 Carbon Assimilation and Stomatal Conductance Results

The Licor 6800 records many different measurements when sampling a specimen, but this study only focuses on net carbon assimilation (A_{net}) and stomatal conductance (GSW). Licor measurements were taken during Trip 2 (DOY 175-179) and Trip 6 (DOY 316-319).

3.4.1 Carbon Assimilation and Stomatal Conductance Results — Ashe Juniper 1 (AJ1)

All assimilation and stomatal conductance measurements taken during 2021 for AJ1 can be found below in **Figure 55** and **Figure 56**, respectively. These measurements include predawn, afternoon and dusk recordings. Note that the x-axes both start at DOY 155, as we are only concerned with the dates where Licor data was obtained.

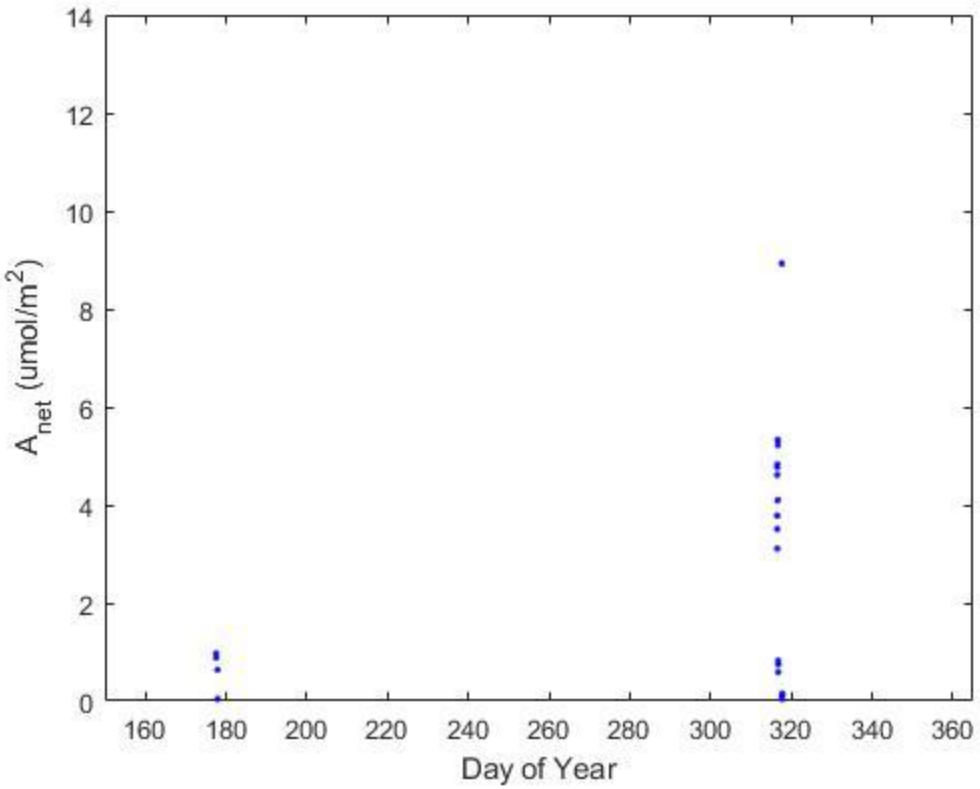

Figure 55: *All assimilation measurements for AJ1 during 2021. n=25, where n is number of sampling points.*

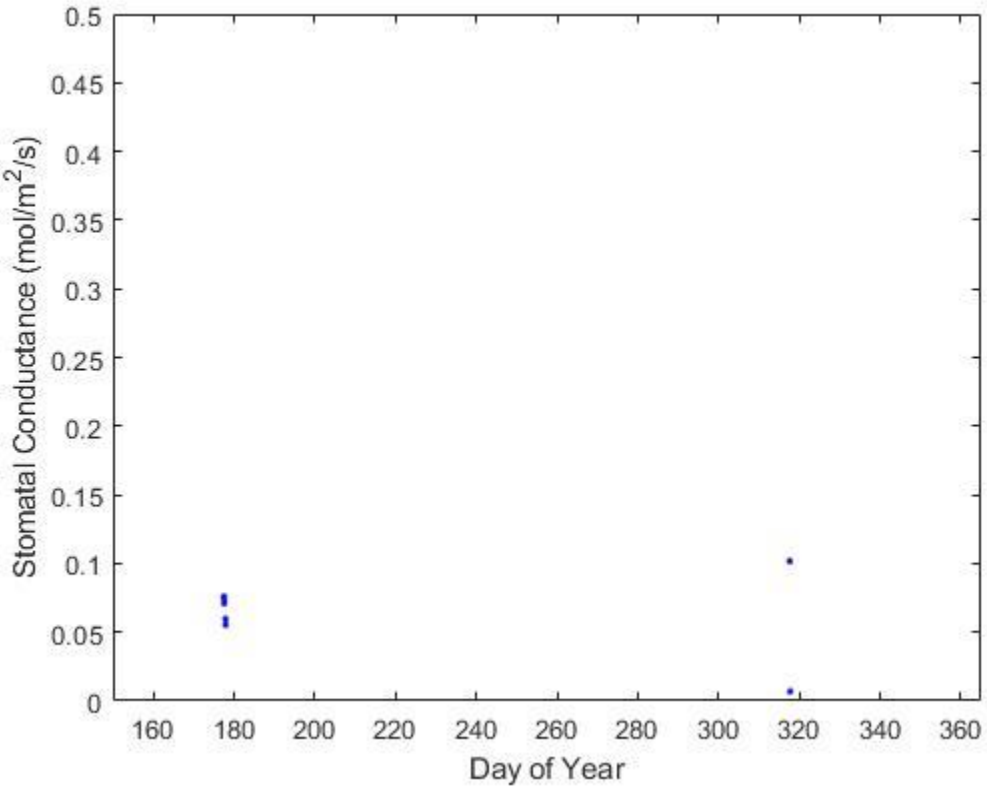

Figure 56: *All stomatal conductance measurements for AJ1 during 2021. n=9, where n is number of sampling points.*

3.4.1a AJ1 Carbon Assimilation, Stomatal Conductance, and Sap Flux

Assimilation compared to sap flux for AJ1 during Trip 2 can be found below in **Figure 57**. After that, stomatal conductance and sap flow are plotted together in **Figure 58**.

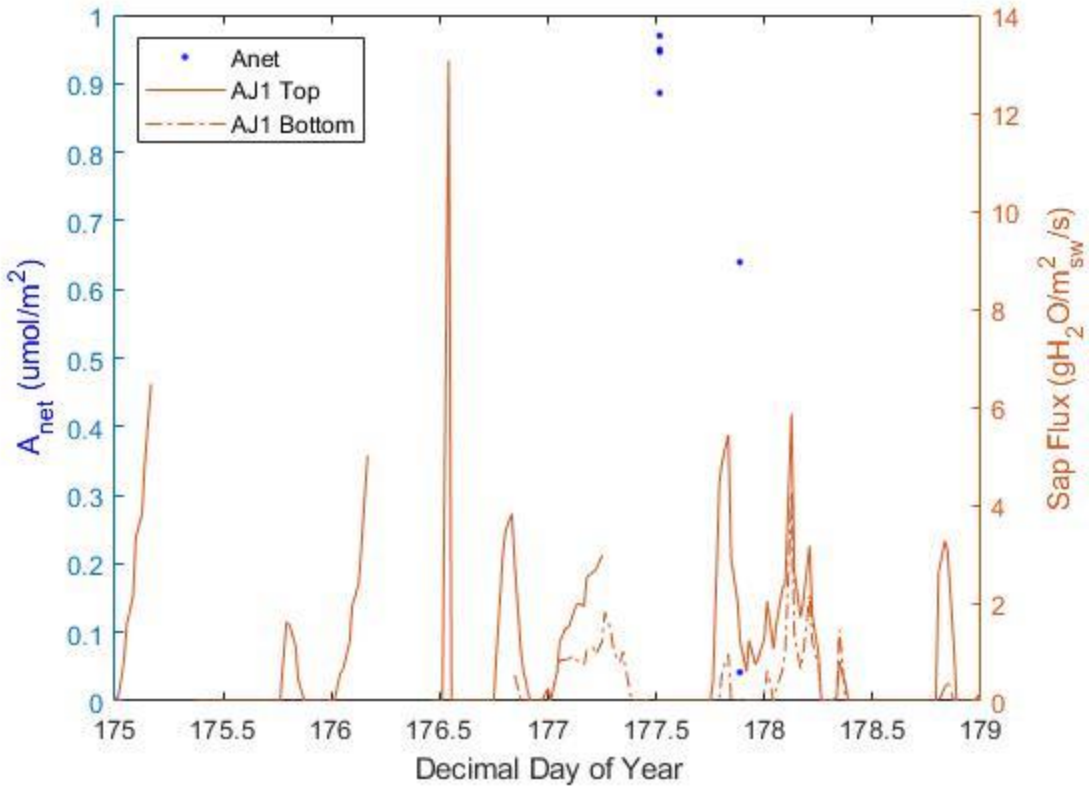

Figure 57: *Assimilation and sap flow for AJ1 during Trip 2 (DOY 175-DOY 179). Whole numbers on the x-axis are midnight. Numbers with half decimals (i.e, 176.5) represent noon of that day. n=6, where n is the number of sampling points.*

As seen in **Figure 32**, AJ1's bottom sensor failed to record data until late DOY 176. Although there are only 6 data points, they fortunately were taken at both the heat of the day and at dusk. Assimilation, or the rate of photosynthesis, is highest around 1:00 pm. This makes sense, as maximum photosynthetic active radiation (PAR) is highest in the midafternoon. Assimilation then decreases throughout the evening, until reaching its lowest point (least amount of photosynthesis) just before midnight. Stomatal conductance for AJ1 during the same period can be found below (**Figure 58**).

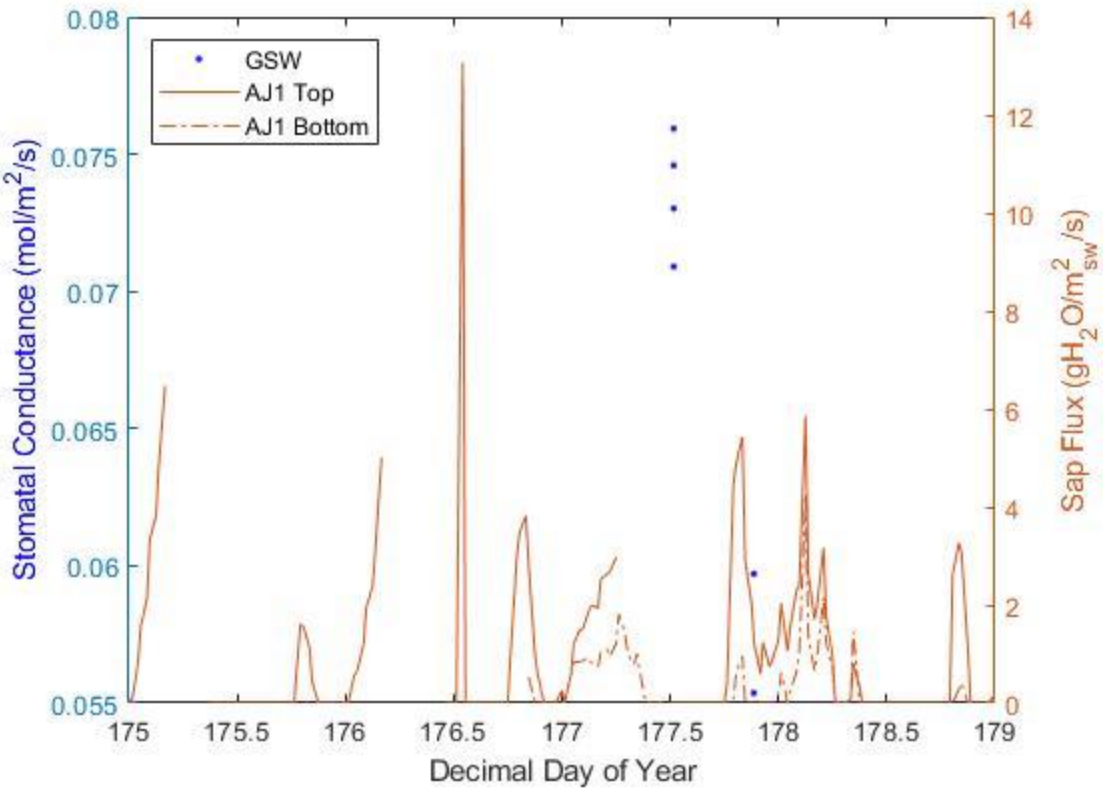

Figure 58: *Stomatal conductance and sap flow for AJ1 during Trip 2 (DOY 175-DOY 179). Whole numbers on the x-axis are midnight. Numbers with half decimals (i.e, 176.5) represent noon of that day. n=6, where n is the number of sampling points.*

As with assimilation, stomatal conductance is highest around 1:00 pm, meaning this is when the stomates are most open, allowing gas exchange with the atmosphere. Stomatal conductance decreases quickly during the heat of the day and reaches its lowest point at night, just before midnight.

Next, we examine the same parameters for Trip 6. Assimilation and sap flow can be found below in **Figure 59**. Note that the sap flow data is gap-filled.

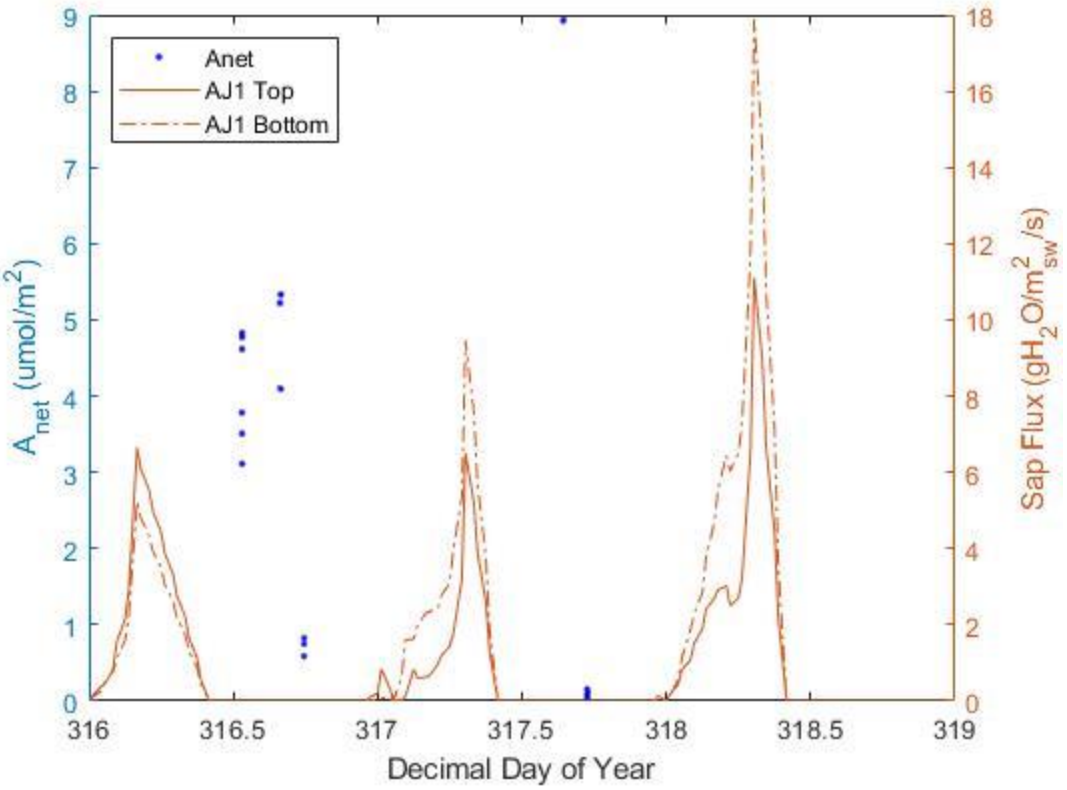

Figure 59: *Assimilation and sap flow for AJ1 during Trip 6 (DOY 316-DOY 319). Whole numbers on the x-axis are midnight. Numbers with half decimals (i.e, 317.5) represent noon of that day. n=16, where n is the number of sampling points. Sap flow data for Trip 6 was gap-filled.*

Unfortunately, neither sap flux nor assimilation recordings offer much insight into the patterns of AJ1 for Trip 6. Assimilation decreases from the heat of the day onward on DOY 316, and afternoon measurements for DOY 317 show a dramatic drop in assimilation over a very short time change. Stomatal conductance and sap flow (gap-filled) can be seen below in **Figure 60**.

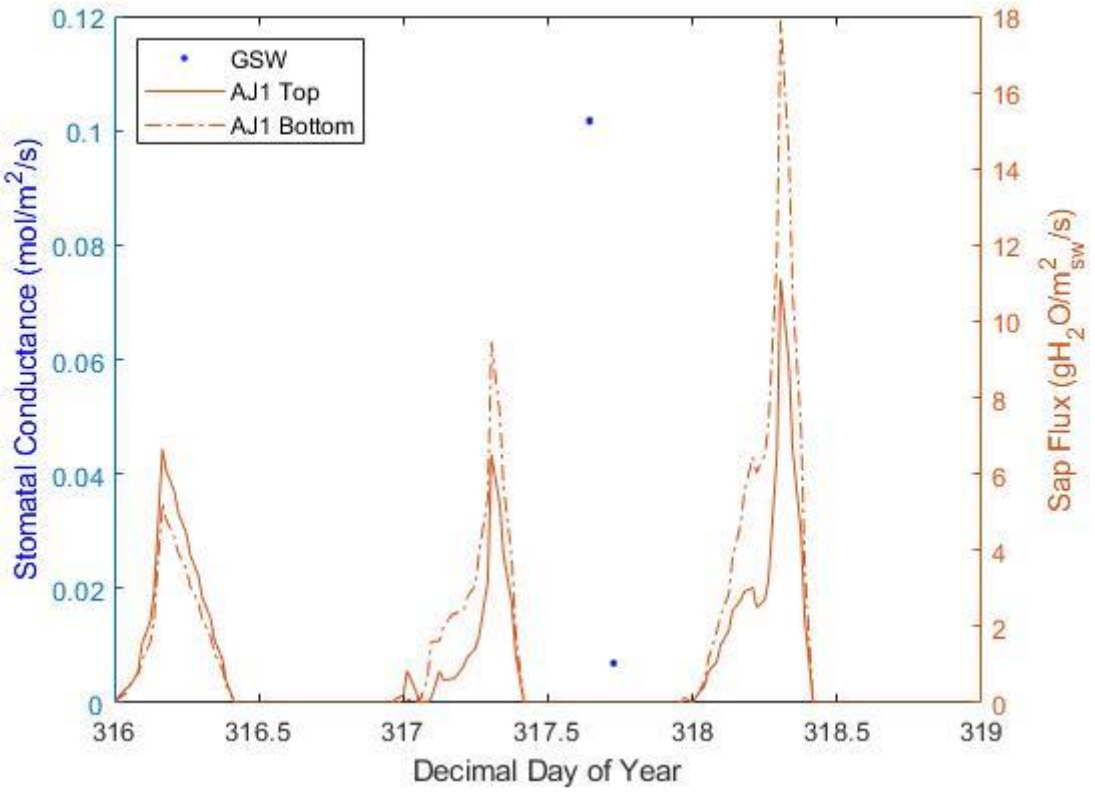

Figure 60: *Stomatal conductance and sap flow for AJ1 during Trip 6 (DOY 316-DOY 319). Whole numbers on the x-axis are midnight. Numbers with half decimals (i.e, 317.5) represent noon of that day. n=5, where n is the number of sampling points. Sap flow data for Trip 6 was gap filled.*

Due to sap flow data being gap-filled, all that is truly observable is that stomatal conductance is highest around 3:00 pm in DOY 317, before decreasing to near zero after only a short period of time, likely indicating extreme midday stomatal closure.

3.4.1b AJ1 Carbon Assimilation and Stomatal Conductance Responses to Meteorological Conditions

There was no significant correlation found between AJ1's changes in assimilation and VPD (**Figure S3** in appendices). AJ1's stomatal conductance and VPD regression also

does not show a significant correlation (**Figure S4** in appendices). Therefore, neither assimilation or stomatal conductance appear to be dependent on VPD for AJ1. This may be due to a paucity of sample points. Note that the number of assimilation and stomatal conductance sample points has decreased for these regression plots, as measurements were lost when time-averaging to match the sap flow timestep.

The regression between assimilation and SWP for AJ1 (**Figure S5** in appendices) does not have enough data points for a thorough analysis. A regression between stomatal conductance and SWP for AJ1 (**Figure S6** in appendices) also has inadequate data points for analysis.

3.4.2 Carbon Assimilation and Stomatal Conductance Results — Lacey Oak 6 (O6)

All assimilation measurements for O6 during 2021 can be viewed below in **Figure 61**, and every stomatal conductance measurement can be found in **Figure 62**. Note that both assimilation and stomatal conductance recordings were taken on Trip 2 and Trip 6 at predawn, afternoon, and dusk intervals.

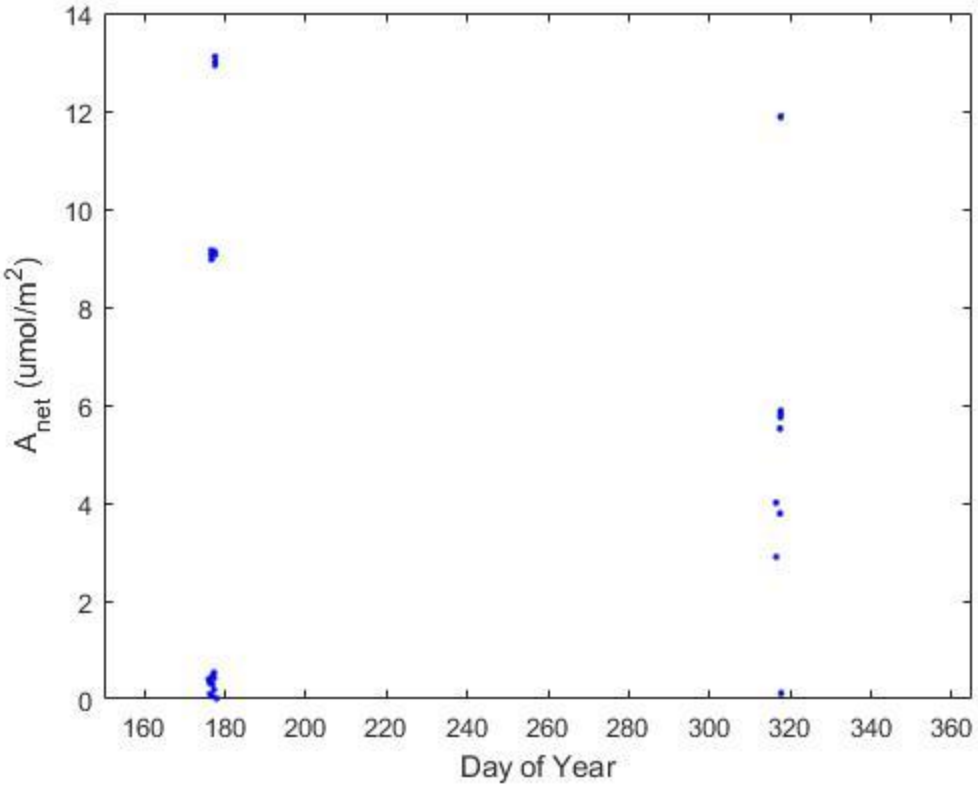

Figure 61: *All assimilation measurements for O6 during 2021. n=31, where n is number of sampling points.*

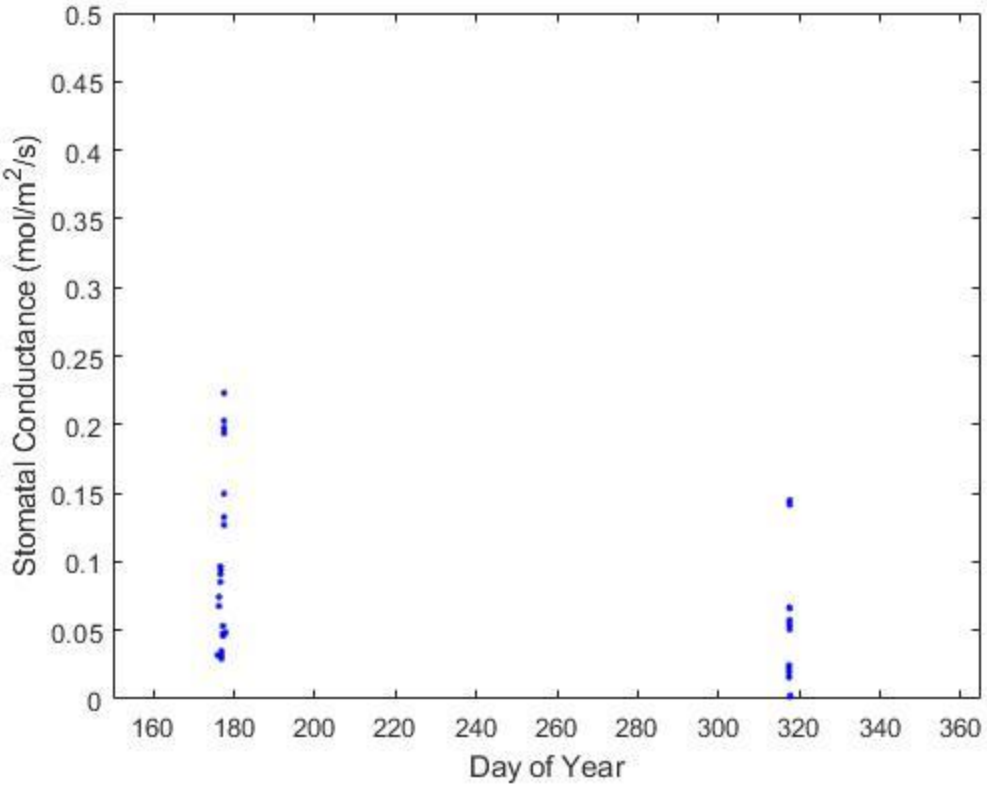

Figure 62: *All GSW measurements for O6 during 2021. n=34, where n is number of sampling points.*

3.4.2a O6 Carbon Assimilation, Stomatal Conductance, and Sap Flux

Assimilation and sap flow for O6 during Trip 2 can be found in **Figure 63**. Assimilation is highest during midday, indicating that this is when O6 is photosynthesizing the most. As expected, assimilation is lowest at night.

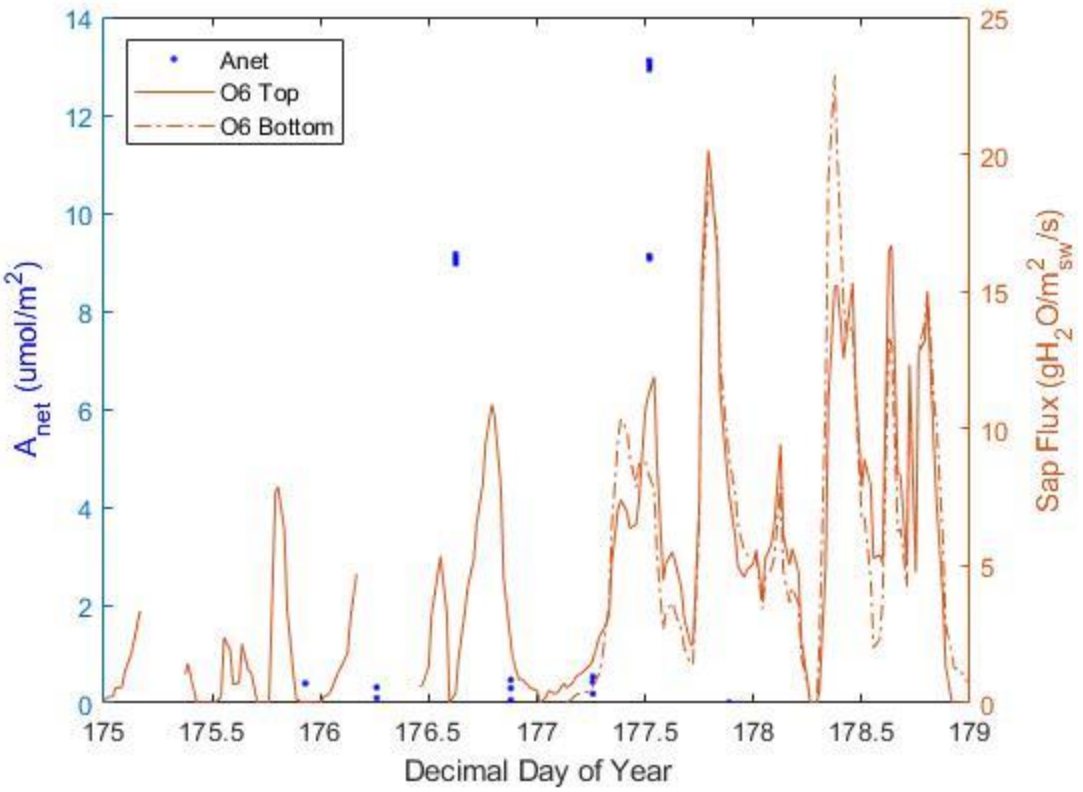

Figure 63: *Assimilation and sap flow for O6 during Trip 2 (DOY 175-DOY 179). Whole numbers on the x-axis are midnight. Numbers with half decimals (i.e, 176.5) represent noon of that day. n=20, where n is the number of sampling points.*

Stomatal conductance measurements plotted with sap flow for the same Trip can be seen below in **Figure 64**. Much like assimilation, stomatal conductance is highest just after noon and lowest just before midnight, meaning that midday is when the stomates are most open and allowing the most gas exchange. Importantly, stomatal conductance declines rapidly after midday indicating a probable stomatal closure due to highly negative leaf water potential.

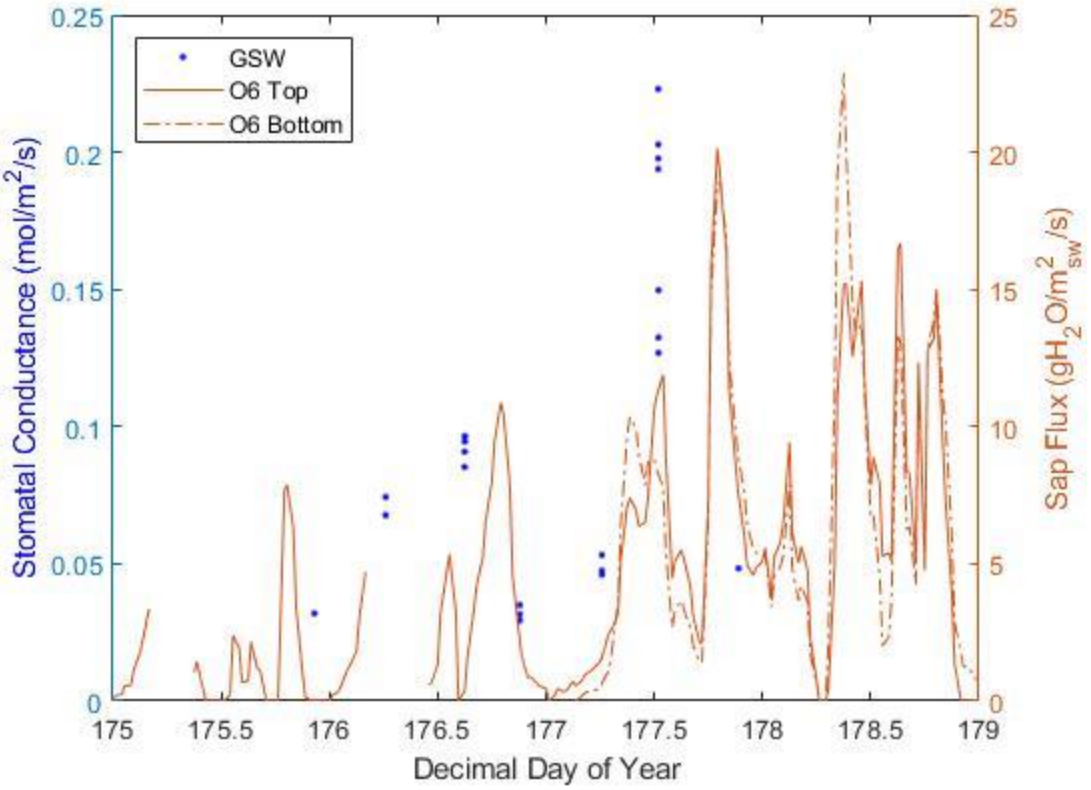

Figure 64: *Stomatal conductance and sap flow for O6 during Trip 2 (DOY 175-DOY 179). Whole numbers on the x-axis are midnight. Numbers with half decimals (i.e, 176.5) represent noon of that day. n=21, where n is the number of sampling points.*

Moving on to Trip 6, assimilation for O6 can be found in **Figure 65**.

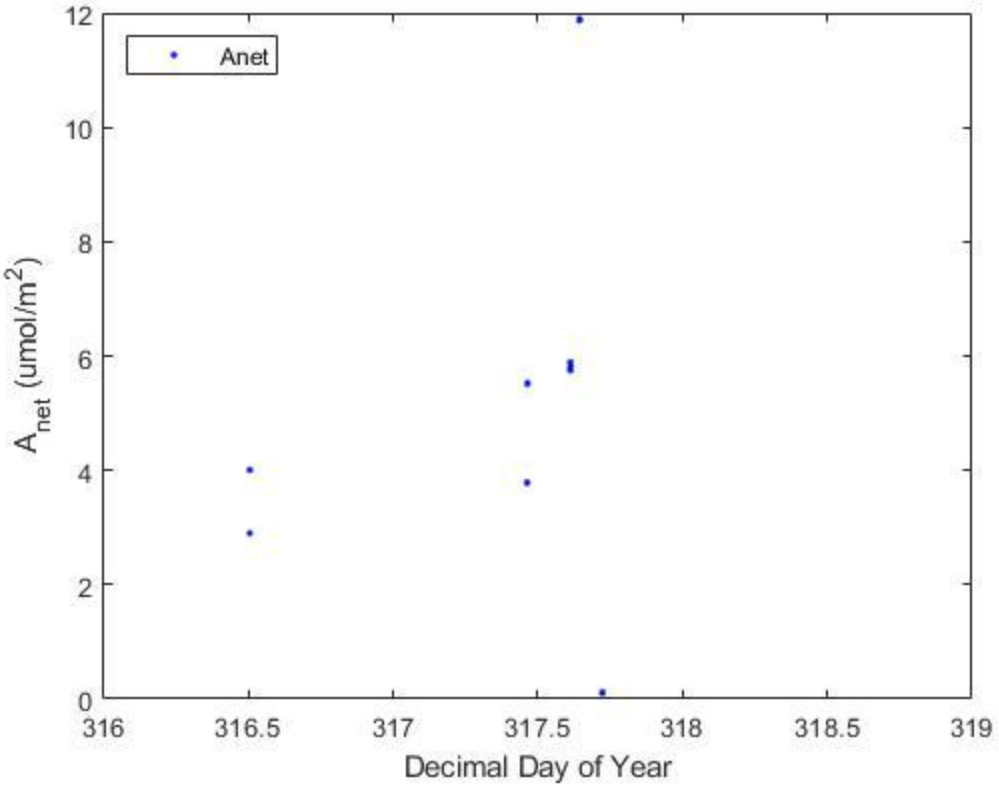

Figure 65: *Assimilation measurements for O6 during Trip 6 (DOY 316-319). Whole numbers on the x-axis are midnight. Numbers with half decimals (i.e, 317.5) represent noon of that day. Note that there is no sap flow data for O6, as both sensors were malfunctioned.*

As we observed in Trip 2 (**Figure 63**), assimilation is highest at midday, meaning that is when O6 is photosynthesizing. However, there is not much assimilation data from Trip 6 for us to analyze. Stomatal conductance for Trip 6 can be found in **Figure 66**.

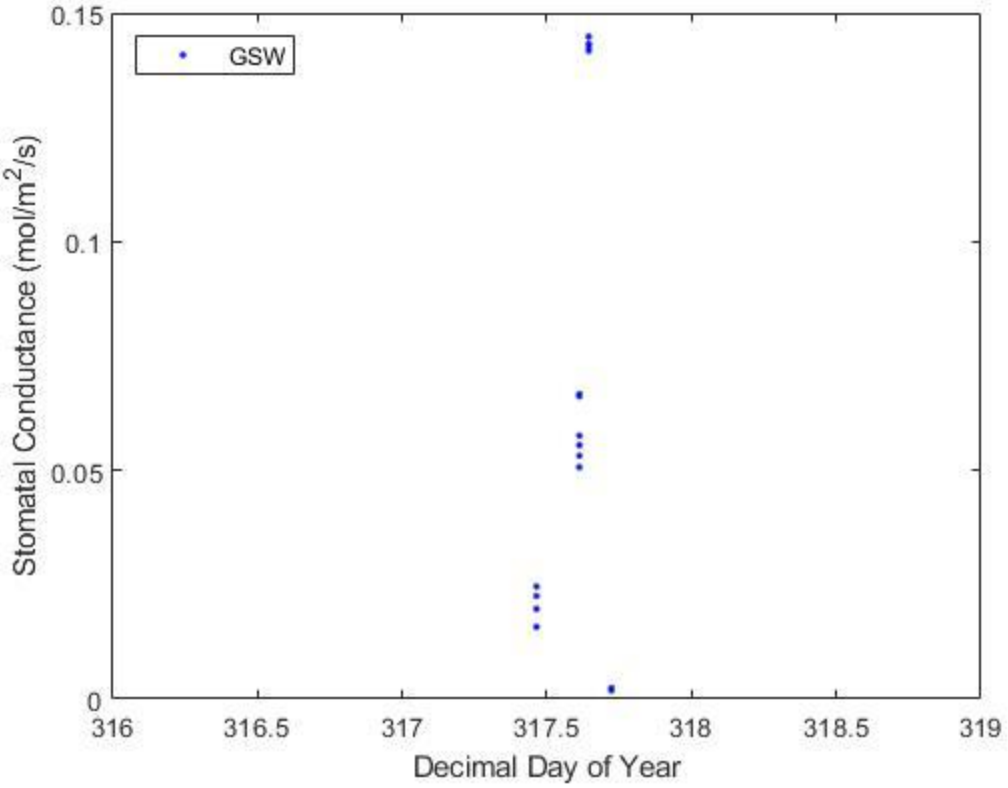

Figure 66: *Stomatal conductance measurements for O6 during Trip 6 (DOY 316-319). Whole numbers on the x-axis are midnight. Numbers with half decimals (i.e, 317.5) represent noon of that day. Note that there is no sap flow data for O6, as both sensors were malfunctioned.*

Stomatal conductance measurements are centered more around midday of DOY 317, which allows the reader to get a sense of stomatal conductance behavior leading up to and away from the heat of the day. As seen in Trip 2 (**Figure 64**), stomatal conductance is highest during the heat of the afternoon and decreases rapidly thereafter.

3.4.2b O6 Carbon Assimilation and Stomatal Conductance Responses to Meteorological Conditions

O6 showed a strong positive relationship between assimilation and VPD (**Figure 67**).

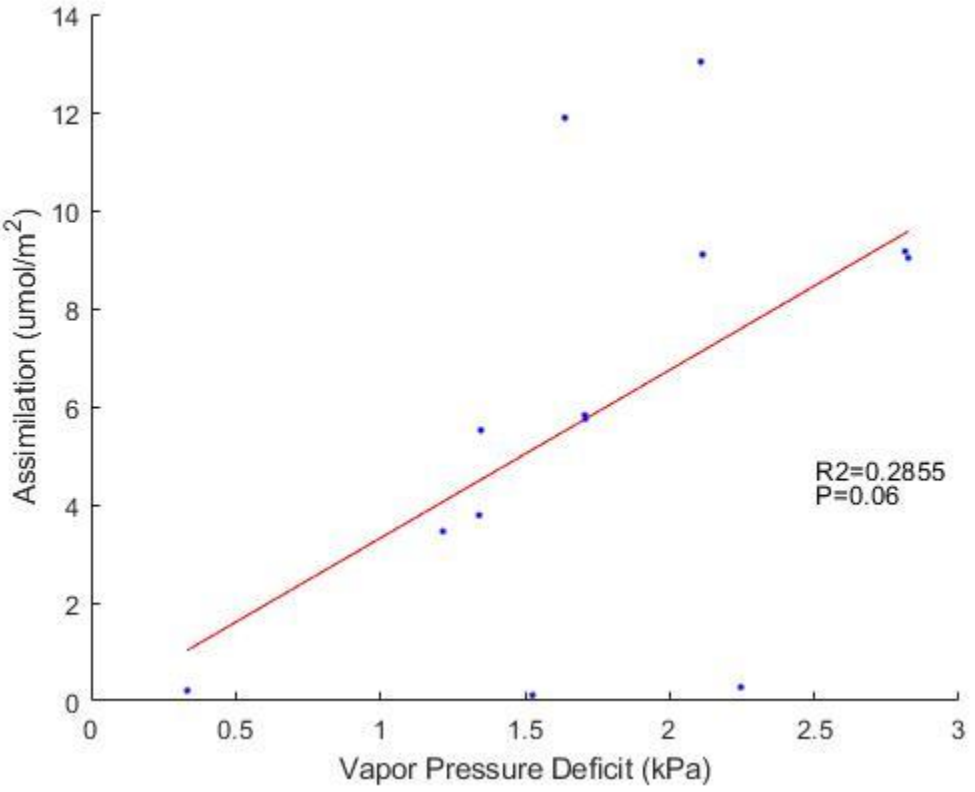

Figure 67: *Assimilation measurements for O6 during 2021 with respect to VPD. Best fit line in red. P value and R2 are reported on graph. n=13, where n is the number of sample points.*

In other words, as VPD increases, assimilation increases as well. However, we observed no correlation of significance between stomatal conductance and VPD **(Figure S7** in appendices**)**. Next, the relationship between assimilation and SWP for O6 can be found below (**Figure 68**).

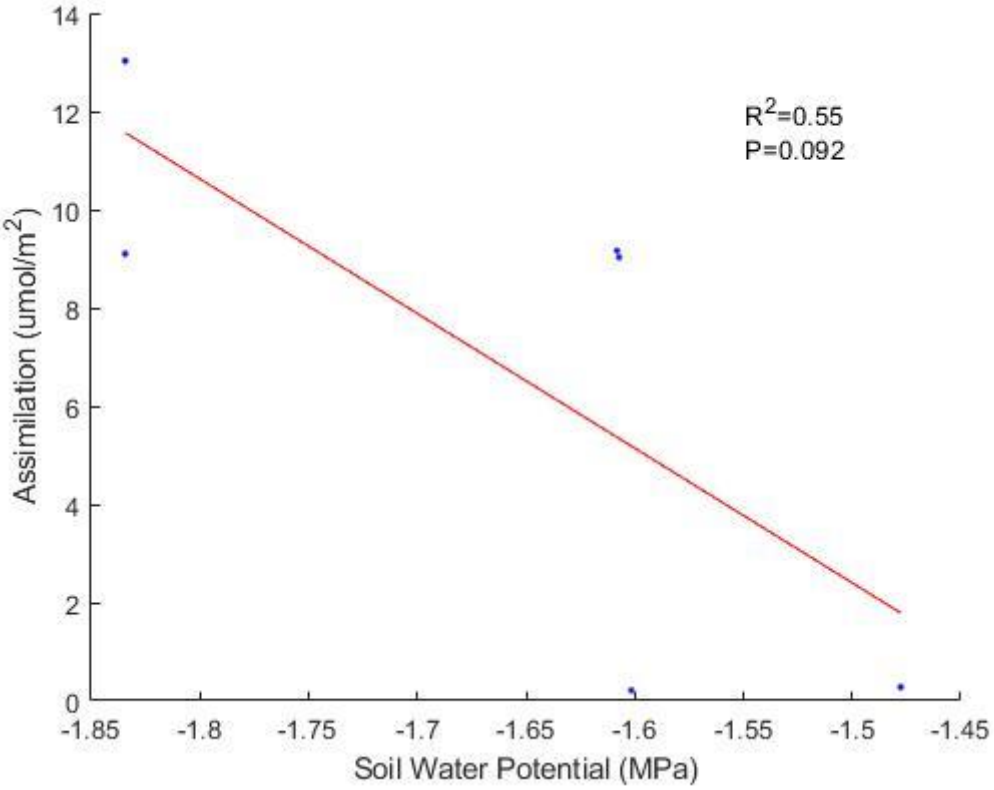

Figure 68: *Assimilation and SWP for O6 during 2021. n=6, where n is the number of sample points. P-value and R^2 are reported on graph.*

Based on the P-value and R-squared, the relationship between assimilation and SWP is strong, but not significant. Below, a regression between stomatal conductance and SWP can be found in **Figure 69**.

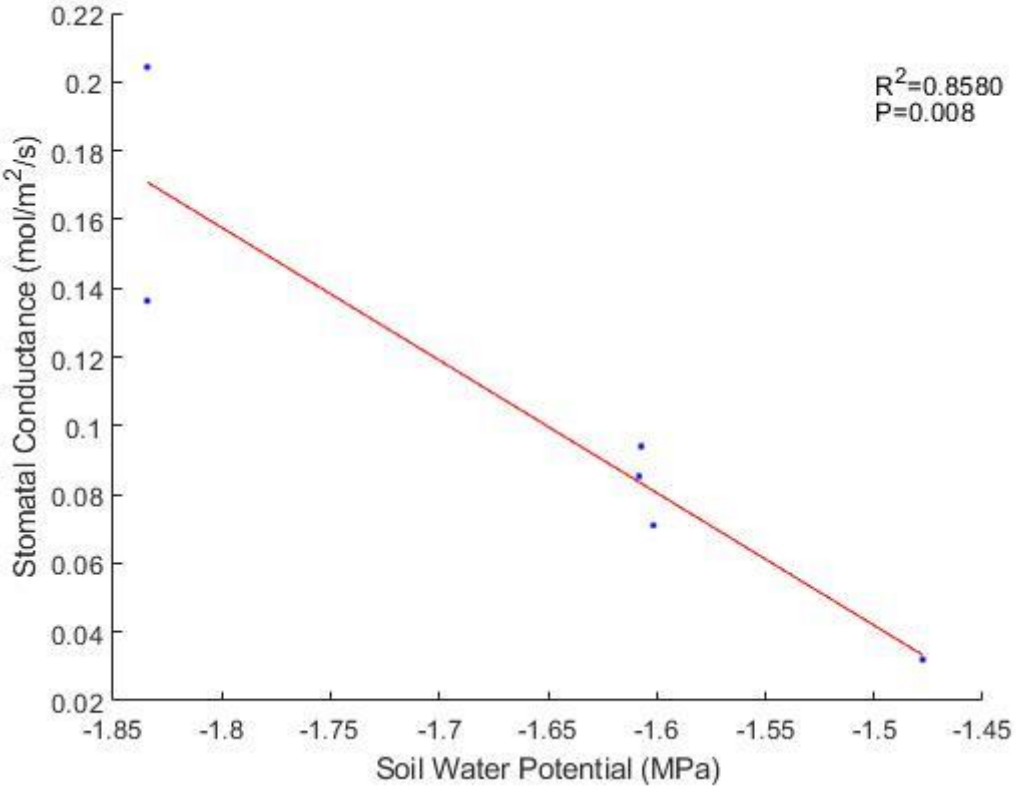

Figure 69: *Stomatal conductance and SWP for O6 during 2021. n=6, where n is the number of sample points. P-value and R^2 are reported on graph.*

As seen above with assimilation, the relationship between stomatal conductance and SWP is very strong, with a relatively weak significance due to a lack of data. Interestingly, the relationships for both assimilation (**Figure 68**) and stomatal conductance (**Figure 69**) with SWP are negative, indicating that stomata are most open when soil is driest.

3.4.3 Carbon Assimilation and Stomatal Conductance Results — Pinyon Pine (P7)

Every assimilation measurement (including predawn, afternoon, and dusk measurements) for P7 from 2021 (taken during Trip 2 and Trip 6) can be seen below in **Figure 70**.

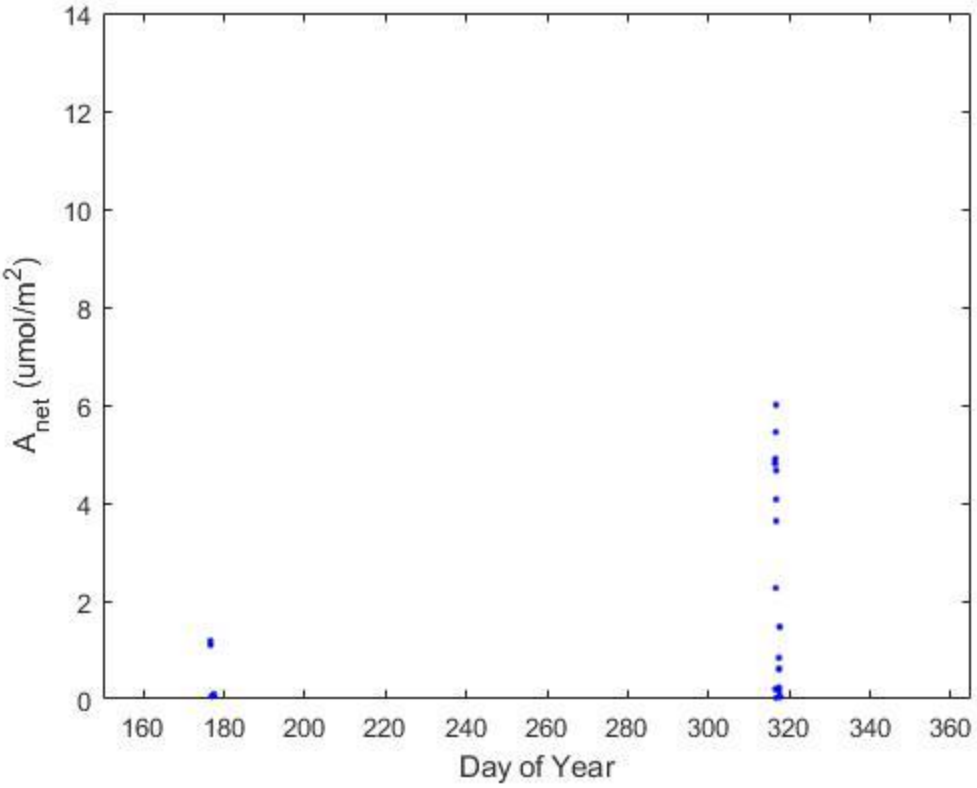

Figure 70: *All assimilation measurements for P7 during 2021. n=22, where n is number of sampling points.*

Stomatal conductance measurements for P7 taken during 2021 can be found in **Figure 71**.

Note that no recordings were taken during Trip 6 for P7.

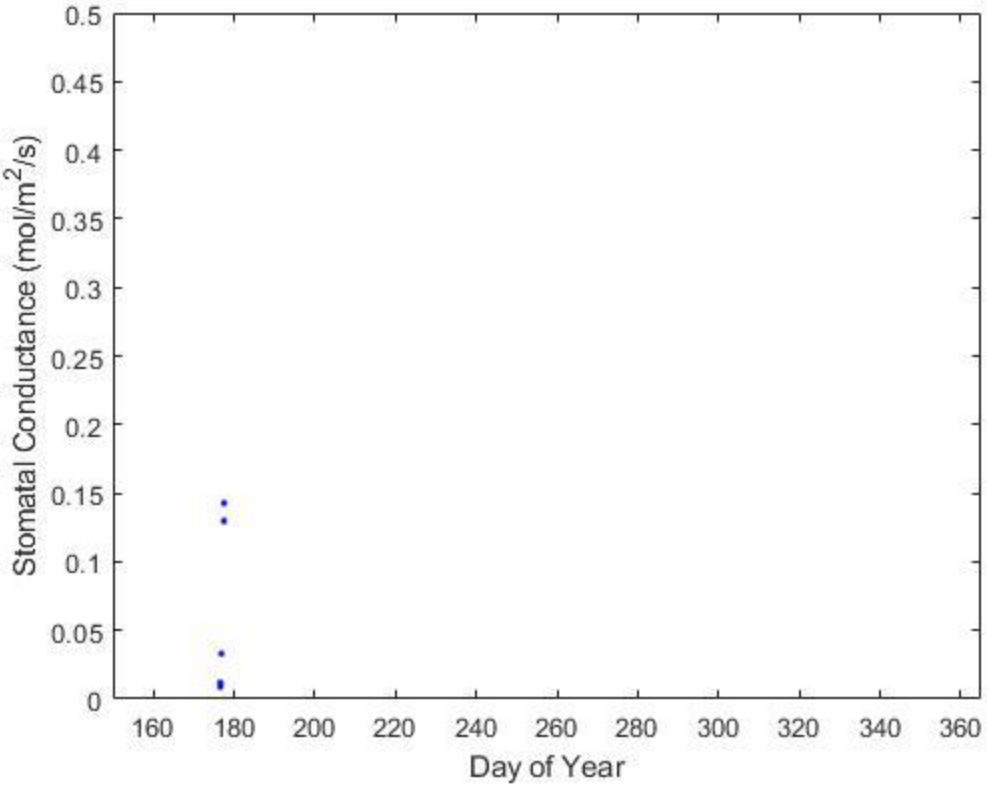

Figure 71: *All stomatal conductance measurements for P7 during 2021. n=7, where n is number of sampling points.*

3.4.3a P7 Carbon Assimilation, Stomatal Conductance, and Sap Flux

Assimilation and sap flow for P7 during Trip 2 can be viewed in **Figure 72**.

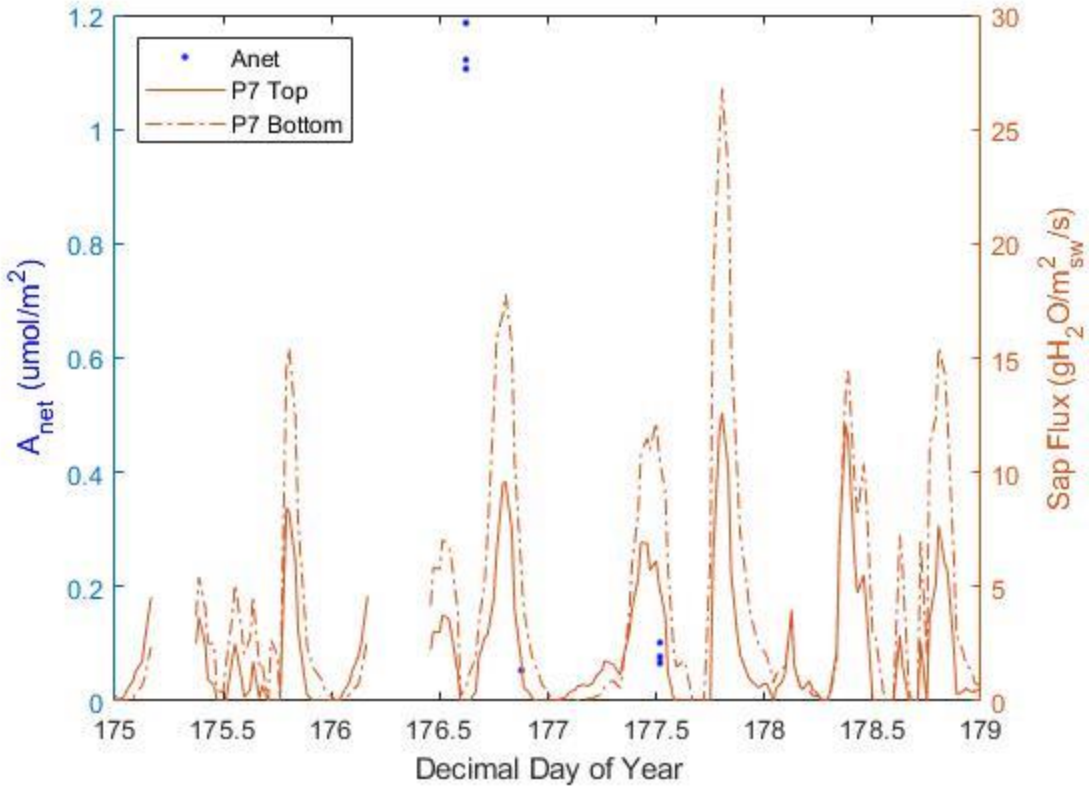

Figure 72: *Assimilation and sap flow for P7 during Trip 2 (DOY 175-DOY 179). Whole numbers on the x-axis are midnight. Numbers with half decimals (i.e, 176.5) represent noon of that day. n=7, where n is the number of sampling points.*

In **Figure 73** below, stomatal conductance and sap flow for P7 during Trip 2 can be viewed. Unfortunately, there are not many assimilation data points during Trip 2 to analyze for P7. The afternoon of DOY 176 has the highest values of the Trip (meaning this is when P7 is photosynthesizing the most), with the following nighttime showing the lowest assimilation value. However, at noon the next day, assimilation is very low.

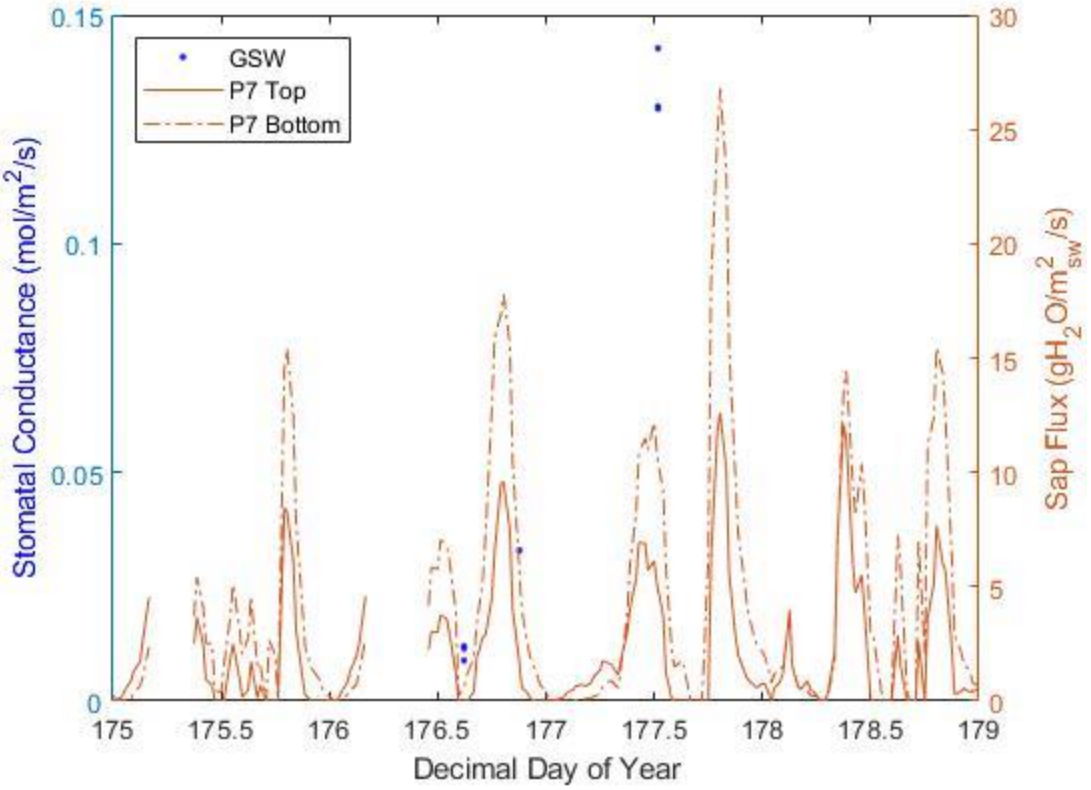

Figure 73: *Stomatal conductance and sap flow for P7 during Trip 2 (DOY 175-DOY 179). Whole numbers on the x-axis are midnight. Numbers with half decimals (i.e, 176.5) represent noon of that day. n=7, where n is the number of sampling points.*

Interestingly, stomatal conductance values are opposite of assimilation values (**Figure 72**). For example, stomatal conductance is highest just after noon of DOY 177 and lowest around 1:30 pm of DOY 176. This means stomates were much more conductive (promoting gas exchange) on DOY 177. It is important to note that in the sap flux trough of DOY 176.5, stomatal conductance values are at their minimum.

Assimilation and sap flow for Trip 6 are plotted below in **Figure 74** for P7. Bear in mind that the sap flow data is gap-filled.

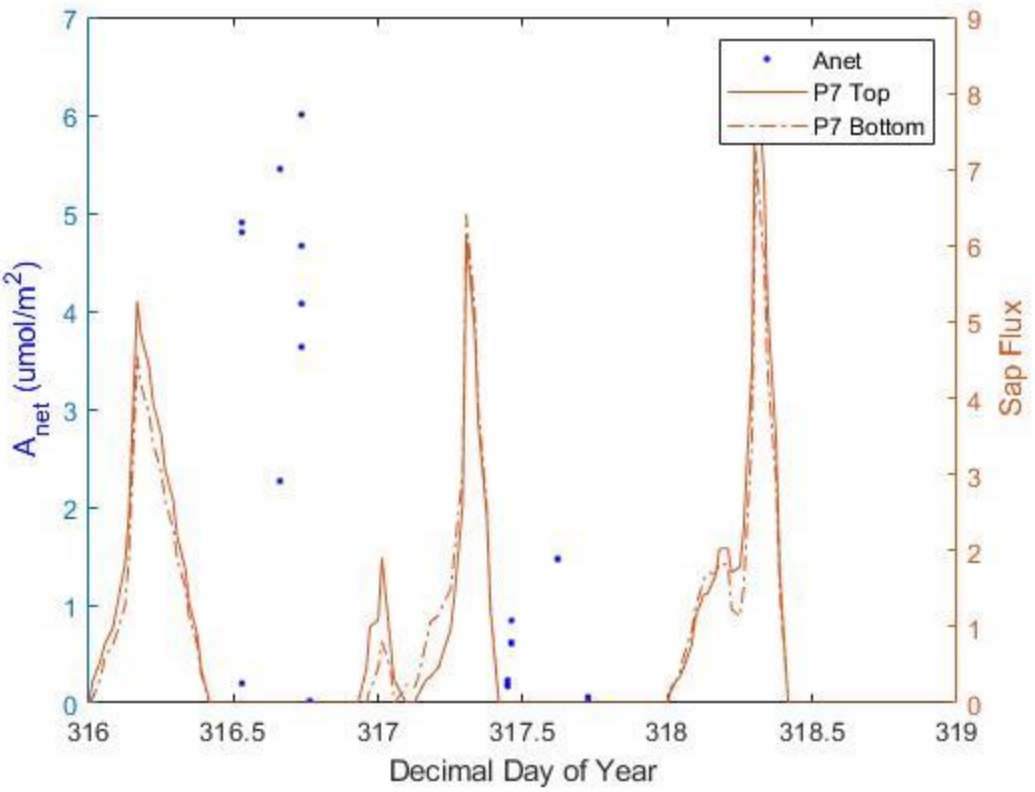

Figure 74: *Assimilation and sap flow for P7 during Trip 6 (DOY 316-DOY 319). Whole numbers on the x-axis are midnight. Numbers with half decimals (i.e, 317.5) represent noon of that day. n=17, where n is the number of sampling points.*

From this figure, it appears that assimilation increases (meaning it photosynthesizes more) throughout the afternoon, but that is the only direct conclusion that can be drawn. Lastly, there are no stomatal conductance measurements from P7 for Trip 6 due to instrument malfunction.

3.4.3b P7 Carbon Assimilation and Stomatal Conductance Responses to Meteorological Conditions

Similar to AJ1 and O6, the number of data points (for both the A_{net} and GSW regressions) is less than the actual number of data points due to time averaging while data processing.

There is no correlation or significance for P7 between assimilation and VPD (**Figure S8** in appendices). As with assimilation, there is no correlation between stomatal conductance and VPD for pine (**Figure S9**). These results indicate that VPD did not strongly affect P7's ability to photosynthesize during this period. However, the lack of data makes a true assessment of this relationship difficult. When analyzing assimilation and SWP for pines, a significant correlation was not discovered (**Figure S10** in appendices). Lastly, there was not a significant correlation found between stomatal conductance and SWP for the pines (**Figure S11** in appendices). This tells us that SWP did not strongly affect P7's photosynthesis during this period.

Chapter 4: Discussion

The purpose of this study was to determine the major environmental stresses for each species, as well as determining what causes the abnormality in diurnal sap flow patterns, where the majority of flow occurs around dawn and dusk (**Figure 1**). We determined that ashe juniper was the only species to show a correlation between both LWP & VPD and LWP & SWP, while lacy oaks and pinyon pines only had a correlation between LWP & VPD. Furthermore, lacy oaks were the only species which had any correlations regarding stomatal conductance and carbon assimilation (assimilation & VPD, assimilation & SWP, and stomatal conductance & SWP. The sap flow abnormality was determined to occur during periods which had stressful environmental conditions, such as high temperature, low precipitation, low SWC and high VPD. Lastly, we determined the sap flow artifact occurred during Trips 5 and 6, as these periods had the lowest SWC, and thus, the lowest wood water content for all 2021.

4.1 Meteorological Conditions

The only meteorological condition that looks different than expected is SWC during the stressful period (**Figure 12**). The maximum SWC value for the stressful period is ~0.14 m^3m^{-3}, while the maximum SWC for the favorable period is ~0.33 m^3m^{-3} (**Figure 14**). Both have a negative trend, but SWC for the stressful period (**Figure 12**) has a cyclical aspect to it, while SWC for the favorable period is a much smoother curve that decreases more gradually. There are a few hypotheses to explain this cyclical pattern in the SWC data. The

first is that it is caused by miniscule amounts of moisture change throughout the day (such as dew condensation and evaporation), and only occurs because of the extremely low SWC values. The second is that these are strong temperature effects on the sensor due to extremely low moisture content. Lastly, these small fluctuations may also be related to low level sensor noise.

4.2 ASHE JUNIPER

4.2.1 Ashe Juniper — Sap Flux

Daily average sap flow from Junipers for the whole year (**Figure 16**) and for the stressful period (**Figure 17**) both show the abnormality, where most of the sap flow occurs at dawn and/or dusk and is near zero during the midday. This is important to understand because it gives us insight into how these trees survive such a harsh environment. Interestingly, daily average sap flux over the favorable period (**Figure 18**) looks much more like the typical inverted parabola characteristic of sap flux in mesic ecosystems, especially in AJ3 and AJ6. Even AJ7's sap flow looks more typical during the favorable period than it did when averaged over the whole year, and AJ1 has shifted its sap flow to occur later in the day during the favorable period. One study conducted by Manandhar et al., showed that when trees are exposed to drought conditions for extended periods, peak transpiration occurs earlier in the day (2021). In almost every daily average example, all the top sensors show large spikes in sap flow during the evening, which in part may be the plant

replenishing internal water stores for the next day. Nearly all sapwood tissue can be used as water storage, and water in the leaves and upper, distal branches is transpired first at the start of a new day, as it is the closest available water to the leaf (Matheny et al., 2015; Scholz et al., 2011). A previous study showed that evening spikes in transpiration of five different tree species in central Germany are linked to changes in water storage and withdrawal (Köcher et al., 2013). After a full day of transpiration, the outer branches and leaves are replenished with water if sufficient soil moisture is available to reduce vulnerability to hydraulic stress the next day. Looking at **Figure 19**, it is clear how favorable environmental conditions, such as temperature, VPD, and SWC, promote typical sap flux patterns and increased flow magnitudes. This is further supported by **Figure 35**, where sap flow over the course of Trip 4 produces the classic, characteristic pattern. Sap flow magnitude is much higher when conditions are favorable for all junipers, with AJ3 showing the largest increase (216%) in sap flow magnitude from the stressful to the favorable period. This agrees with other studies which show that sap flow has been found to decrease during drought conditions across multiple tree species and climates, including one study regarding ashe juniper at another location on Edwards Plateau (Gartner et al., 2009; Kukowski et al., 2013). Trip 1 is the only Trip that has very limited diurnal sap flow, and while VPD and temperature for this period are the lowest of all Trips and SWC is highest, it is not in the growing season. Trips 5 and 6 did not record sap flow data even though the sensors were functioning. We hypothesize this is the sap flow artifact discussed earlier due to low SWC values and the lowest wood water content values of all 6 Trips (Beaman, 2022).

4.2.2 Ashe Juniper — Leaf Water Potential

LWP ranges from near zero to roughly -6 MPa for junipers, but the magnitude varies based on the time of year; in the winter and spring, values are less negative, but become increasingly more negative throughout the summer and into the fall (**Figure 31**). This variability is somewhat expected, as ashe junipers are anisohydric, meaning that they will continue to transpire even when soil water content decreases (Hugalde et al., 2014). LWP shows a similar pattern for every Trip (1 through 6), where AJ1's highest water stress occurs during the afternoon, after AJ1 has likely been transpiring all day. LWP then trends in a positive direction overnight and into the early morning, indicating that AJ1 is re-hydrating its xylem tissues as hypothesized based on the sap flow data (Scholz et al., 2011). It has been shown that transpiration at the start of the day typically comes from internal water storage, so we would expect water content, and thus LWP, to decrease when sap flux begins (Waring & Running, 1978). When AJ1 is hydrated again as indicated by less negative LWP values, sap flow resumes. This supports our theory that the abnormal spikes in sap flux data are due to replenishment of stored water. Trip 6 (**Figure 37**) had the most negative LWP values of all Trips, with much less variability between data points than seen in the other Trips. VPD and temperature were not unusually high for this period, but SWC was extremely low, measuring just 0.06 m^3m^{-3} on average for the whole Trip. One study found a similar result, where stem water stores became exhausted at low SWP values (Köcher et al., 2013). It is also worth noting that Trip 5 (**Figure 36**) and Trip 2 (**Figure 33**) had the next most negative LWP values out of all Trips. Both Trips 2 and 5 had warm temperatures, and Trip 2 had the second lowest SWC of all Trips. SWC was not available

for Trip 5 due to sensor malfunction but is expected to be between 0.05 and 0.1 m^3m^{-3} based on the negative trend in the SWC curve and there being little to no rain received during this time. These results are important, as they could explain why Trips 2 and 5 had such negative LWP values, as well as recording highly variable sap flow. LWP magnitudes for Trip 3 (**Figure 34**) were not far behind that of Trips 2 and 5, as temperature and VPD are still high, but SWC is relatively high for this period in comparison to the other Trips, so that may explain why LWP is not as high as in Trips 2 and 5. Lastly, LWP was the least negative, indicating good hydration, for Trips 1 and 4, respectively. All of which indicate that junipers are more water-stressed as temperature, VPD, and SWC become increasingly more stressful. Trip 4 was in the growing season and had moderately warm temperatures with high SWC, corresponding to the 'favorable period'. Based on the regressions in **Figure 38** and **Figure 39**, VPD and LWP were found to have a weak but significant correlation, while SWP and LWP were found to have a medium strength and significant correlation. As junipers are the only plant that shows a correlation between LWP and SWP, we hypothesize that this is due to junipers having an extensive lateral root system, with not as much focus on the roots growing deep (Mollnau et al., 2014; Northup et al., 2021). These results, taken together, indicate that junipers are more dependent on SWP than on VPD. Therefore, junipers are more reliant on water supply than they are dependent on atmospheric water demand. With future climate change potentially increasing VPD and decreasing SWP, junipers could face increasing risk of mortality.

4.2.3 Ashe Juniper — Carbon Assimilation and Stomatal Conductance

Carbon assimilation and stomatal conductance measurements were recorded during Trips 2 and 6. While sap flow for Trip 2 is inconsistent and has gaps, assimilation for Trip 2 (**Figure 57**) is highest in the afternoon and lowest at night, meaning that AJ1 is photosynthesizing more during the day, as expected. Assimilation for Trip 6 (**Figure 59**) shows similar results, where assimilation is highest in the afternoon and lowest at night. However, DOY 317 shows that assimilation can have large differences in magnitude over a short change in time, indicating that AJ1 will decrease photosynthesis if environmental conditions are stressful enough. This supports our theory of stomatal closure during stressful periods leading to the abnormalities in the sap flow pattern. Stomatal conductance during Trip 2 (**Figure 58**) shows a similar pattern to assimilation, where the stomata are more conductive in the middle of the day than at night. Higher stomatal conductance values explains why LWP values are more negative during the middle of the day; if the stomates are more open, more water is transpired, increasing the water-stress (e.g. lowering the LWP) of the plant. One study in southern Italy found that when hydraulic conductivity is decreased due to drought conditions, LWP and stomatal conductance of *P. Pinaster* decreased as well (Ripullone et al., 2007). Stomatal conductance decreases very quickly at the end of DOY 177 (**Figure 58**), implying that the stomata are closing as night starts. This is what allows us the see if the trees should be transpiring or not; if the stomata are open, then water is being lost. It is important to note that sap flow is being observed one to several meters away along the xylem's flow path from where LWP, carbon assimilation, and stomatal conductance measurements are

being taken at the leaf. This distance is likely the source of the time lag between the midmorning sap flux spike in DOY 177 and the higher stomatal conductance values just a few hours later (**Figure 58**). Stomatal conductance is low when sap flow starts again in the evening, which may indicate the plant closing its stomata in order to build up water stores overnight (Scholz et al., 2011). During Trip 6, however, (**Figure 59** and **Figure 60**), assimilation can be seen decreasing rapidly in the midafternoon for both DOY 316 and 317. A similar sharp decrease can be seen in stomatal conductance for the afternoon of DOY 317, indicating that AJ1 does close its stomata in the afternoon to avoid stressful conditions. One study has shown that drought conditions will cause stomatal closure earlier in the day in *Vitis vinifera* (Manandhar et al., 2021), while another study shows that other oak and pine species will reduce stomatal conductance at midday and early afternoon to protect the plant from further water loss (Mirfenderesgi et al., 2016). The fact that Trip 6 was the Trip with lowest SWP, recorded inconclusive sap flow data, and AJ1 had the strongest relationship between water-stress and SWP, likely indicate that the junipers will potentially cease photosynthesizing and close their stomata when environmental factors become stressful. However, junipers and their drought-tolerant nature may be less-vulnerable than other species, as no correlation or significance was found between carbon assimilation and VPD (**Figure S3**), along with no correlation or significance being found between stomatal conductance and VPD (**Figure S4**). Assimilation and SWP (**Figure S5**), along with assimilation and stomatal conductance (**Figure S6**) only have two values for this study, hindering our abilities to draw conclusions about AJ1's assimilation and stomatal conductance responses to SWP

changes. Based on the regressions displayed earlier, we can conclude that SWP is the most limiting factor in this environment for ashe junipers (**Figure 39**).

4.3 LACEY OAK

4.3.1 Lacey Oak — Sap Flux

Daily average sap flow for both the entire year (**Figure 21**) and the stressful period (**Figure 22**) highlight the sap flux abnormality in lacey oaks. In general, the oaks tend to have larger and more frequent sap flow spikes at dawn and dusk than the junipers. As with the junipers, the evening sap flow spikes may be from water-storage accumulating for use the next day (Köcher et al., 2013; Scholz et al., 2011). However, the more common morning sap flow spikes in the oaks could indicate that they have a greater need for water storage, not only having to fill back up at the end of the day, but also filling up before the day starts as well. In general, the oaks are the tallest trees in this study (**Table 2**). Scholz et al., found that taller trees have a greater volume of stored water, so the refilling of this additional water storage could explain the occurrence of more common morning and evening sap flux spikes in the oaks than the junipers (2011). Notice how the morning sap flow spikes practically disappear during the favorable period (**Figure 23**), which was also the case for junipers (**Figure 18**). This, on top of the fact that the oaks have sap flow spikes in the morning during the stressful period (**Figure 22**), indicates that the oaks could have a need to store more water to survive than junipers do, especially since the oaks appear to be refilling so often. O5 tends to have the most variability in sap flow, and the variability becomes even more

unpredictable during the stressful period (**Figure 22**) but trends back to a more natural curve during the favorable period (**Figure 23**), indicating that sap flow behaves erratically during stressful environmental conditions. Furthermore, changes in sap flow patterns and magnitudes can be observed when conditions are favorable versus when they are stressful (**Figure 24**). O6 was found to increase sap flow 225% during the favorable period as compared to the stressful, and the diurnal sap flow pattern for every oak is very similar to a typical inverted parabola. Typical sap flow with varying degrees of dawn and dusk sap flow spikes can be observed for the first four days of the stressful period in **Figure 43**, reinforcing the idea that oaks will shift their sap flux patterns with environmental conditions. Sap flux was not recorded during Trip 6, although the sensors were functioning. As with the junipers, we hypothesize this is the sap flow artifact discussed earlier due to low SWC values and the lowest wood water content values of all 6 Trips (Beaman, 2022).

4.3.2 Lacey Oak — Leaf Water Potential

LWP for the oaks shares a similar pattern with junipers, where LWP becomes increasingly negative throughout the morning, reaching maximum water-stress in the afternoon, before trending less negative throughout the night and early morning. LWP magnitudes are relatively the same for every Trip, with values ranging from near zero to roughly -4 MPa. However, Trip 5 (**Figure 44**) has by the far the least negative values of any Trip with the most negative value at just -0.84 MPa. Some variability is expected, as lacey oaks are anisohydric just as junipers are. VPD and temperature were moderate for Trip 5, but unfortunately, no SWC values were recorded during this period. O6 was found to have a

strong relationship between VPD and LWP (**Figure 46**), meaning that the plant is under more water-stress during higher VPD values. Such a strong relationship alone puts the oaks at an increased vulnerability to climate change, as increasing VPD would be detrimental to lacey oaks. However, O6 did not show a relationship between SWP and LWP. This independence from soil water suggests that oaks could have the ability to root to deeper depths, accessing unknown water sources in this karst landscape that junipers cannot, as junipers are generally knows as being shallow-rooted, while oaks have been found to have very deep roots (Jackson et al., 1997; Northup et al., 2021; Schwinning, 2008).

4.3.3 Lacey Oak — Carbon Assimilation and Stomatal Conductance

As with juniper, assimilation and stomatal conductance measurements were recorded on Trips 2 and 6. While sap flow for the first half of Trip 2 (**Figure 63**) is inconsistent, assimilation shows us a similar pattern to what was observed in junipers, where assimilation is highest in the day and lowest at night, showing that O6 is photosynthesizing during the day as one would expect. If we look at stomatal conductance during Trip 2 (**Figure 64**), it's clear that the stomata are regulated more during DOY 176, when sap flow is very low and inconsistent. We have established that sap flow is low and inconsistent during the day when environmental conditions are more stressful, so the stomates being more regulated during this time is highly likely. Midday stomata closure has been shown to occur in oaks and pines during drought conditions (Matheny et al., 2014; Mirfenderesgi et al., 2016). When sap flow increases from DOY 176 to DOY 177, stomatal conductance increases by 130%, furthering the idea that these plants will regulate their stomates more

during stressful environmental conditions. While there is no sap flow data, assimilation in Trip 6 (**Figure 65**) shows the same pattern, with higher rates at midday. Looking at stomatal conductance for Trip 6 (**Figure 66**), one should notice that the magnitude has decreased by 40% from Trip 2 (**Figure 64**), which is important because Trip 6 has the lowest SWC values of all the Trips. In fact, assimilation for O6 was found to have a strong but not significant correlation (r^2=0.55, P-value=.092) with SWP (**Figure 68**), while stomatal conductance was found to have a very strong and significant correlation (r^2=0.858, P-value=.008) with SWP (**Figure 69**). Both relationships tell us that oaks will be less productive and limit their stomata more closely as SWP values become more negative. Furthermore, assimilation from O6 was found to have a strong and significant correlation (r^2=0.2855, P-value=.06) with VPD (**Figure 67**). This is yet another reason that lacey oaks are vulnerable to climate change, more so even than the other species of this study.

4.4 PINYON PINE

4.4.1 Pinyon Pine — Sap Flux

The sap flux abnormality can be seen in P4, P6, and P7 for daily average plots of the whole year (**Figure 26**). P2 produces more typical sap flux patterns than the others, especially the bottom sensor. If we observe sap flow during the stressful period (**Figure 27**), it is clear that flow shifts to earlier in the morning and ceases for the rest of the day for all four pines. During this same period, P2's bottom sensor and P6's top sensor show variability after the

morning spike, which could potentially be equated to stem-water storage being replenished (Köcher et al., 2013; Matheny et al., 2015). Another study in Austria found similar results, where spruce trees would show a reduction in midday sap flow during drought conditions (Gartner et al., 2009). As with juniper (**Figure 18**) and oak (**Figure 23**), the pines' sap flow patterns returns to more typical shapes when environmental conditions are favorable (**Figure 28**). Moreover, sap flow was found to increase for every pine from the stressful period to the favorable period, with P6 having the highest increase in flow at 350% (**Figure 29**). Diurnal sap flow for P7 during Trip 4, which coincides with the first four days of the favorable period, show typical inverted parabolas, with morning and evening spikes in flow visible. Taken together, these results indicate that stressful environmental conditions (such as elevated temperature and VPD) affect pine's sap flow occurrence and magnitude. Trips 5 and 6 only recorded sap flow during the morning period, just as we observed with junipers. Based on the low wood water content values during this time (Beaman, 2022), we hypothesize that this is an example of the sap flow artifact.

4.4.2 Pinyon Pine — Leaf Water Potential

Pinyon pine showed very similar LWP values for each trip, regardless of time of year. With ranges from near zero to just above -3 MPa, pines have the smallest range of LWP values in this study. This should come as no surprise, because unlike junipers and oaks, the pines are isohydric, meaning that they will quit transpiring if soil water content becomes too low (Hugalde et al., 2014). In general, P7 shows a similar daily LWP pattern as AJ1 and O6, where LWP is most negative in the afternoon, with values trending less negative

throughout the night and early morning. However, Trip 6 (**Figure 53**) shows LWP is most negative at night and in the early morning, with less negative values in the middle of the day. Studies from a Brazilian savannah environment (Cerrado) and the southwest United States showed that predawn LWP trends more negative with increasing nighttime water loss (via transpiration), especially during low SWP values (Bucci et al., 2005; Donovan et al., 1999; Williams & Ehleringer, 2000). With Trip 6 having the lowest SWP of all Trips, this is the likely hypothesis for the nighttime LWP maximums. The sap flow data is gap-filled during this Trip, so it only provides an approximation of what sap flow may have looked like. LWP shows more variability between Trips 1-6 than O6 did, but not as much as AJ1. Trip 2 (**Figure 49**) has the most negative LWP values, along with having the most inconsistent sap flow of all Trips that have sap flow data. Trip 2 (May 18-22) had the highest temperatures and VPD along with the second lowest SWC. Out of all six Trips, Trip 4 (**Figure 60**) has the least negative LWP values, which coincides with the favorable period. P7 was shown to have a weak but significant relationship (r^2=0.1671, P-value=$6.65x10^{-8}$) between LWP and VPD (**Figure 54**), but no correlation between LWP and SWP (**Figure S2**). Much like O6 (**Figure S1**), this could mean P7 has a less-obvious water source that AJ1 (**Figure 39**) does not have access to. This could be a byproduct of location, rooting depth and age, or tree and root morphology. O6 and P7 are located more closely to one another than either are to AJ1.

4.4.3 Pinyon Pine — Carbon assimilation and Stomatal Conductance

Assimilation from P7 during Trip 2 (**Figure 72**) shows that values can be high one day (seen in DOY 176) but low the next (DOY 177). Assimilation during the middle of DOY 177 is near zero, just as low of values as the night before, meaning that P7 is not photosynthesizing in the middle of the day. Stomatal conductance during the same trip (**Figure 73**) shows similar results, but stomatal conductance is near zero during DOY 176 (when assimilation is highest for the Trip) and highest during DOY 177 (when assimilation is near zero). A previous study also showed that some C3 desert shrubs will have conductive stomata and photosynthesize at night (Donovan et al., 1999), while another study showed that assimilation and stomatal conductance will approach zero during midday during the dry season in a similar environment in Israel (Klein et al., 2016). Minimum stomatal conductance values coincide with a lag in sap flow during the midafternoon of DOY 176, with higher rates later that evening when sap flow is higher. The maximum stomatal conductance values occur at the same time as midday sap flow during DOY 177. Assimilation for Trip 6 (**Figure 74**) shows a similar pattern as Trip 2, where values are high one day and less than one-third of the magnitude the next day. Unfortunately, sap flow during this period is gap-filled, and there are no stomatal conductance values. Moreover, neither assimilation or stomatal conductance was found to be correlated with either VPD or SWP (**Figure S8** through **Figure S11**). This lack of correlation may be due to the small number of data points. However, the fact that we can observe stomatal conductance, assimilation and sap flow values near zero in the middle of the day support our hypothesis that pinyon pines will regulate their stomata in response to stressful conditions, albeit if not

as much as oaks. While other species may be more vulnerable to stressful conditions, future climate change could prove detrimental to pinyon pines in hot semi-arid environments.

Chapter 5: Conclusion

This study revealed different transpiration, leaf water potential, assimilation and stomatal conductance patterns from ashe juniper, lacey oak and pinyon pine. All three species showed sap flux increases that occur near dusk and dawn when environmental conditions are stressful. When conditions are favorable, diurnal sap flow patterns shifts back to midday, resembling an inverted parabola, along with having sap flow magnitude increase by at least 100% for every tree. The cause of these abnormal dawn and dusk sap flow spikes is challenging to pinpoint, as the relationships between variables are highly interrelated. Leaf water potential shows a similar daily pattern for all the trees (excluding P7 during Trip 6), where LWP is least negative (least stressed) in the morning, trending increasingly negative during the day, before trending back to less negative values as the late evening and night continue. Junipers were found to have a weak relationship between LWP and VPD, along with a medium correlation between LWP and SWP, indicating that they leave stomata open and incur water stress during dry conditions. Lacey oaks were found to have a strong correlation between VPD and LWP, indicating that they become more stressed than junipers with increasing VPD. However, no relationship was found between LWP and SWP for oaks, or for pinyon pines. This may indicate that pines and oaks rely on a different water source than the junipers. The pines showed a weak

correlation between LWP and VPD, indicating that all three species are vulnerable to increasing climate change, with oaks being the most vulnerable and junipers being the least. The strong correlation between LWP and SWP tells us that juniper is more reliant on shallow soil waters than the other species, which puts the junipers at an elevated risk. Leaf-level carbon assimilation and stomatal conductance showed no relationships between VPD and SWP for junipers. However, the lack of data points makes it challenging to draw conclusions from this analysis. Oaks showed a correlation between assimilation and VPD, a strong relationship between assimilation and SWP, and a very strong relationship between stomatal conductance and VPD. Taken together, this indicates that increasing drought conditions will affect lacey oaks' ability to assimilate carbon and photosynthesize, making the oaks more vulnerable to atmospheric drought. With only one weak correlation between VPD and LWP, the pines being able to shift transpiration earlier in the day when environmental conditions are stressful, and their ability to close stomata to maintain relatively constant LWP, the pines are the least vulnerable of the three species to climate change at this location. However, our results indicate that future climate change puts all species in hot semi-arid climates, and even other species in the Texas hill country, at elevated risk of mortality. Considering that vegetation plays a vital role in regulating numerous climatic feedback loops, humans should be concerned with furthering research about vegetation adaptations, especially those already in dry environments.

Appendices

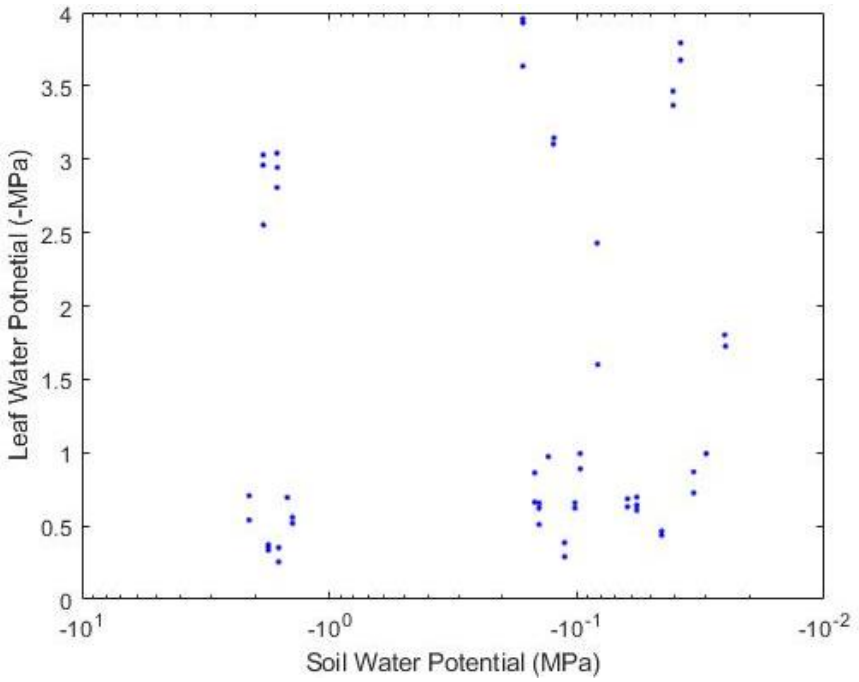

Figure S1: *LWP and SWP for all LWP measurements from O6 in 2021. R2 and P values are not listed because no correlation was found.*

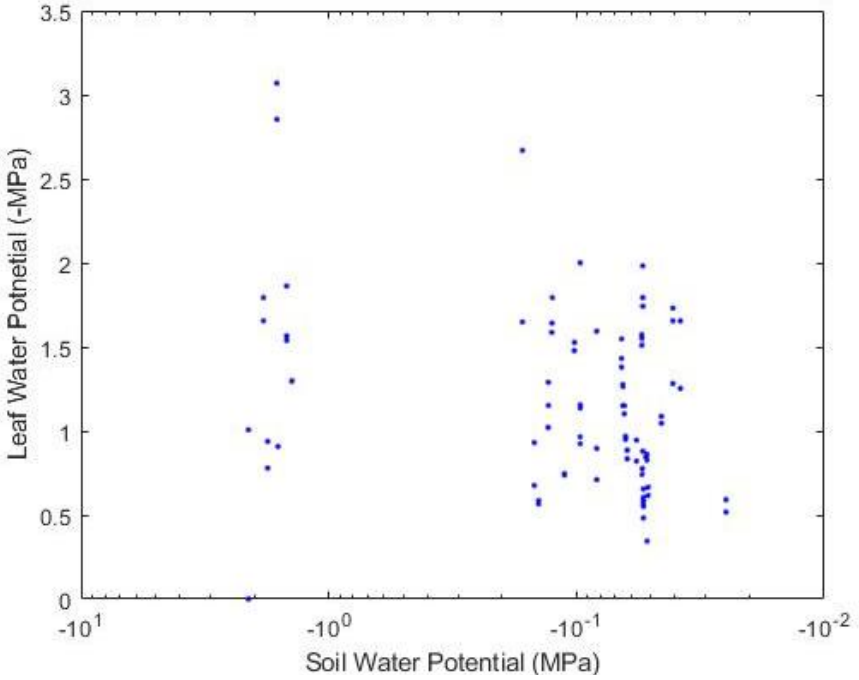

Figure S2: *LWP and SWP for all LWP measurements from P7 in 2021. R2 and P values are not listed because no correlation was found.*

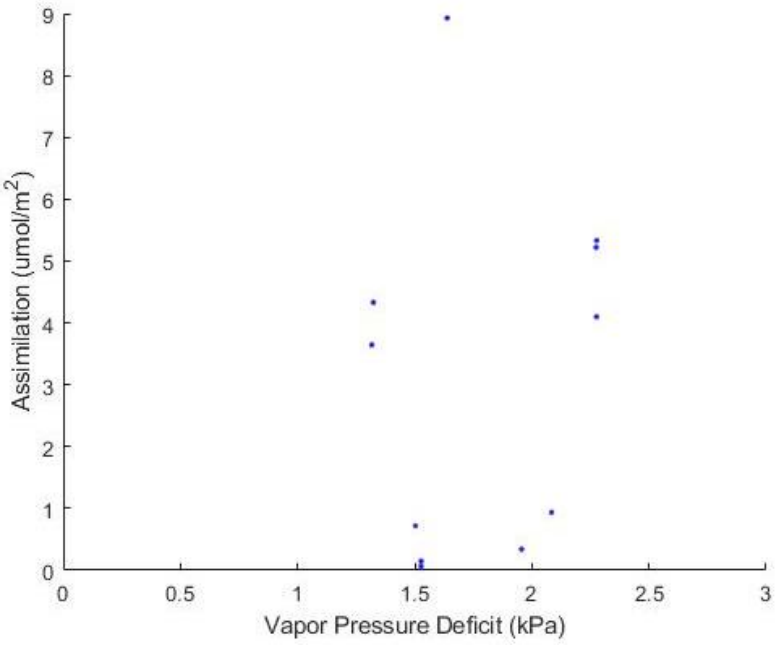

Figure S3: *Assimilation measurements for AJ1 during 2021 with respect to VPD. No P value or R2 reported, as no correlation or significance was found. n=12, where n is the number of sample points.*

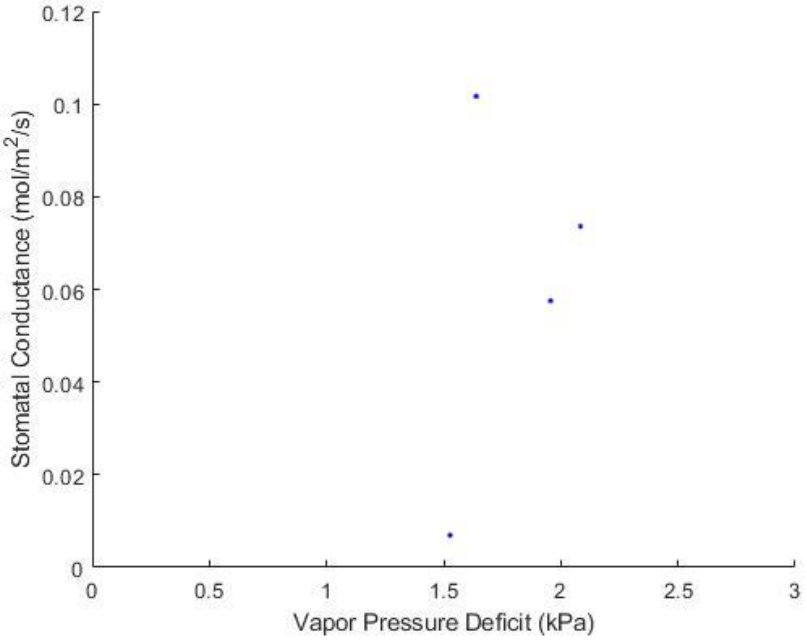

Figure S4: *Stomatal conductance measurements for AJ1 during 2021 with respect to VPD. No P value or R2 reported, as no correlation or significance was found. n=4, where n is the number of sample points.*

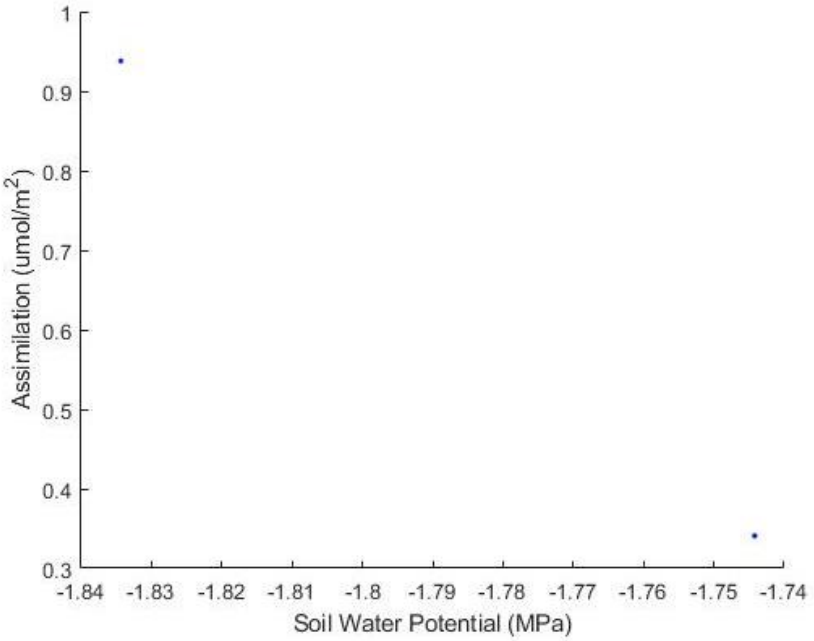

Figure S5: *Assimilation and SWP for AJ1 during 2021. n=2, where n is the number of sample points. No P-value or R2 reported, as there are only 2 points.*

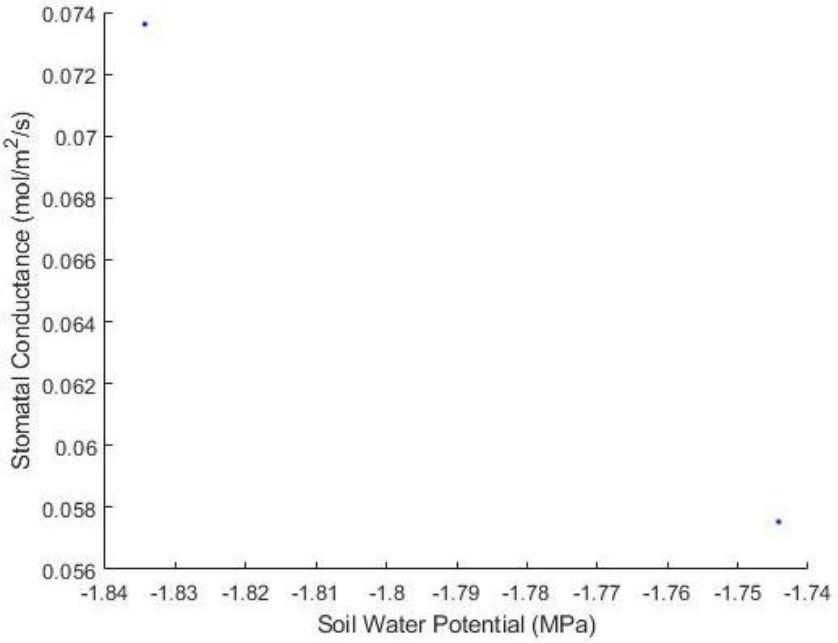

Figure S6: *Stomatal conductance and SWP for AJ1 during 2021. n=2, where n is the number of sample points. No P-value or R2 reported, as there are only 2 points.*

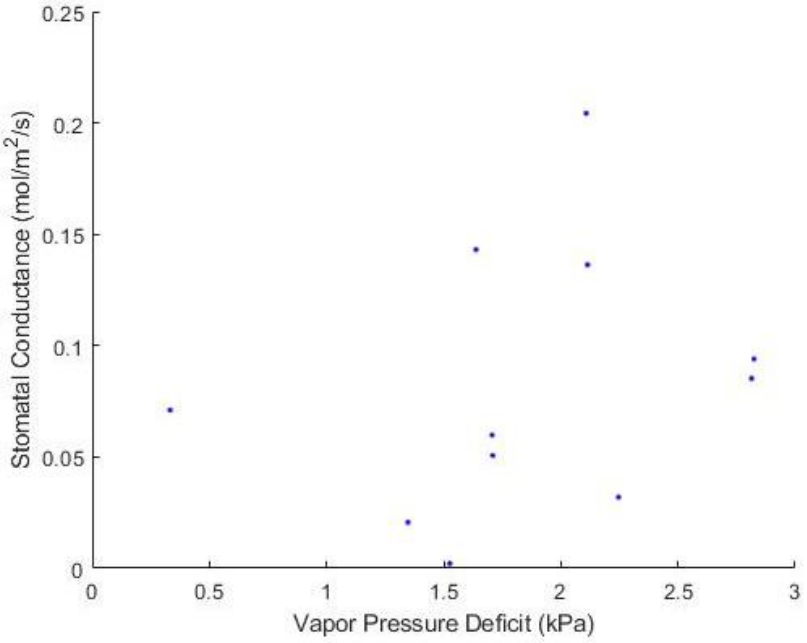

Figure S7: *Stomatal conductance measurements for O6 during 2021 with respect to VPD. No P value or R2 reported, as no correlation or significance was found. n=11, where n is the number of sample points.*

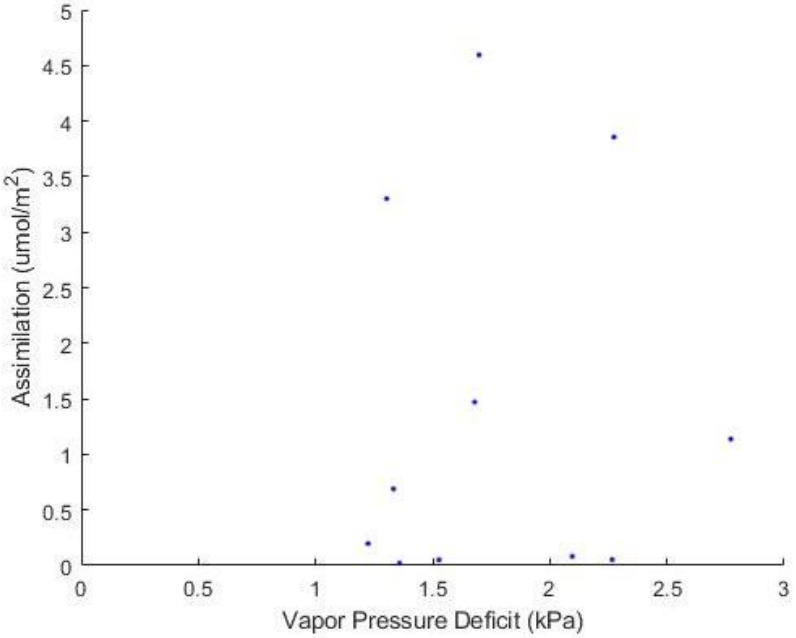

Figure S8: *Assimilation measurements for P7 during 2021 with respect to VPD. No P value or R2 are reported, as no correlation or significance was found. n=11, where n is the number of sample points.*

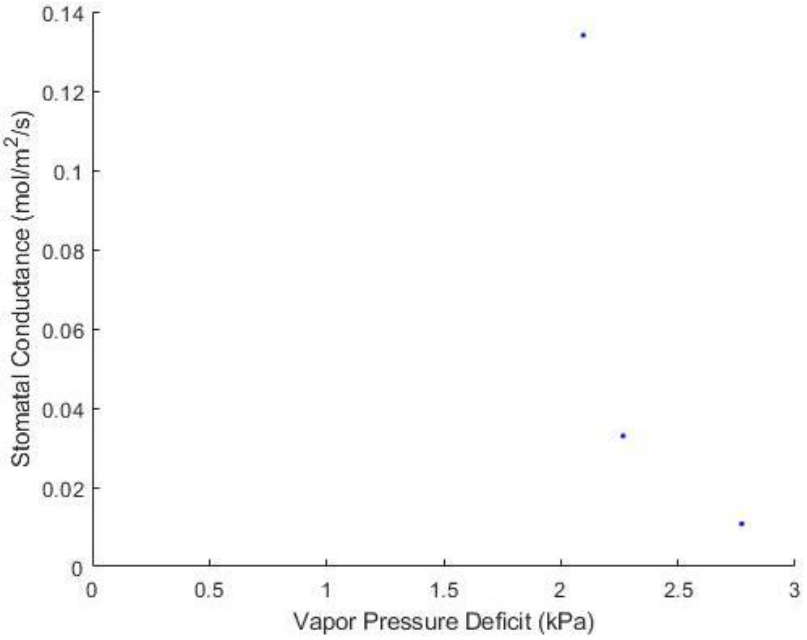

Figure S9: *Stomatal conductance measurements for P7 during 2021 with respect to VPD. No P value or R2 are reported, as no correlation or significance was found. n=3, where n is the number of sample points.*

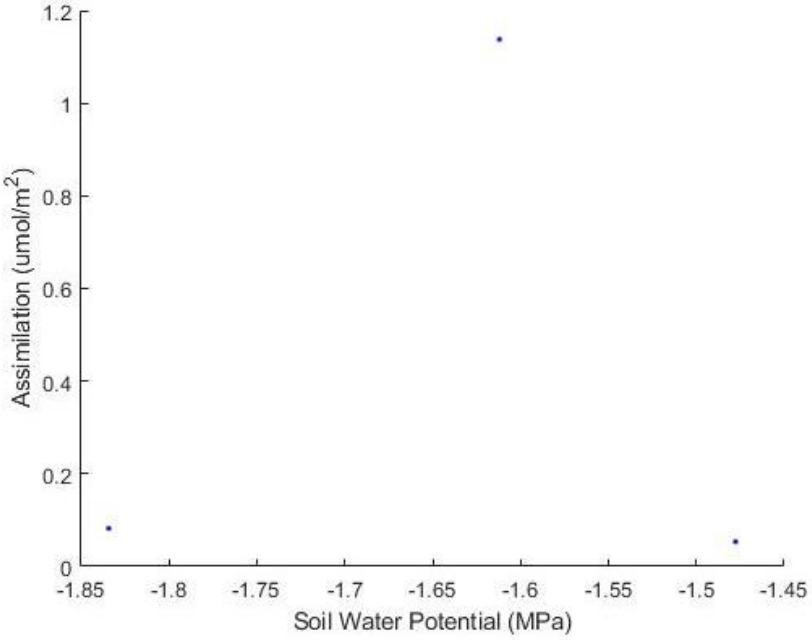

Figure S10: *Assimilation and SWP for P7 during 2021. n=3, where n is the number of sample points. No P-value or R2 reported, as no relationship was found.*

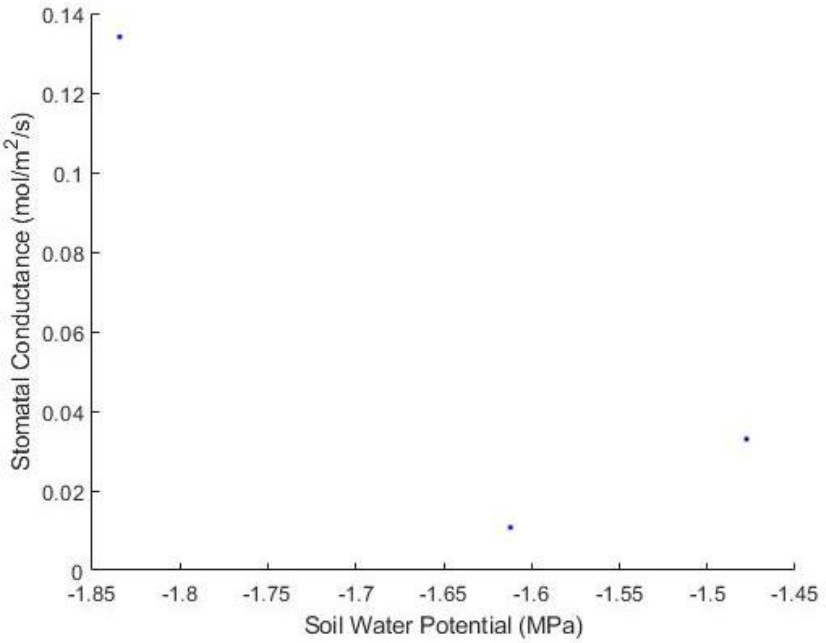

Figure S11: *Stomatal conductance and SWP for P7 during 2021. n=3, where n is the number of sample points. No P-value or R2 reported, as no relationship or significance was found.*

Table S1: *All LWP values in this study. Species number identifies which species the recording is from. Ashe Juniper = 1, Lacy Oak = 2, and Pinyon Pine = 3.*

DOY	Hour	Minute	Species Number	-PSI	-MPa
29	22	35	3	87.5	0.603292
29	22	40	3	92.7	0.639144
29	22	42	3	96.4	0.664655
29	22	46	3	89.3	0.615702
29	22	35	3	87.5	0.603292
29	22	40	3	92.7	0.639144
29	22	44	3	96.4	0.664655
29	22	48	3	89.3	0.615702
30	06	11	1	210	1.4479
30	06	18	1	245	1.689216
30	06	20	1	280	1.930533
30	06	22	1	100	0.689476
30	06	24	1	100	0.689476
30	06	26	1	92	0.634318

30	07	11	1	110	0.758424
30	07	14	1	107	0.737739
30	07	15	1	92	0.634318
30	12	11	1	290	1.99948
30	12	16	1	294	2.027059
30	12	18	1	297	2.047744
30	22	45	1	125	0.861845
30	22	50	1	117	0.806687
30	22	52	1	146	1.006635
30	22	54	1	139	0.958372
30	06	11	1	210	1.4479
30	06	18	1	245	1.689216
30	06	20	1	280	1.930533
30	06	22	1	100	0.689476
30	06	24	1	100	0.689476
30	06	26	1	92	0.634318
30	07	11	1	110	0.758424
30	07	14	1	107	0.737739
30	07	15	1	92	0.634318
30	08	14	1	92.5	0.637765
30	08	16	1	92.5	0.637765
30	08	18	1	90	0.620528
30	12	13	1	290	1.99948
30	12	16	1	294	2.027059
30	12	18	1	297	2.047744
30	15	08	1	290	1.99948
30	15	11	1	290	1.99948
30	15	14	1	285	1.965007
30	20	16	1	142.5	0.982503
30	20	18	1	135	0.930793
30	20	20	1	140	0.965266
30	21	14	1	130	0.896319
30	21	16	1	127.5	0.879082
30	21	16	1	135	0.930793
30	22	47	1	125	0.861845
30	22	50	1	117	0.806687
30	22	52	1	146	1.006635
30	22	54	1	139	0.958372

30	06	31	3	95	0.655002
30	06	33	3	85	0.586055
30	06	35	3	82.5	0.568818
30	07	03	3	87.5	0.603292
30	07	05	3	85	0.586055
30	07	06	3	82.5	0.568818
30	12	00	3	225	1.551321
30	12	02	3	228	1.572005
30	12	05	3	219	1.509952
30	22	58	3	112.5	0.775661
30	23	01	3	112.5	0.775661
30	23	03	3	107.5	0.741187
30	06	31	3	95	0.655002
30	06	33	3	85	0.586055
30	06	35	3	82.5	0.568818
30	07	03	3	87.5	0.603292
30	07	05	3	85	0.586055
30	07	06	3	82.5	0.568818
30	08	22	3	70	0.482633
30	08	27	3	87.5	0.603292
30	08	29	3	80	0.551581
30	08	32	3	80	0.551581
30	12	01	3	225	1.551321
30	12	04	3	228	1.572005
30	12	07	3	219	1.509952
30	15	19	3	127.5	0.879082
30	15	26	3	287.5	1.982244
30	15	28	3	260	1.792638
30	15	31	3	252.5	1.740927
30	20	24	3	120	0.827371
30	20	25	3	120	0.827371
30	20	27	3	50	0.344738
30	20	29	3	125	0.861845
30	21	02	3	122.5	0.844608
30	21	04	3	122.5	0.844608
30	21	05	3	117.5	0.810134
30	22	58	3	112.5	0.775661
30	23	01	3	112.5	0.775661

30	23	03	3	107.5	0.741187
31	09	04	3	136.4	0.940445
31	09	06	3	140.2	0.966645
31	09	08	3	137.9	0.950787
31	09	55	3	167.6	1.155562
31	09	57	3	166.8	1.150046
31	09	58	3	159.8	1.101783
31	11	03	3	184.9	1.274841
31	11	08	3	166.8	1.150046
31	11	10	3	183.6	1.265878
31	11	12	3	182.1	1.255536
31	11	59	3	224.4	1.547184
31	12	02	3	200.1	1.379641
31	12	04	3	202.4	1.395499
31	12	06	3	207.6	1.431352
31	09	04	3	136.4	0.940445
31	09	06	3	140.2	0.966645
31	09	08	3	137.9	0.950787
31	09	55	3	167.6	1.155562
31	09	57	3	166.8	1.150046
31	09	58	3	159.8	1.101783
31	11	03	3	184.9	1.274841
31	11	08	3	166.8	1.150046
31	11	10	3	183.6	1.265878
31	11	12	3	182.1	1.255536
31	11	59	3	224.4	1.547184
31	12	02	3	200.1	1.379641
31	12	04	3	202.4	1.395499
31	12	06	3	207.6	1.431352
175	22	02	1	334	2.30285
175	22	05	1	335	2.309745
175	22	07	1	322	2.220113
175	22	22	2	81	0.558476
175	22	25	2	75.2	0.518486
175	22	27	2	75	0.517107
175	22	12	3	188	1.296215
175	22	14	3	190.1	1.310694
175	22	16	3	188.2	1.297594

176	06	03	1	227	1.565111
176	06	05	1	233.1	1.607169
176	06	08	1	234.9	1.619579
176	14	55	1	496.4	3.422559
176	14	57	1	465	3.206063
176	14	59	1	449.4	3.098505
176	20	55	1	389.2	2.683441
176	20	58	1	356	2.454535
176	21	01	1	378	2.606219
176	06	21	2	38	0.262001
176	06	23	2	51	0.351633
176	06	25	2	37	0.255106
176	14	38	2	441	3.040589
176	14	40	2	407	2.806167
176	14	43	2	426.9	2.943373
176	21	13	2	100.7	0.694302
176	21	15	2	99.4	0.685339
176	06	12	3	127.9	0.88184
176	06	16	3	131.6	0.90735
176	06	18	3	128.4	0.885287
176	14	46	3	445	3.068168
176	14	48	3	413.8	2.853052
176	14	50	3	429.8	2.963368
176	21	06	3	270	1.861585
176	21	08	3	223	1.537531
176	21	09	3	227	1.565111
177	06	29	1	283	1.951217
177	06	32	1	271.8	1.873996
177	06	35	1	343.2	2.366282
177	12	24	1	414.8	2.859946
177	06	09	2	54	0.372317
177	06	11	2	48.5	0.334396
177	06	14	2	51.3	0.353701
177	12	36	2	370	2.551061
177	12	38	2	439.2	3.028179
177	12	40	2	429.1	2.958542
177	06	20	3	113	0.779108
177	06	23	3	136	0.937687

177	06	25	3	136	0.937687
177	12	28	3	240	1.654742
177	12	30	3	260	1.792638
177	12	32	3	246	1.696111
178	12	21	1	506.7	3.493575
178	12	22	1	453.4	3.126084
178	21	35	1		0
178	21	16	2	102.3	0.705334
178	21	18	2	97.1	0.669481
178	21	20	2	78.4	0.540549
178	21	23	3		0
178	21	26	3	146	1.006635
178	21	29	3		0
218	20	48	1	220	1.516847
218	20	55	1	265	1.827111
218	20	59	1	195	1.344478
218	21	05	3	290	1.99948
218	21	17	3	140	0.965266
219	06	07	1	255	1.758164
219	06	09	1	149	1.027319
219	06	12	1	148	1.020424
219	06	14	1	144	0.992845
219	15	02	1	373	2.571745
219	15	04	1	375	2.585535
219	15	06	1	355	2.44764
219	20	22	1	265	1.827111
219	20	24	1	223	1.537531
219	20	27	1	243	1.675427
219	06	30	2	48	0.330948
219	06	34	2	42	0.28958
219	06	36	2	56	0.386107
219	14	52	2	450	3.102642
219	14	58	2	456	3.144011
219	20	39	2	132	0.910108
219	20	41	2	141	0.972161
219	20	42	2	152	1.048004
219	06	20	3	108	0.744634
219	06	22	3	107	0.737739

219	06	24	3	103	0.71016
219	14	37	3	230	1.585795
219	14	40	3	238	1.640953
219	14	44	3	260	1.792638
219	20	32	3	167	1.151425
219	20	34	3	187	1.28932
219	20	37	3	148	1.020424
220	03	18	1	125	0.861845
220	03	20	1	127	0.875635
220	03	22	1	123	0.848055
220	06	00	1	130	0.896319
220	06	02	1	148	1.020424
220	06	04	1	142	0.979056
220	13	21	1	355	2.44764
220	13	22	1	398	2.744114
220	13	23	1	425	2.930273
220	03	04	2	95	0.655002
220	03	06	2	74	0.510212
220	03	08	2	90	0.620528
220	06	18	2	96	0.661897
220	06	19	2	125	0.861845
220	06	20	2	96	0.661897
220	13	13	2	527	3.633539
220	13	14	2	570	3.930013
220	13	16	2	574	3.957592
220	03	10	3	72	0.496423
220	03	12	3	82	0.56537
220	03	14	3	85	0.586055
220	06	10	3	140	0.965266
220	06	12	3	98	0.675686
220	06	14	3	135	0.930793
220	13	07	3	239	1.647848
220	13	09	3	334	2.30285
220	13	10	3	387	2.668272
250	20	21	1	323.7	2.231834
250	20	23	1	209.4	1.443763
250	20	25	1	324	2.233902
250	16	29	2	488.3	3.366711

250	16	31	2	502.3	3.463238
250	16	32	2	541.6	3.734202
250	19	53	2	261.3	1.801601
250	19	55	2	246.3	1.698179
250	19	57	2	250.2	1.725069
250	16	19	3	185.9	1.281736
250	16	22	3	240	1.654742
250	16	24	3	251	1.730585
250	20	08	3	85.7	0.590881
250	20	14	3	75	0.517107
251	13	22	1	365.2	2.517966
251	13	24	1	370	2.551061
251	13	28	1	382.8	2.639314
251	20	05	1	221	1.523742
251	20	07	1	220.1	1.517537
251	20	08	1	219	1.509952
251	07	46	1	187.9	1.295525
251	07	48	1	167.1	1.152114
251	07	51	1	191	1.316899
251	03	13	1	212	1.461689
251	03	15	1	257	1.771953
251	03	17	1	234	1.613374
251	13	35	2	550	3.792118
251	13	37	2	533	3.674907
251	13	38	2	552	3.805908
251	20	11	2	78.2	0.53917
251	20	12	2	67.3	0.464017
251	20	13	2	63.2	0.435749
251	07	38	2	126.3	0.870808
251	07	40	2	126	0.86874
251	07	41	2	105.2	0.725329
251	03	22	2	144	0.992845
251	03	24	2	145	0.99974
251	03	25	2	115	0.792897
251	13	31	3	181.7	1.252778
251	13	32	3	156	1.075583
251	13	33	3	240	1.654742
251	20	00	3	151.3	1.043177

251	20	02	3	157.6	1.086614
251	20	03	3	151.6	1.045246
252	03	23	1	188	1.296215
252	03	24	1	185	1.275531
252	03	26	1	186	1.282425
252	06	31	1	160	1.103162
252	20	06	1	336	2.316639
252	20	08	1	319	2.199428
252	20	09	1	317	2.185639
252	03	16	2	88	0.606739
252	03	17	2	93	0.641213
252	03	18	2	101	0.696371
252	06	21	2	98.5	0.679134
252	06	22	2	99.2	0.68396
252	06	23	2	91.4	0.630181
252	19	53	2	232	1.599584
252	19	59	2	352	2.426956
252	20	00	2	251	1.730585
252	03	19	3	137	0.944582
252	03	20	3	119	0.820476
252	03	22	3	137	0.944582
252	06	24	3	113.3	0.781176
252	06	26	3	128.4	0.885287
252	06	27	3	121	0.834266
252	20	02	3	231	1.59269
252	20	03	3	103	0.71016
252	20	04	3	130	0.896319
252	20	05	3	130	0.896319
253	03	25	1	233.3	1.608548
253	03	29	1	247.6	1.707143
253	03	31	1	228.2	1.573384
253	06	39	1	216.6	1.493405
253	06	41	1	226	1.558216
253	06	43	1	256	1.765059
253	03	36	2	127	0.875635
253	03	37	2	129	0.889424
253	03	39	2	144	0.992845
253	06	24	2	96.5	0.665344

253	06	26	2	95.4	0.65776
253	06	28	2	90.3	0.622597
253	03	18	3	134	0.923898
253	03	22	3	167.5	1.154872
253	03	23	3	164.7	1.135567
253	06	31	3	221.4	1.5265
253	06	33	3	214.3	1.477547
253	06	36	3	202.1	1.393431
297	20	20	1	450	3.102642
297	20	24	1	440	3.033694
297	20	26	1	447.5	3.085405
297	23	10	1	420	2.895799
297	23	16	1	440	3.033694
297	23	20	1	412	2.840641
297	19	38	2	124	0.85495
297	19	45	2	95	0.655002
297	20	00	2	77.5	0.534344
297	20	05	2	77.5	0.534344
297	22	48	2	122.5	0.844608
297	22	55	2	75	0.517107
297	22	58	2	60	0.413686
297	23	02	2	75	0.517107
297	23	40	2	85	0.586055
297	23	45	2	85.06	0.586468
297	23	48	2	75	0.517107
297	19	10	3	55	0.379212
297	19	20	3	150	1.034214
297	19	25	3	55	0.379212
297	19	28	3	140	0.965266
297	19	32	3	105	0.72395
297	22	26	3	75	0.517107
297	22	32	3	135	0.930793
297	22	36	3	130	0.896319
297	22	40	3	122.5	0.844608
297	23	30	3	115	0.792897
297	23	32	3	120	0.827371
297	23	34	3	117.5	0.810134
298	00	05	1	410	2.826852

298	00	08	1	402.5	2.775141
298	00	12	1	410	2.826852
298	06	43	1	372.5	2.568298
298	06	47	1	365	2.516587
298	06	51	1	354	2.440745
298	07	40	1	365	2.516587
298	07	44	1	377	2.599325
298	07	48	1	365	2.516587
298	15	15	1	510	3.516328
298	15	22	1	512.5	3.533565
298	15	26	1	512.5	3.533565
298	20	10	1	467.5	3.2233
298	20	16	1	470	3.240537
298	20	19	1	455	3.137116
298	21	18	1	450	3.102642
298	21	25	1	450	3.102642
298	21	28	1	450	3.102642
298	06	24	2	25	0.172369
298	06	28	2	55	0.379212
298	06	31	2	22.5	0.155132
298	06	34	2	12.5	0.086185
298	06	36	2	15	0.103421
298	07	23	2	22.5	0.155132
298	07	28	2	42.5	0.293027
298	07	31	2	25	0.172369
298	07	34	2	32.5	0.22408
298	20	33	2	75	0.517107
298	20	35	2	42.5	0.293027
298	20	37	2	60	0.413686
298	21	03	2	62.5	0.430923
298	21	05	2	75	0.517107
298	21	07	2	55	0.379212
298	06	10	3	60	0.413686
298	06	15	3	105	0.72395
298	06	18	3	120	0.827371
298	06	21	3	110	0.758424
298	07	09	3	22.5	0.155132
298	07	12	3	100	0.689476

298	07	15	3	92.5	0.637765
298	07	18	3	107.5	0.741187
298	15	48	3	100	0.689476
298	15	50	3	75	0.517107
298	15	54	3	245	1.689216
298	15	58	3	302.5	2.085665
298	16	06	3	125	0.861845
298	16	08	3	142.5	0.982503
298	20	24	3	150	1.034214
298	20	26	3	140	0.965266
298	20	29	3	145	0.99974
298	21	10	3	130	0.896319
298	21	12	3	127.5	0.879082
298	21	13	3	130	0.896319
299	07	32	1	275	1.896059
299	07	35	1	360	2.482114
299	07	38	1	357.5	2.464877
299	07	41	1	365	2.516587
299	08	02	1	367.5	2.533824
299	08	05	1	362.5	2.499351
299	08	08	1	365	2.516587
299	19	00	1	455	3.137116
299	07	06	2	50	0.344738
299	07	09	2	47.5	0.327501
299	07	12	2	47.5	0.327501
299	08	28	2	50	0.344738
299	08	31	2	42.5	0.293027
299	08	34	2	35	0.241317
299	19	19	2	80	0.551581
299	19	22	2	90	0.620528
299	19	24	2	70	0.482633
299	20	12	2	90	0.620528
299	20	14	2	92.5	0.637765
299	20	16	2	100	0.689476
299	21	09	2	77.5	0.534344
299	21	12	2	95	0.655002
299	21	16	2	97.5	0.672239
299	07	18	3	102.5	0.706713

299	07	20	3	100	0.689476
299	07	25	3	87.5	0.603292
299	08	16	3	90	0.620528
299	08	17	3	105	0.72395
299	08	25	3	105	0.72395
299	19	10	3	170	1.172109
299	19	12	3	170	1.172109
299	19	14	3	160	1.103162
299	20	20	3	70	0.482633
299	22	23	3	155	1.068688
299	22	26	3	152.5	1.051451
299	22	28	3	140	0.965266
299	21	00	3	115	0.792897
299	21	02	3	145	0.99974
299	21	06	3	130	0.896319
316	15	01	1	682	4.702226
316	17	46	1	665	4.585015
316	17	50	1	672	4.633279
316	17	53	1	643	4.433331
316	21	57	1	643	4.433331
316	22	00	1	657	4.529857
316	22	02	1	652	4.495384
316	15	39	2	320	2.206323
316	15	44	2	310	2.137376
316	15	46	2	305	2.102902
316	18	20	2	205	1.413426
316	18	23	2	210	1.4479
316	18	26	2	195	1.344478
316	22	27	2	135	0.930793
316	22	29	2	138	0.951477
316	22	31	2	140	0.965266
316	12	44	2	280	1.930533
316	12	48	2	230	1.585795
316	12	53	2	185	1.275531
316	15	17	3	42	0.28958
316	15	20	3	34	0.234422
316	15	23	3	22	0.151685
316	15	25	3	57	0.393001

316	17	56	3	60	0.413686
316	18	00	3	32	0.220632
316	18	10	3	35	0.241317
316	22	06	3	48	0.330948
316	22	10	3	152	1.048004
316	22	13	3	172	1.185899
316	22	16	3	278	1.916743
316	12	29	3	45	0.310264
316	12	34	3	65	0.448159
316	12	36	3	85	0.586055
317	07	02	1	660	4.550542
317	07	05	1	622	4.288541
317	07	08	1	630	4.343699
317	10	50	1	667	4.598805
317	10	54	1	852	5.874336
317	10	58	1	655	4.516068
317	11	04	1	668	4.6057
317	15	10	1	698	4.812542
317	15	13	1	716	4.936648
317	15	18	1	459	3.164695
317	06	48	2	165	1.137635
317	06	51	2	125	0.861845
317	06	55	2	125	0.861845
317	11	22	2	475	3.275011
317	11	25	2	435	2.999221
317	11	27	2	350	2.413166
317	14	58	2	430	2.964747
317	15	02	2	415	2.861325
317	15	04	2	350	2.413166
317	21	36	2	150	1.034214
317	21	40	2	140	0.965266
317	21	42	2	155	1.068688
317	06	29	3	260	1.792638
317	06	37	3	255	1.758164
317	06	41	3	257	1.771953
317	11	01	3	12	0.082737
317	11	07	3	94	0.648107
317	11	11	3	17.2	0.11859

317	15	23	3	42	0.28958
317	15	25	3	12	0.082737
317	15	28	3	41	0.282685
317	21	50	3	299	2.061533
317	21	51	3	276	1.902954
317	21	54	3	272	1.875375
318	06	43	2	140	0.965266
318	06	47	2	132	0.910108
318	06	49	2	120	0.827371
318	06	26	3	82	0.56537
318	06	28	3	153	1.054898
318	06	30	3	180	1.241057
318	06	36	3	186	1.282425

REFERENCES

Anderegg, W. R. L., Trugman, A. T., Bowling, D. R., Salvucci, G., & Tuttle, S. E. (2019). Plant functional traits and climate influence drought intensification and land–atmosphere feedbacks. *Proceedings of the National Academy of Sciences of the United States of America*, *116*(28), 14071–14076. https://doi.org/10.1073/pnas.1904747116

Asawa, T., & Fujiwara, K. (2020). Estimation of Sensible and Latent Heat Fluxes of an Isolated Tree in Japanese Summer. *Boundary-Layer Meteorology*, *175*(3), 417–440. https://doi.org/10.1007/s10546-020-00507-y

Barker, R. A., & Ardis, A. F. (1996). Hydrogeologic framework of the Edwards-Trinity aquifer system, west-central Texas. *US Geological Survey Professional Paper*, *1421 B*.

Barker, R. A., Bush, P. W., & Baker, E. T. (1994). *GEOLOGIC HISTORY AND HYDROGEOLOGIC SETTING OF THE EDWARDS-TRINITY AQUIFER SYSTEM, WEST-CENTRAL TEXAS Water-Resources Investigations Report 94-4039*.

Beaman, L. (2022). *Evaluating Biomass Water Storage and Sap Flux in Three Semi-Arid Tree Species in Central Texas* [Masters Thesis]. The University of Texas at Austin.

Belko, N., Zaman-Allah, M., Diop, N. N., Cisse, N., Zombre, G., Ehlers, J. D., & Vadez, V. (2013). Restriction of transpiration rate under high vapour pressure deficit and non-limiting water conditions is important for terminal drought tolerance in cowpea. *Plant Biology*, *15*(2), 304–316. https://doi.org/10.1111/j.1438-8677.2012.00642.x

Bucci, S. J., Goldstein, G., Meinzer, F. C., Franco, A. C., Campanello, P., & Scholz, F. G. (2005). Mechanisms contributing to seasonal homeostasis of minimum leaf water potential and predawn disequilibrium between soil and plant water potential in Neotropical savanna trees. *Trees - Structure and Function*, *19*(3), 296–304. https://doi.org/10.1007/s00468-004-0391-2

Campbell, G. (1974). A simple method for determining unsaturated conductivity from moisture retention data. *Soil Science*, *117*(6), 311–314.

Davis, T. W., Kuo, C. M., Liang, X., & Yu, P. S. (2012). Sap flow sensors: Construction, quality control and comparison. *Sensors*, *12*(1), 954–971. https://doi.org/10.3390/s120100954

Dennis Baldocchi. (2014). *Personal Communication*.

Donovan, L. A., Griseâ, D. J., West, J. B., Pappert, R. A., Alder, N. N., & Richards, J. H. (1999). *Predawn disequilibrium between plant and soil water potentials in two cold-desert shrubs*.

Gams, I. (1993). Origin of the term "karst," and the transformation of the classical karst (kras). *Environmental Geology*, *21*(3), 110–114. https://doi.org/10.1007/BF00775293

Gartner, K., Nadezhdina, N., Englisch, M., Čermak, J., & Leitgeb, E. (2009). Sap flow of birch and Norway spruce during the European heat and drought in summer 2003. *Forest Ecology and Management*, *258*(5), 590–599. https://doi.org/10.1016/j.foreco.2009.04.028

Granier, A. (1985). *Une nouvelle méthode pour la mesure du flux de sève brute dans le tronc des arbres*.

Granier, A. (1987). Evaluation of transpiration in a Douglas-fir stand by means of sap flow measurements. In *Tree Physiology* (Vol. 3). Heron Publishing.

Grossiord, C., Buckley, T. N., Cernusak, L. A., Novick, K. A., Poulter, B., Siegwolf, R. T. W., Sperry, J. S., & McDowell, N. G. (2020). Plant responses to rising vapor pressure deficit. In *New Phytologist* (Vol. 226, Issue 6, pp. 1550–1566). Blackwell Publishing Ltd. https://doi.org/10.1111/nph.16485

Howell, T. A., & Dusek, D. A. (1995). *COMPARISON OF VAPOR-PRESSURE-DEFICIT CALCULATION METHODS-SOUTHERN HIGH PLAINS*.

Hugalde, I. P., Vila, ;, & Hernán F. (2014). *Isohydric or anisohydric behavior in grapevines... An endless controversy? Isohydric or anisohydric behaviour in grapevine…, a never-ending controversy?* https://www.researchgate.net/publication/298079737

Jackson, R. B., Mooney, H. A., & Schulze, E.-D. (1997). A global budget for fine root biomass, surface area, and nutrient contents. In *Ecology* (Vol. 94). www.pnas.org.

Kholová, J., Hash, C. T., Kakkera, A., Koová, M., & Vadez, V. (2010). Constitutive water-conserving mechanisms are correlated with the terminal drought tolerance of pearl millet [Pennisetum glaucum (L.) R. Br.]. *Journal of Experimental Botany*, *61*(2), 369–377. https://doi.org/10.1093/jxb/erp314

Kirschbaum, M. U. F. (2004). Direct and indirect climate change effects on photosynthesis and transpiration. In *Plant Biology* (Vol. 6, Issue 3, pp. 242–253). https://doi.org/10.1055/s-2004-820883

Klein, T., Cohen, S., Paudel, I., Preisler, Y., Rotenberg, E., & Yakir, D. (2016). Diurnal dynamics of water transport, storage and hydraulic conductivity in pine trees under seasonal drought. *IForest*, *9*(5), 710–719. https://doi.org/10.3832/ifor2046-009

Köcher, P., Horna, V., & Leuschner, C. (2013). Stem water storage in five coexisting temperate broad-leaved tree species: Significance, temporal dynamics and dependence on tree functional traits. *Tree Physiology*, *33*(8), 817–832. https://doi.org/10.1093/treephys/tpt055

Kukowski, K. R., Schwinning, S., & Schwartz, B. F. (2013). Hydraulic responses to extreme drought conditions in three co-dominant tree species in shallow soil over bedrock. *Oecologia*, *171*(4), 819–830. https://doi.org/10.1007/s00442-012-2466-x

Long, A. T., Udall, S. L., & Nolan, T. B. (1963). *Ground-Water Geology of Edwards County Texas UNITED STATES DEPARTMENT OF THE INTERIOR*.

Manandhar, A., Preisler, Y., & Holbrook, N. M. (2021). Diurnal Shifts in Stomatal Regulation in Response to Water Availability. *In AGU Fall Meeting 2021*.

Matheny, A. M., Bohrer, G., Garrity, S. R., Morin, T. H., Howard, C. J., & Vogel, C. S. (2015). Observations of stem water storage in trees of opposing Hydraulic strategies. *Ecosphere*, *6*(9). https://doi.org/10.1890/ES15-00170.1

Matheny, A. M., Bohrer, G., Stoy, P. C., Baker, I. T., Black, A. T., Desai, A. R., Dietze, M. C., Gough, C. M., Ivanov, V. Y., Jassal, R. S., Novick, K. A., Schäfer, K. V. R.,

& Verbeeck, H. (2014). Characterizing the diurnal patterns of errors in the prediction of evapotranspiration by several land-surface models: An NACP analysis. *Journal of Geophysical Research: Biogeosciences*, *119*(7), 1458–1473. https://doi.org/10.1002/2014JG002623

Mirfenderesgi, G., Bohrer, G., Matheny, A. M., Fatichi, S., de Moraes Frasson, R. P., & Schäfer, K. V. R. (2016). Tree level hydrodynamic approach for resolving aboveground water storage and stomatal conductance and modeling the effects of tree hydraulic strategy. *Journal of Geophysical Research: Biogeosciences, 121*(7), 1792–1813. https://doi.org/10.1002/2016JG003467

Mitchell, P. J., Benyon, R. G., & Lane, P. N. J. (2012). Responses of evapotranspiration at different topographic positions and catchment water balance following a pronounced drought in a mixed species eucalypt forest, Australia. *Journal of Hydrology*, *440–441*, 62–74. https://doi.org/10.1016/j.jhydrol.2012.03.026

Mollnau, C., Newton, M., & Stringham, T. (2014). Soil water dynamics and water use in a western juniper (Juniperus occidentalis) woodland. *Journal of Arid Environments*, *102*, 117–126. https://doi.org/10.1016/j.jaridenv.2013.11.015

Nizinski, J., & Saugier, B. (1989). FOR A MATURE OAK FOREST. In *Agricultural and Forest Meteorology* (Vol. 47).

Northup, A. P., Keitt, T. H., & Farrior, C. E. (2021). *Cavitation-resistant junipers cease transpiration earlier than cavitation-vulnerable oaks under summer dry conditions _ Enhanced Reader*.

Oishi, A. C., Hawthorne, D. A., & Oren, R. (2016). Baseliner: An open-source, interactive tool for processing sap flux data from thermal dissipation probes. *SoftwareX*, *5*, 139–143. https://doi.org/10.1016/j.softx.2016.07.003

Oishi, A. C., Oren, R., & Stoy, P. C. (2008). Estimating components of forest evapotranspiration: A footprint approach for scaling sap flux measurements. *Agricultural and Forest Meteorology*, *148*(11), 1719–1732. https://doi.org/10.1016/j.agrformet.2008.06.013

Oki, T., & Kanae, S. (2006). *Global Hydrological Cycles and World Water Resources*. https://www.science.org

Oogathoo, S., Houle, D., Duchesne, L., & Kneeshaw, D. (2020). Vapour pressure deficit and solar radiation are the major drivers of transpiration of balsam fir and black spruce tree species in humid boreal regions, even during a short-term drought. *Agricultural and Forest Meteorology*, *291*. https://doi.org/10.1016/j.agrformet.2020.108063

Palmer, Arthur, N. (1991). Origin and morphology of limestone caves.pdf. In *Geological Society of America Bulletin* (Vol. 103, pp. 1–21).

Rechner, A. (2020). *A Comparison of Transpiration Rates from Three Semi-Arid Tree Species in Response to Partial Stand Clearing*. The University of Texas at Austin.

Rempe, D. M., & Dietrich, W. E. (2018). Direct observations of rock moisture, a hidden component of the hydrologic cycle. *Proceedings of the National Academy of Sciences of the United States of America*, *115*(11), 2664–2669. https://doi.org/10.1073/pnas.1800141115

Ripullone, F., Guerrieri, M. R., Nole', A., Magnani, F., & Borghetti, M. (2007). Stomatal conductance and leaf water potential responses to hydraulic conductance variation in Pinus pinaster seedlings. *Trees - Structure and Function*, *21*(3), 371–378. https://doi.org/10.1007/s00468-007-0130-6

Scholes, R. J. (2020). The future of semi-arid regions: A weak fabric unravels. *Climate*, *8*(3). https://doi.org/10.3390/cli8030043

Scholz, F. G., Phillips, N. G., Bucci, S. J., Meinzer, F. C., & Goldstein, G. (2011). *Hydraulic Capacitance: Biophysics and Functional Significance of Internal Water Sources in Relation to Tree Size* (pp. 341–361). https://doi.org/10.1007/978-94-007-1242-3_13

Schwinning, S. (2008). *The Water Relations of Two Evergreen Tree Species in a Karst Savanna* (Vol. 158, Issue 3).

Texas Water Science Center (USGS TWSC). (2014, February 1). Geologic Database of Texas.

Thomsen, J. E., Bohrer, G., Matheny, A. M., Ivanov, V. Y., He, L., Renninger, H. J., & Schäfer, K. V. R. (2013). Contrasting hydraulic strategies during dry soil conditions in Quercus rubra and Acer rubrum in a sandy site in Michigan. *Forests*, *4*(4), 1106–1120. https://doi.org/10.3390/f4041106

Waring, R. H., & Running, S. W. (1978). Sapwood water storage: its contribution to transpiration and effect upon water conductance through the stems of old-growth Douglas-fir. *Plant Cell Environ.*, 131–140.

Williams, D. G., & Ehleringer, J. R. (2000). INTRA-AND INTERSPECIFIC VARIATION FOR SUMMER PRECIPITATION USE IN PINYON-JUNIPER WOODLANDS. In *Ecological Monographs* (Vol. 70, Issue 4).